SYNTHESIZING FIELD, LABORATORY, AND IN-SITU STUDIES TO DETERMINE THE ENVIRONMENTAL FATE OF LAMPRICIDE 3-TRIFLUOROMETHYL-4-NITROPHENOL (TFM)

by

Lauryn Dee Angell

A thesis submitted in partial fulfillment of

the requirements for the degree of

Master of Science

(Environmental Chemistry & Technology)

at the

UNIVERSITY OF WISCONSIN-MADISON

2024

ABSTRACT

Understanding the fate of organic compounds in river systems is important for protecting watersheds and human health. While individual mechanisms of compound transformation and transport can be quantified, determining their relative importance under various photochemical and biogeochemical conditions poses another challenge. Aquatic pesticide treatments provide an opportunity for scientists to conduct controlled field studies and validate a systematic research framework for assessing chemical fate. This research synthesizes laboratory and *in-situ* experiments with field studies on the lampricide 3-trifluoromethyl-4-nitrophenol (TFM), a compound that has been applied to tributaries of the Great Lakes since the 1950s to control for the invasive sea lamprey (*Petromyzon marinus*). Tandem studies of a photoreactive tracer (uranine), a sorptive tracer (rhodamine-WT), and a conservative tracer (bromide) are used to quantify specific loss processes. Our study of two treatments in the Upper Peninsula of Michigan reveal physical transport processes and local hydrologic conditions largely control the residence time of TFM in the hyporheic zone, where most biogeochemical transformations occur. Evidence of transient subsurface storage (i.e., reincorporation of TFM back into the water column over treatment timescales) suggests photodegradation may be important, yet *in-situ* batch experiments and modeled solar irradiance reveal environmental photodegradation kinetics are much slower than laboratory kinetics. Alignment between *in-situ* experiments, kinetic models, and field observations highlights the importance of using a synergistic approach to predict compound persistence in the environment.

To my mother

Claresa Lee Cummings Angell

whose strength and sacrifices led to my education, opportunities, and privilege

ACKNOWLEDGEMENTS

Like most research, this work is the culmination of ideas influenced by a village of mentors, peers, and predecessors. To my thesis mentor and advisor, Professor Christy Remucal, thank you for believing in me, taking a chance on me, and helping me learn how to conduct graduate-level research. I was so fascinated by and passionate about environmental contaminants, and your expertise has pushed me to learn more than I ever expected. The level of achievement and balance you maintain inspires me to continuously assess and improve the seemingly small, daily habits that end up making a big difference. To our longtime collaborator, Professor Adam Ward, with your help and excitement, I expanded my knowledge beyond the laboratory and dove far past my comfort zone to gain new, valuable skills in the field. Thank you both for reiterating my worth as a scientist and person. Additional thanks to Assistant Professor Haoran Wei, who also read this thesis and served on my MS committee.

I knew little about the Midwest before applying to graduate school, and living in Wisconsin has expanded my perspectives on personal communication, water resources, the Great Lakes region, and much more. I am proud to have been a member of the Remucal Group and the EC&T community, which we refined from the inside-out post-pandemic. These are special groups to belong to and ones comprised of tenacious young scientists who fight for ideas that matter and uplift underrepresented voices. Kaitlyn Gruber, Jenna Swenson, Seo Won Cho, Savannah Finley, and AnnaBeth Thomas, thank you for helping me navigate one of the most difficult chapters of my life— a chapter when I grew more as a person than every other chapter combined.

I am grateful to the Great Lakes Fishery Commission for funding this research and graciously understanding the impact of COVID-19 on our research timelines and goals. Thank you to UW-Madison's Center for Limnology for the Anna Grant Birge Memorial Award, which provided additional financial support for field sampling and analysis. Analysis was conducted at the UW-Madison Core Facility for Advanced Water Analysis, housed in the Water Science & Engineering Laboratories (WSEL). Conducting research at WSEL has been a wild ride full of improvisation and collaboration. A couple Becker Travel Supplements from the Department of Civil & Environmental Engineering were also awarded, allowing me to present my findings at regional and national conferences.

It was an exciting, new experience coordinating with Supervising Fish Biologists Lori Criger and Christopher Gagnon from the U.S. Fish and Wildlife Service – Marquette Biological Station. Their teams welcomed us and kept us in the loop during TFM treatments. In a remote but breathtaking region of the Upper Peninsula of Michigan, our field study could not have been done without the willingness of undergraduate researchers Elizabeth (Lily) Wagner, Josie Jaquet, and Alexander Lemmenes. Thank you to the Water@UW REU Program for supporting Lily's research experience during the time we needed her most. You three kept me laughing during the more stressful times.

Molly Cain, Ph.D., your presence in the field was extremely helpful and your ideas about science and life inspire me to be the best version of myself. Paige Becker, Ph.D., thank you for jumping on this project, joining zoom meetings, and answering my calls and texts despite all the fires you were already fighting. Reid Milstead, Ph.D., thank you for staying awake with me all night to sample, listening to my long-winded stories, and watching bad TV with me. Amber M. White, Ph.D., thank you for answering so, so many of my questions. You are an incredible scientist and my research was greatly improved by collaborating with the aquatic herbicide team. James Lazarcik, M.S., interacting with you has raised the standards I hold for my personal and professional relationships. Your thought-provoking words and level of discretion has allowed me

to understand nuance and break away from limited, black-and-white thinking. During times when I needed to make critical decisions or find mental clarity, you helped me.

TABLE OF CONTENTS

TABLE OF TABLES

TABLE OF FIGURES

INTRODUCTION

Developing a Research Framework: TFM as a Model Compound

There is a critical need to link laboratory experiments with true environmental conditions to predict the fate of polar organic compounds. Rates of compound loss in aquatic and terrestrial systems can be magnitudes faster or slower than loss in laboratory experiments, making compound fate difficult to predict using lab studies alone.[1–3] Polar and ionizable compounds are of specific concern due to their increased solubility, reactivity, and environmental mobility.[4] Controlled experiments performed *in-situ*, or "on-site", connect laboratory and field studies, which can increase the predictive power of kinetic and equilibrium models and improve our understanding of a compound's environment fate.[5]

The application of aquatic pesticides provides scientists with an opportunity to perform robust field studies on "model compounds" using crucial information like the mass of compound applied, application location, and target concentration. By synthesizing field observations with results from controlled experiments conducted both *in-situ* and in the laboratory, this research develops a framework to comprehensively assess the environmental fate of 3-trifluoromethyl-4-nitrophenol (TFM). TFM is a lampricide that has been directly applied to tributaries of the Laurentian Great Lakes of North America since the 1950s to reduce populations of the invasive sea lamprey (*Petromyzon marinus*).[6] Sea lamprey grow to become parasitic and have historically devastated native (and commercially relevant) fish populations of lake trout, white fish, blue pike, walleye, etc.[7,8] Sea Lamprey Control values an integrated pest-management approach (i.e., using electrical and mechanical barriers, physical traps, and pheromones), but chemical control using TFM is the most effective and widely used approach.[9,10] TFM is an effective model compound because it is structurally similar to other compounds of concern and mechanistic studies are broadly applicable to polar organic compounds in general.

Lampricide applications are highly controlled. TFM is a Restricted Use Pesticide for Great Lakes tributaries, with most being treated in 3-5 year cycles to target sea lamprey in their larval, non-parasitic stage.[7,11–14] Over 30,000 kg of TFM are applied annually and the target in-stream concentrations range from 1-14 mg/L (~5-67 μM).[15,16] 12-hour, continuous-rate injections are typically conducted because an exposure of 9-hours at or slightly above the minimum lethal concentration (MLC) is required to achieve 99.9% sea lamprey mortality. The "stream-specific" minimum lethal concentration (SMLC) is determined by pretreatment on-site toxicity tests or river pH, alkalinity, and discharge.[7,17–19]

With an improved understanding of TFM fate, we can estimate the potential for low-level concentrations of TFM and its persistent degradation products, such as trifluoroacetic acid (TFA).[15,20] There is evidence of increasing TFA concentrations in surface waters[21–24] and lampricide-treated tributaries drain to the Great Lakes, a vital fresh water resource.[25,26] Although TFA is a photoproduct of TFM based on laboratory irradiations, TFM photodegradation in the environment is expected to be minimal or only relevant under specific conditions (shallow depth, little cloud cover, etc.).[2] This exemplifies the broad applicability of TFM studies and the need for a holistic research approach. However, there is a narrower research goal, in alignment with the Great Lakes Fishery Commission (GLFC), to continuously optimize integrated treatment practices by maintaining lethal levels while minimizing impact on non-target species and the ecosystems they inhabit.[9,10,27]

TFM Environmental Fate

The dominant loss and transformation pathways of TFM are well understood, but their relative importance under various photochemical and biogeochemical conditions has not been investigated simultaneously. Reactive processes like abiotic and biotic degradation can reduce the mass of TFM recovered at downstream sites. The relevant degradation reactions for TFM in the environment are photodegradation (half-life ($t_{1/2}$) ~ days) and microbial degradation ($t_{1/2}$ ~ weeks).[2,15,28–30] TFM does not undergo hydrolysis, and volatilization is negligible due to its low vapor pressure and ionized state above pH 6.4.[6,20,31,32] While sorption of TFM to riverbed and hyporheic sediment may facilitate microbial degradation and impact in-stream concentrations, TFM is considered environmentally mobile based on its organic carbon-normalized distribution coefficient (K_{OC}) of 35 – 290 Kg/L.[33,34]

In addition to reactive processes, physical processes such as river discharge (including advection and dispersion as water travels downstream) and transient storage in the hyporheic zone can strongly control the retention and transport of compounds.[35–37] The hyporheic zone is a dynamic, shallow region of the riverbed with heterogeneous redox conditions and high microbial activity where transformation kinetics are difficult to quantify with accuracy.[37,38] Over days to weeks, TFM may be temporarily stored in the hyporheic zone and slowly released back into the water column, contributing to low-level, legacy concentrations. However, river discharge and hyporheic exchange are controlled by complex factors including seasonal precipitation events, sediment permeability and organic content, and spatiotemporal variable channel characteristics.[39,40] Over longer time scales (i.e., weeks to months), biodegradation of TFM by sediment microbes in the hyporheic zone may also contribute to the release of metabolites in-stream. Overall, we hypothesize the persistence of TFM may be greater than reflected in isolated studies and will be highly dependent on individual stream characteristics and hyporheic dynamics.

Hydrological Tracer Studies

In this research, field studies of TFM, a photoreactive tracer (uranine), a sorptive tracer (rhodamine WT), and a conservative tracer (bromide) were performed on treated tributaries of Lake Michigan. *In-situ* photochemistry and streamside mesocosm experiments with TFM and the tracers were used to bridge in-stream mass flux determinations with compound-specific, laboratory-derived equilibrium and kinetic constants.

Uranine (UR), also known as fluorescein, is photolabile and has been used to quantify rates of compound photodegradation in surface waters.[41–43] Rhodamine-WT (RWT) can be effectively used as a conservative tracer in marine environments and aquifer studies, but it does exhibit particle interactions in organic matter-rich environments such as rivers, bogs, and wetlands and should be used cautiously or as a sorptive tracer.[42,44–46] RWT is a multi-compound mixture consisting of two isomers with distinct sorptive properties.[47–49] The meta isomer is more sorptive, but RWT distribution coefficients refer to the combined behavior of both isomers. Both uranine and RWT absorb visible light and strongly fluoresce (**Supplemental Information (SI) Section 1**). Bromide (Br^-) is commonly used as a conservative, or non-reactive, hydrological tracer to assess physical transport dynamics and time of water passage over a flow path. Loss of bromide would be attributed to storage in the riverbed hyporheic zone.[50]

METHODS

Field Studies: TFM Treatments, a Multi-Tracer Study, and an *In-Situ* Column Study

In July of 2022, we studied TFM treatment of two large tributaries of the Manistique River in the Upper Peninsula of Michigan, USA: the Fox River and the Driggs River (**Figure 1**). As a part of the Sea Lamprey Control Program, scientists from the U.S. Fish and Wildlife Service (USFWS) conducted the treatments and TFM was the only chemical applied. The Fox and Driggs River treatments were selected because they were the first applications conducted at tributary headwaters. Because there was no background TFM, we anticipated these rivers would be more amenable to mass balance analysis and time of passage studies.

Fox River TFM Treatment Study

There are multiple tributary confluences along the Fox River, which is net gaining (i.e., there is a net increase in water discharge over the river flow path). To account for dilution from the added water volume and maintain SMLCs, TFM was applied at multiple points of the Fox River (**Figure 2, a**). We refer to the earliest, most upstream applications as primary (1°) applications and downstream, "boost" applications as secondary (2°) applications. 1° and 2° applications are conducted identically, and the boost begins once the upstream "chemical block" arrives. We collected samples at two well-mixed points: an *upper site* 80 m downstream of a 2° application and a *lower site* 240 m downstream of another 2° application (**Figure 2, a**). The lower site captured converging chemical blocks from the West Branch and Casey Lake outlet. Relative to the 1° application at Casey Lake outlet, there was a 1.8 km and 7.6 km flow path to the upper and lower sites, respectively. Site coordinates and flow paths from application points are summarized for both the Fox and Driggs Rivers in **SI Section 2.** Because of the complexity of the

Fox River, our field studies served to refine sampling techniques, analytical sensor deployment, and stream-side sediment-column operation, as well as develop rapport with USFWS.

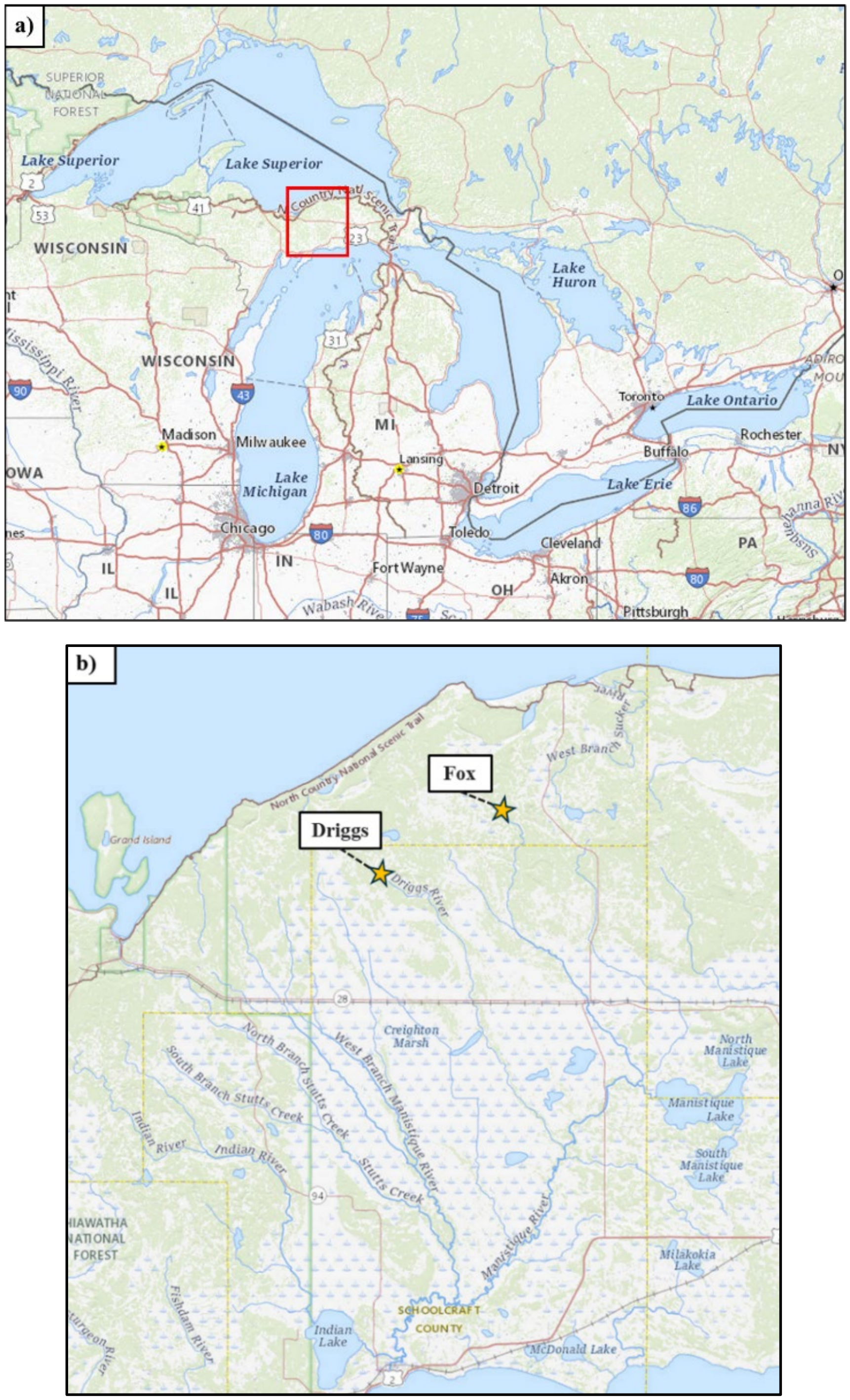

Figure 1. a) A map of the Great Lakes region of the United States. The Manistique River system, located in the Upper Peninsula of Michigan, is boxed in red. **b)** The major tributaries of the Manistique River with stars indicating the two tributaries we studied.[51]

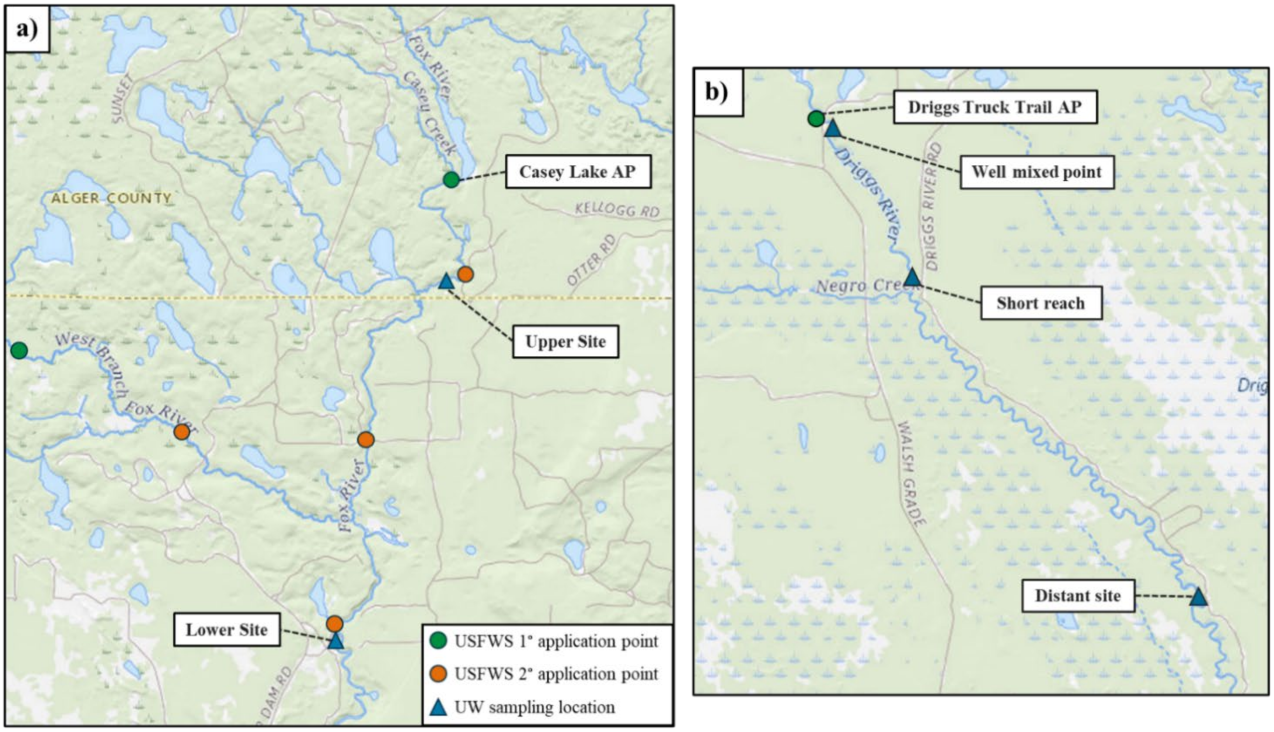

Figure 2. TFM application points and our sampling sites for the **a)** Fox and **b)** Driggs River treatments.

Throughout treatment, USFWS performs spectrophotometric analysis on discrete water samples to quantify TFM and ensure SMLCs are maintained.[52] We quantified TFM by collecting river water samples for laboratory analysis and deploying fluorescent dissolved organic matter (fDOM) sensors for *in-situ* analysis. We validated this continuous monitoring approach to develop higher resolution concentration time series for TFM, leading to more accurate mass calculations.

fDOM, the fraction of chromophoric or colored DOM (cDOM) that fluoresces, can be used as a surrogate to indirectly monitor dissolved organic carbon (DOC) concentrations, an important water quality parameter. For this reason, fDOM is commonly monitored in wastewater-impacted streams and river systems.[53–56] The fDOM sensors (YSI item #599104-01, λ_{excite} = 365 ± 5 nm, $\lambda_{emission}$ = 480 ± 40 nm)[57] were attached to YSI EXO water quality Sonde II field instruments positioned in the river thalweg and middle of the water column. Individual sensors were calibrated *ex-situ* by relating the acquired fDOM signals to corresponding TFM concentrations measured in discrete water samples. Water samples were collected immediately downstream (~2 m) of the sensors to not influence turbidity and light scattering during readings.

Samples collected adjacent to the analytical sensors were syringe filtered (0.45 μm, nylon) with zero headspace into 40 mL amber vials with Teflon-lined lids. All glassware was amber and baked at 450 °C for 8 hours before sampling. The samples did not require additional preservation to maintain analyte stability. During the Fox River treatment, a bulk water sample (1 L) was collected, and vacuum-filter sterilized (0.45 μm, nylon) on site for use in *in-situ* photochemistry experiments once the in-stream TFM concentration stabilized (collected mid-day). All TFM and tracer study samples were stored on-site for ~1 week in the dark on ice and then transported to UW-Madison for analysis.

Driggs River TFM Treatment Study

The Driggs River treatment offered a more controlled field study; unlike the Fox River study, our sampling sites on the Driggs River were all located upstream of any 2° applications, allowing us to better model the system as a plug flow reactor and perform mass balance analysis (**Figure 2, b**). Mass analysis was performed to **a)** determine the relative importance of dominant loss mechanisms to the overall attenuation of TFM in-stream and **b)** assess the accuracy of kinetic-based predictions relative to actual field observations. USFWS conducted the 1° application at Driggs Truck Trail, and we quantified TFM at three sites: a *well-mixed point*, a *short reach*, and a *distant site*, which respectively had 0.2 km, 2.8 km, and 11.2 km flow paths from the application point. These sites were selected with the broad goal of predicting TFM fate over shorter stream reaches and a relatively longer flow path. Sample processing and *in-situ* analysis were conducted as described for the Fox River.

Driggs River Tracer Study

To better characterize the dominant loss processes over the short reach, we conducted a multi-tracer study using organic and inorganic solutes with predictable fates. On July 31, 2022, four days after the TFM treatment, a pulse injection of a photoreactive tracer (uranine), a sorptive tracer (rhodamine-WT), and a conservative tracer (bromide) was conducted at the same 1° application point used during treatment. Tracer dosing was calculated based on historical and pre-treatment discharge measurements. The study was conducted post-treatment to avoid interference with the lampricide application process. In addition, the organic tracers absorb light and their presence during treatment would have interfered with the *in-situ* quantification of TFM via fDOM sensing.

Like the TFM treatment, concentration time series were developed for the fluorescent tracers using in-stream optical sensors (fluorometers) that were calibrated *ex-situ* based on discrete water sample results. The fluorometers used were Turner Designs Cyclops-7 Interchangeable Loggers by Precision Measurement Engineering (PME). Each fluorometer was wavelength-specific to either uranine or RWT. The dynamic range for the Uranine and RWT sensors were respectively 0-500 ppb and 0-1000 ppb.[58] The bromide time series was developed from analysis of the discrete water samples.

In-situ Sediment Column

During TFM treatment and the tracer study at the Driggs River, treated water was passed through a streamside, sediment-packed column to observe TFM-sediment interactions and simulate a hyporheic flow path. This flow-through experiment served as a middle-tier, *in-situ* study to bridge our analysis of field observations with batch-style laboratory sorption and biodegradation experiments. Treated water was pumped from the well-mixed point sampling location to the sediment column using a battery-powered peristaltic pump and a deep-cycle marine battery. The influent and effluent lines were constructed of soft plastic and the column itself was plastic. The column was vertically saturated and flowing upward with the effluent line immediately draining into a secondary container. Column joints were waterproofed using Teflon tape and the packed sediment was retained using a series of mesh frits and cork liners. When packing the column, the top few centimeters of the riverbed were hand-cored, collected in a bucket, stirred, and then gradually added to the column as a slurry (**SI Section 2**).

Data from the effluent container were reduced as a fourth "site". Like the in-stream studies, analytical sensors were deployed in the container (either an fDOM sensor for TFM or fluorometers for the organic tracers) and it was periodically sampled for laboratory analysis. To collect the samples, runoff from the effluent container was directed to a 60 mL syringe with a 0.45 µm nylon filter to gradually collect a time-integrated sample over ~15-minute intervals. The container was covered with a tarp to avoid interference from wet deposition. The column set-up was positioned amongst tall grass to provide some shade cover, but the temperature was not controlled otherwise. The column was equilibrated with river water for 24-48 hours before each breakthrough curve study.

During TFM treatment, steady-state influent and effluent concentrations (C_0 and C_{out}, respectively) were used to calculate a comprehensive rate of compound loss, assuming constant column flow (Q) and volume (V) (**Equation 1**).[59]

$$R = (C_0 - C_{out})\frac{Q}{V}$$

Equation 1

Mass Analysis

The mass (m) of a compound recovered at a given site was determined from the product of water discharge (Q) and the in-stream concentration (C_t) integrated over the entire treatment period, including the rising and falling limbs of the time series (**Equation 2**). This analysis was performed for TFM, bromide, RWT, and uranine in the Driggs River.

$$m = Q \int_{t_0}^{t_f} C(t)dt$$

Equation 2

A daily, site-specific water discharge value (Q) was computed as the sum of discharge values (q_x) for *x* number of discrete subsections over the river profile (**Equation 3**).

$$Q = \sum q_x$$

Equation 3

For a given subsection (x), q_x was calculated following the mid-section method using velocity and depth measurements recorded on-site using a McBurney flow meter and top-setting wading rod (**Equation 4**).[60]

$$q_x = \overline{V}_x \left(\frac{W_{x-1} + W_x}{2}\right) d_x$$

Equation 4

V_x is the subsection velocity averaged over ~1 minute of river flow. W_x and W_{x-1} are the widths of successive subsections and d_x is the vertical depth.

The mass recovery at downstream sites (short reach and distant site) was determined relative to the mass calculated at the well-mixed point (**Equation 5**). Uncertainty of the mass recovery was propagated from the uncertainty of the time-integrated concentration value.

$$\% \ m_{recovered} = \left(\frac{m_{downstream}}{m_{WMP}}\right) * 100\%$$

Equation 5

Laboratory Sorption Studies

Batch equilibrium and kinetic laboratory studies of TFM sorption to sediment were adapted from methods by the United States Environmental Protection Agency (US EPA) and the International Organisation for Economic Co-operation and Development (OECD).[61,62] All batch sorption studies were performed using pretreatment sediment from the Driggs River. The organic content of the sediment was determined using the loss-on-ignition method as described previously.[63] Briefly, the wet sediment was air dried in large batches and then baked at 550 °C in triplicate crucibles for four hours to mineralize all organic material to $CO_{2\,(g)}$. The difference in mass between the dry and ignited sediment is the fraction of organic content (f_{oc}), which impacts the degree of TFM sorption.[33]

Sorption-Desorption Kinetics: TFM

Sorption kinetics experiments were conducted using a ~1:7 sediment-to-buffer ratio. In 50 mL centrifuge tubes (batch reactors), 5 g of sediment was equilibrated with 34 mL of phosphate buffer (20 mM, pH 7.2-7.3) overnight on an incubator-shaker table at 150 RPM at 24 °C. The sediment was air-dried in a laboratory hood for 3 days before sieving to 2 mm. Samples were centrifuged at 4000 RPM for 10 minutes before recording the equilibrated pH. The reactors were spiked with 80 µL of TFM standard to achieve an initial aqueous concentration of 12 µM and then placed on the shaker table for specific time intervals (5 min, 30 min, and 1, 2, 4, 6, 8, 15, and 24 hours). Because 6 mL of the aqueous fraction was removed at the time of sampling (post-centrifuge, **SI Section 14**), sacrificial reactors were prepared in triplicate *for each time condition* to maintain consistent sediment-buffer ratios. Buffer blanks and sediment-buffer blanks were also studied following this procedure. Filtered aliquots were analyzed by high-performance liquid chromatography (HPLC) and the final pH was recorded immediately after sampling. Aqueous concentrations at a given time (C_t) and the experiment start (C_i) were used to determine a first-order kinetic constant (k_{sorb}, or k in **Equation 6**) and the characteristic time (τ, **Equation 7**).

$$\ln\left(\frac{C_t}{C_0}\right) = -k(t)$$

Equation 6

$$\tau = \frac{1}{k}$$

Equation 7

In desorption kinetic experiments, TFM-sorbed sediment was prepared in bulk by equilibrating 200 g of dry, sieved sediment with 1.4 L of buffered, ultrapure water containing 12 μM TFM (20 mM phosphate, pH 7.2). The suspension was equilibrated on a shaker table overnight (19 hours) at 150 RPM in the dark. The sediment was collected by gently pouring the suspension through a glass funnel with a mesh screen. Sacrificial reactors were prepared in triplicate by adding ~6 g of wet, TFM-sorbed sediment to 50 mL centrifuge tubes. The mass of the empty tube and lid was recorded before adding the wet sediment. The percent moisture of the sediment at the time of reactor preparation was determined by oven drying ~10 g of the wet sediment in an aluminum foil dish, in triplicate, at 100 °C for 2-3 hours. With the correction for percent moisture, a 1:5.7 sediment-water ratio was maintained by adding 42 mL of buffered, ultrapure water (20 mM phosphate). Upon addition of the buffer, reactors were placed on the shaker table and sampled at 0 min, 30 min, 1 hr, 2 hr, 4 hr, 8 hr, or 15 hr. Samples were centrifuged at 4000 RPM for 10 minutes before removing an aliquot for filtration and analysis. The kinetic constant describing the first-order loss of TFM from the sediment phase (k_{desorb}) was determined using **Equation 8**, where C_t and C_{eq} refer to the *aqueous* concentration at a given time and equilibrium, respectively.

$$\ln\left(1-\frac{C_t}{C_{eq}}\right) = -k_{desorb}t$$

Equation 8

Sorption Isotherms: TFM, RWT, UR

Batch sorption experiments were conducted to establish equilibrium isotherms for TFM and uranine (UR). RWT sorption studies were limited by compound sorption to syringe filters during aliquot removal (**SI Section 14**). Triplicate batch reactors were prepared following the same approach used in sorption kinetics experiments: 50 mL centrifuge tubes contained a ~1:7 sediment-to-buffer ratio (5 g dry, sieved sediment to 34 mL of 20 mM phosphate, pH = 7.2- 7.3). The reactors were equilibrated on a shaker table overnight, initial pH was recorded, then the test compounds were added. TFM reactors were prepared at 0, 5, 10, 15, 20, 25, and 30 μM and UR reactors were prepared at 0, 100, 200, 300, 400, and 500 ppb (0.12 -0.30 μM UR). Reactors were shaken on an incubator-shaker table at 150 RPM in the dark at an average temperature of 28 °C (TFM) and 23 °C (UR). Equilibration time was determined for each compound based on preliminary experiments and literature values; equilibrium aqueous concentrations were determined after 10 hours for TFM and 24 hours for UR. Aliquots were removed post-centrifugation and filtered (0.45 μm, nylon) for HPLC analysis.

A theoretical mass balance (**Equation 9**) was used to determine the concentration of sorbed compound (q_e, in mg analyte/kg dry sediment).

$$q_e = \frac{V}{m}(C_0 - C_{eq})$$

Equation 9

where V is the aqueous phase volume (in L), C_0 is the initial aqueous concentration (in mg/L), and C_{eq} is the equilibrium aqueous concentration (in mg/L). A linear distribution coefficient (K_d) was determined (**Equation 10**) and normalized by sediment organic content (f_{oc}) to obtain K_{oc} (**Equation 11**).

$$q_e = K_d C_{eq}$$

Equation 10

$$K_{oc} = \frac{K_d}{f_{oc}}$$

Equation 11

Laboratory Microcosm Studies

Pretreatment water and sediment from the Fox and Driggs Rivers were used in batch microcosm experiments to quantify TFM biodegradation kinetics. Separate incubation reactors for the Fox River and the Driggs Rivers were conducted in triplicate, at room temperature, in 4 L amber glass jars, and held in the dark. TFM degradation by the water microbial community was studied using 3 L of unfiltered river water and degradation by the sediment microbial community was studied using 2 L of river water (0.2 µm nylon filtered) river water with 500 g of wet sediment. Abiotic controls contained 2 L of 0.2 µm filtered river water. Reactors were spiked with a TFM standard to achieve aqueous concentrations of ~20 µM, which is reflective of typical in-stream concentration during treatment. Aliquots were 0.45 µm syringe filtered for HPLC analysis; there was <4% total volume change by the end of incubation. pH was measured throughout the experiment (pH 6.5 – 7.5). Dissolved oxygen (DO) and temperature in the reactors were measured after 14 days. pH, DO, and temperature results are in **SI Section 11**. Biodegradation kinetics (k_{bio}) and half-lives ($t_{1/2}$) were modeled following pseudo-first order loss (**Equation 6** and **Equation 13,** respectively).

$$t_{1/2} = \frac{\ln(2)}{k_{bio}}$$

Equation 13

Photodegradation Studies

Laboratory Photodegradation Experiments (365 nm Bulbs)

Laboratory photodegradation experiments were conducted with TFM, uranine, and RWT in a Rayonet merry-go-round photoreactor with 14 bulbs that emit light at 365 nm (± 9 nm at half max), which is within the solar spectrum (UV-A region) and largely overlaps with the absorption spectrum of TFM (**Figure 3**). To study direct and indirect photodegradation kinetics, solutions of 20 μM TFM, 1 μM UR, and 0.32 μM RWT were individually buffered to pH 7.5-8 (5 mM phosphate) in either ultrapure water or river water and irradiated in triplicate in borosilicate glass tubes. Dark controls were prepared identically to direct control solutions. The light intensity in the photoreactor was measured by irradiating a chemical actinometer (1 mM pyridine and 10 uM *p*-nitroanisole) alongside the samples.[64]

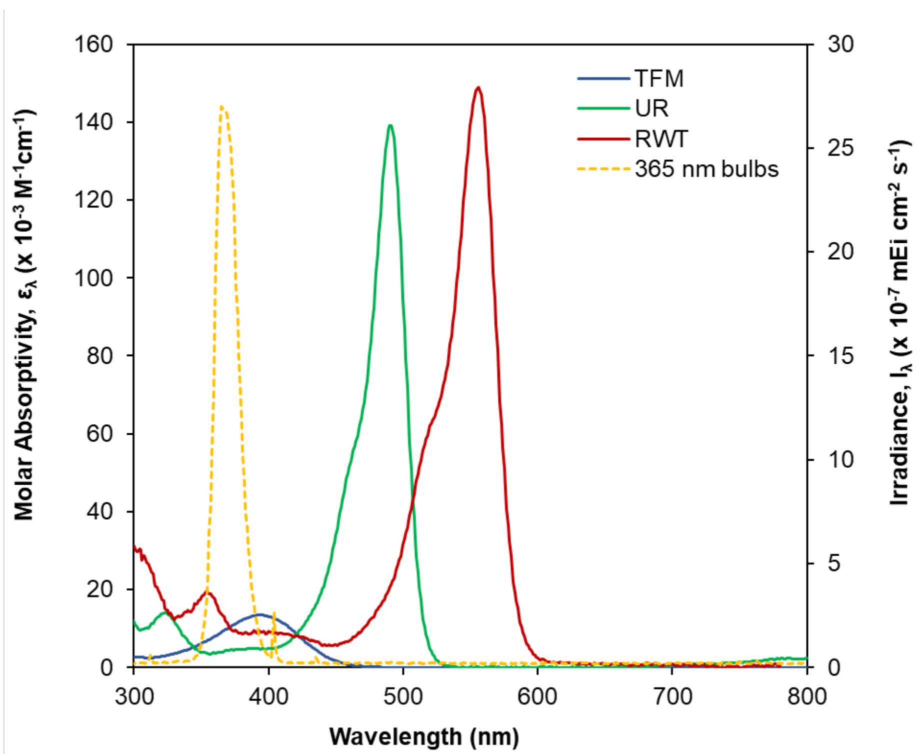

Figure 3. The molar absorptivities of TFM, uranine, and RWT near pH 7.5 as a function of wavelength (*left axis*, solid lines) overlaid with the light intensity of the 365 nm bulb intensity (*right axis*, dashed line) (i.e., the action spectra of each compound in laboratory experiments).

For each compound and condition, the observed photodegradation kinetics (k_{obs}) were modeled as first-order loss following **Equation 6**. The kinetic constants were corrected for light screening using a unitless, wavelength-weighted, average screening factor ($\mathrm{S_{weighted}}$) to determine the correct kinetic constant (k_{screened}, **Equation 14**).

$$k_{\mathrm{screened}} = \frac{k_{\mathrm{obs}}}{\mathrm{S_{weighted}}}$$

Equation 14

The wavelength-weighted, average screening factor ($\mathrm{S_{weighted}}$, **Equation 15**) is a function of light intensity ($\mathrm{I_\lambda}$) in mEi cm^{-2} s^{-1} and the screening factor ($\mathrm{S_\lambda}$, unitless), which are both wavelength-specific values. In laboratory experiments, values were summed over 300-455 nm, and in sunlight kinetic models, values were summed over a larger distribution of 280-800 nm.

$$\mathrm{S_{weighted}} = \sum_{\lambda=300}^{455} \frac{\mathrm{I_\lambda S_\lambda}}{\sum_{300}^{455} \mathrm{I_\lambda}}$$

Equation 15

The wavelength-specific screening factor ($\mathrm{S_\lambda}$, **Equation 16**) accounts for the decadic absorbance (α_λ) in cm^{-1} and pathlength (l) in cm. Pathlength refers to either the UV-visible spectrophotometer cell length in laboratory experiments or the water column depth in sunlight kinetic models.

$$\mathrm{S_\lambda} = \frac{1 - 10^{-\alpha_\lambda \mathrm{l}}}{2.303\ \alpha_\lambda \mathrm{l}}$$

Equation 16

We also calculated a quantum yield (Φ_A), or photochemical reaction efficiency, for each test compound (A) using chemical actinometry (**Equation 17**).[23,65,66] Φ_A can be derived from the photodegradation kinetic constants and integrated rates of light absorption (k_{abs}) of the compound and actinometer (ACT). Photodegradation kinetic constants for the actinometer were not corrected for light screening. Note that rate constants are in (s^{-1}) and quantum yields are unitless.

$$\Phi_{A} = \left(\frac{k_{\text{screened,A}}}{k_{\text{obs,ACT}}}\right)\left(\frac{k_{\text{abs,ACT}}}{k_{\text{abs,A}}}\right)\Phi_{\text{ACT}}$$

Equation 17

The quantum yield of the actinometer (Φ_{act}) is known and has been well studied.[64,67] The integrated rate of light absorption (k_{abs}, **Equation 18**) is a function of wavelength-specific values (I_λ, α_λ, and S_λ) summed over a wavelength distribution, where $[C]_A$ is the concentration of compound A in molar and j is a unit correction factor of one Ei mol^{-1}.

$$k_{abs} = \sum_{\lambda=300}^{455} \frac{2.303\ I_\lambda \alpha_\lambda S_\lambda}{[C]_A j}$$

Equation 18

The light intensity at each wavelength (I_λ) was calculated using a correction factor to shift a reference spectrum (i.e., a spectrum describing the intensity *distribution*, as shown for the 365 nm bulbs in **Figure 3**) to the actual intensity for a given experiment. The correction factor is the ratio of the integrated rate of light absorption of the actinometer based on the reference spectrum (calculated using **Equation 18**) and its true integrated rate of light absorption based on the actual photodegradation rate constant measured during experimentation (**Equation 19**).

$$k_{\text{obs}} = k_{\text{abs}}\Phi \qquad \rightarrow \qquad k_{\text{abs,ACT}} = \frac{k_{\text{obs,ACT}}}{\Phi_{\text{ACT}}}$$

Equation 19

In-situ Photodegradation Experiments (Sunlight)

A batch photochemistry experiment was conducted near the Fox River using natural sunlight as the irradiance source. A bulk water sample was collected mid-treatment of the Fox

River and vacuum-filtered (0.45 μm, nylon) within 24 hours. HPLC analysis later revealed it contained 18.7 μM TFM. A 1.29 μM uranine direct control was also prepared using ultrapure water. Like the laboratory experiments, both solutions were prepared at 5 mM phosphate and buffered to pH 7-8 using dropwise addition of concentrated NaOH. pH was qualitatively determined before and after irradiation using indicator strips. A chemical actinometer solution containing 1 mM pyridine and 10 μM *p*-nitroanisole was also irradiated.

The solutions were split in to four borosilicate glass tubes: three for triplicate sunlight irradiation and one dark control. Solutions were held in a standard test tube rack, positioned in sunlight, and periodically rotated throughout the day. Weather conditions varied from unobstructed sunlight to periodic cloud cover, with little to no precipitation. Aliquots were removed every 3-4 hours and held in the dark on ice before transport to UW-Madison for HPLC analysis. Like the lab experiments, the *in-situ* quantum yields of TFM and uranine were calculated using the measured kinetic constants (light screening corrected) and solution-specific absorbance spectra. However, light intensity from 280-800 nm was modeled by shifting reference solar spectra (wavelength *distributions*) using the actinometer correction factor. The reference solar spectra were generated using the Simple Model of Atmospheric Transfer of Sunshine (SMARTS) following input parameters, or 'cards' (**SI Section 13**).[3,68,69] Because of diurnal variability in light intensity, we generated solar spectra hourly over the treatment day (July 27, 2022) to establish a 24-hour average, or diurnal average, solar spectrum (**Figure 4**). The kinetic constants were corrected for light screening using the actinometer-corrected diurnal average solar spectrum.

a)

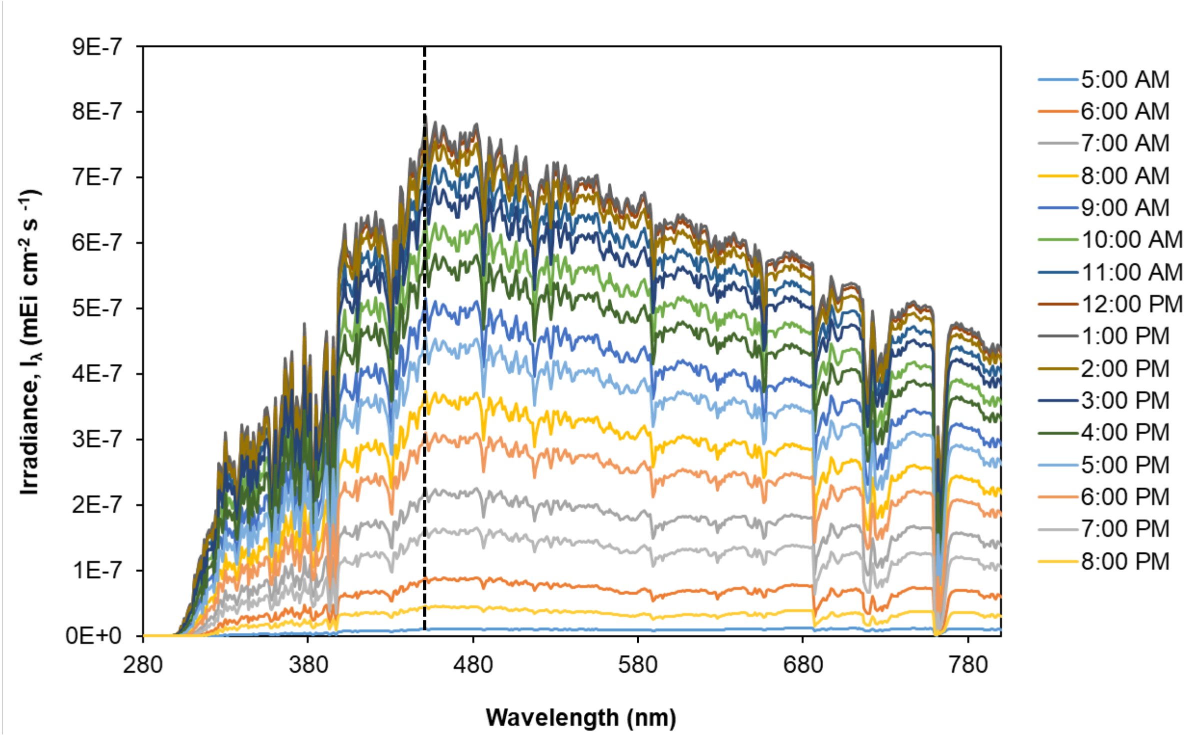

b)

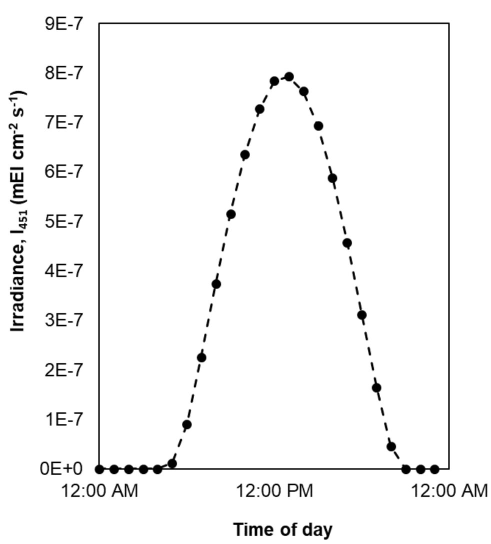

c)

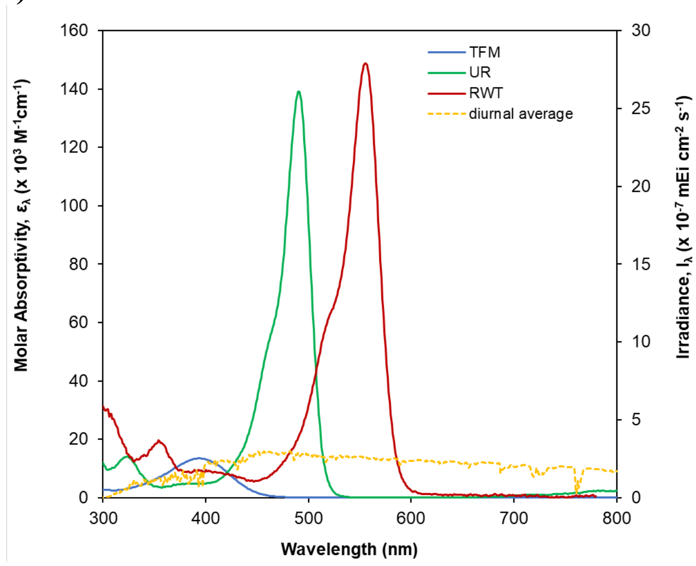

Figure 4. **a)** The reference solar spectra generated hourly for the treatment site using SMARTS (with the peak irradiance wavelength (λ = 451 nm) indicated by the dashed line). **b)** Visualization of the peak solar irradiance over the day. **c)** The molar absorptivities of TFM, uranine, and RWT near pH 7.5 as a function of wavelength (*left axis*) overlaid with the actinometer-corrected, diurnal average solar spectrum (*right axis, plotted to scale with the 365 nm bulb irradiance in Fig. 3*).

Modeling Photodegradation Kinetics In-Stream

The laboratory-determined quantum yields and modeled solar spectra were used to predict in-stream photodegradation rate constants for TFM (20 μM) and uranine (1 μM) at the well-mixed point of the Driggs River. Predictions considered continuous noontime irradiance, diurnal average irradiance, and light attenuation throughout the water column. Kinetic constants were averaged over the water column depth by increasing the pathlength (l) in **Equation 16**. Depth profiles of the Driggs River are in **SI Section 2**.

Analytical Methods

TFM was quantified in field and laboratory samples using an Agilent 1260 Infinity high-performance liquid chromatography (HPLC) system with either diode-array detection (DAD) or multi-wavelength UV-visible detection (MWD). Samples with TFM concentrations <1 μM were analyzed using liquid chromatography-tandem mass spectrometry (LC-MS/MS). PNA was quantified in laboratory and *in-situ* photochemistry samples using HPLC-DAD/MWD. HPLC methods are summarized in **SI Section 7**.

For the analysis of tracer study and *in-situ* photochemistry samples, a method was developed to quantify mixtures of TFM and the fluorescent tracers using absorbance and fluorescence detection (FLD), respectively. Tracer study samples were buffered to pH 7.2 (10 mM phosphate) before analysis. Bromide was quantified in tracer study samples using a ThermoFisher Dionex 4-mm ICS-2100/ICS-1100 ion chromatograph (IC).

The analysis of pretreatment waters included pH, total organic carbon (TOC), inorganic carbon, alkalinity, cations, anions, and UV-visible absorbance. Alkalinity was measured using a Hanna Instruments Potentiometric Titrator (HI 901) with a pH electrode (HI 1131). A GE M5310C

Total Organic Carbon analyzer was used to measure TOC and inorganic carbon. A Shimadzu UV-visible spectrometer (UV-2401PC) was used to obtain spectra from 200 – 800 nm. Cations were quantified using ion chromatography (IC) and anions were quantified using ICP-OES.

RESULTS & DISCUSSION

Fox River TFM Treatment: fDOM Sensor Validation

We validated the use of fDOM sensors to quantify in-stream TFM during the Fox River TFM treatment. As the TFM concentration increased, there was a corresponding decrease in DOM fluorescence at λ_{emit} = 480 ± 40 nm.[57] The fDOM sensors were calibrated *ex-situ* using TFM concentrations measured in discrete water samples. Concentration time series for TFM in the Fox River were generated with this technique to assess its sensitivity, reproducibility, and accuracy.

Signal correction and *ex-situ* calibration were performed as follows. First, TFM was quantified in filtered water samples by HPLC to develop a discretized concentration time series (**Figure 5, a**). fDOM emission was acquired at 2-15 min intervals before, during, and after treatment to create a continuous signal record (**Figure 5, b**). The signal baseline was identified (**Figure 5, c)** and subtracted (**Figure 5, d**) using peak analyzer in OriginPro. The magnitude of signal quenched (ΔfDOM) at a given time (**Figure 5, e**) was related to the corresponding measured TFM concentration to establish a sensor-specific, linear calibration (**Figure 5, f**). Over a range of 0-25 μM TFM, we observed a strongly linear, inverse relationship between in-stream TFM concentration and fDOM emission signal (R^2 = 1 for four different sensors). Response factors between individual sensors ranged from 0.8-2.9 ΔfDOM per unit change in concentration (μM). Calibrations were fixed at the origin because zero ΔfDOM was assigned to the no-TFM condition. Using the calibration equation, ΔfDOM was converted to TFM concentration, resulting in a continuous time series (**Figure 5, g-h**). Additional calibration examples are in **SI Section 9**.

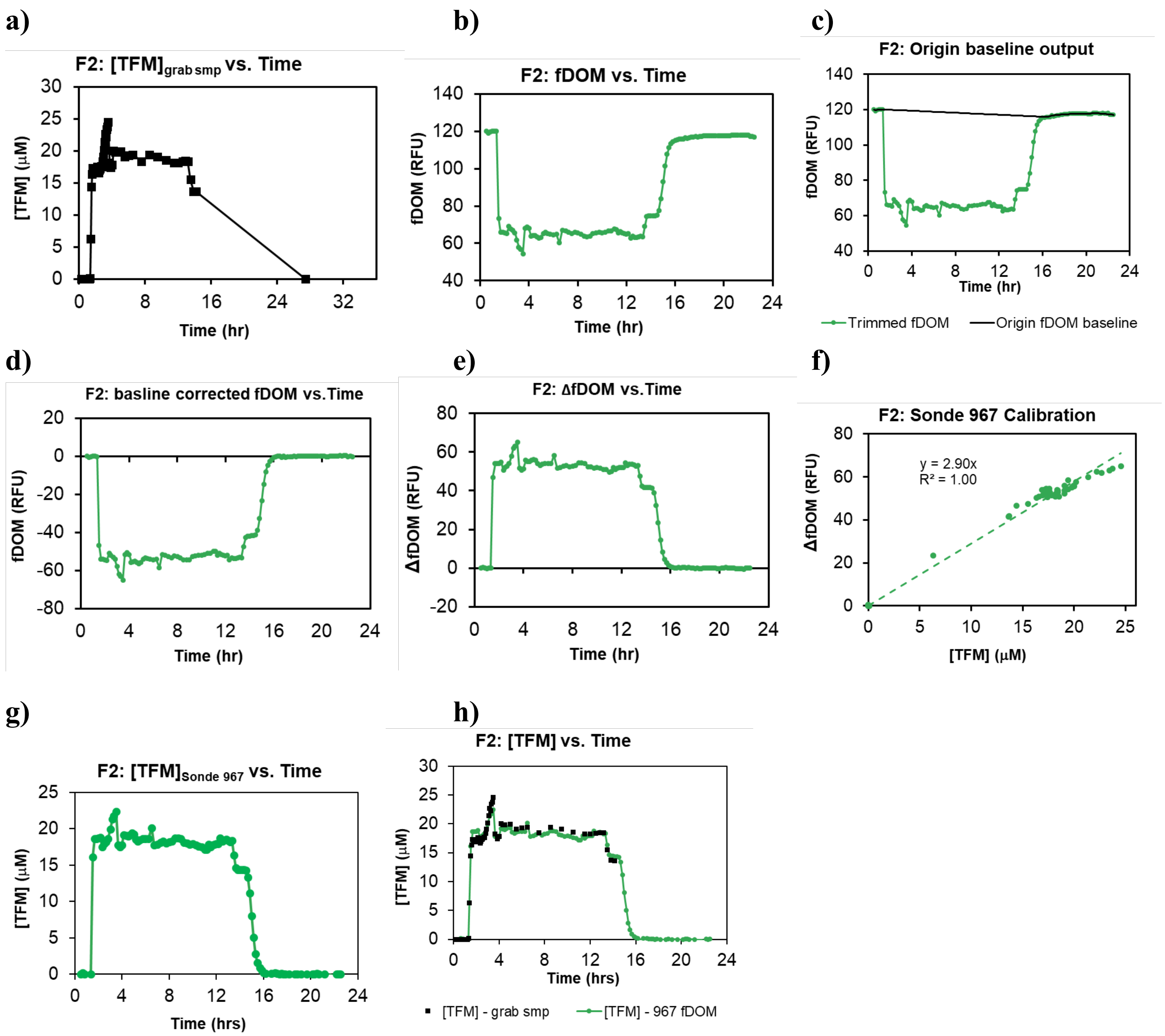

Figure 5. The signal correction and *ex-situ* calibration process: the **a)** discretized TFM concentration time series, **b)** raw fDOM signal, **c)** superimposed baseline identified in Origin, **d)** baseline corrected fDOM signal, **e)** ΔfDOM signal, **f)** linear calibration, **g)** continuous TFM time series (fDOM-attributed), and **h)** overlay of the discretized and continuous time series.

The attenuation of fluorescence signals from pre-treatment levels (ΔfDOM) can be attributed to light screening, a well-documented phenomenon that is caused by competitive absorption of incident light (e.g., in high DOC solutions).[55,70,71] TFM absorbs light in the UV-A region at circumneutral pH (λ_{peak} = 375 nm; **Figure 3**), which strongly overlaps with the fDOM sensor incident light (λ_{excite} = 365 nm).[20] We propose using ΔfDOM monitoring as an effective quantification method for TFM or other compounds with similar optical properties (i.e., compounds that absorb light in the UV-A region and do not fluoresce near 480 nm). This method is applicable for waters with non-zero initial fDOM signals, considering there must be an adequate fDOM signal to attenuate by the light screening compound.

There are benefits of *in-situ* analysis and *ex-situ* sensor calibration. Importantly, the increased signal acquisition frequency offers high temporal resolution compared to water sampling alone. Next, little supervision of the instrument is required once a dynamic calibration is achieved by sampling during concentration gradients. Finally, the *relative* change in fDOM signal (ΔfDOM) encompasses many water chemistry variables. Specifically, signal attenuation is distinct from true fluorescence quenching that is driven by changes in temperature, pH, or increased salinity and aqueous metal concentrations.[72,73] Those parameters are assumed to be relatively constant for specific sites over the treatment timescale (~12-18 hours), allowing us to measure ΔfDOM rather than quantify and correct absolute fDOM measurements for comparison site to site.[56,71]

Continuous concentration time series were developed for TFM in duplicate at the upper Fox River site, illustrating the reproducibility between independent sensors, robustness of *ex-situ* calibration, and accuracy of results (**Figure 6**). Assessing accuracy, the average concentration was 18.3 ± 0.6 μM (RSD = 3.3%, n = 48) over a 9.7-hour period after the initial mixing period of the two lampricide blocks. "n" refers to the number of measurements included in the average calculation over the steady-state period. This average aligns with the target TFM concentration for this reach, 17.9 μM, which was set to maintain the SMLC of 11.6 μM for a reach ~2.7 km downstream.

The discrete time series at the lower site of the Fox River illustrates the complex combination of physical and reactive processes impacting TFM fate over the flow path. The average concentration, 14.5 ± 0.8 μM (RSD = 5.6%, n = 13), was typical of TFM treatments. Qualitatively, there is evidence of advection based on the 6-hour time of passage and evidence of dispersion of the lampricide block based on the tailing of the time series falling limb. However, it is difficult to discern how dispersion, transient hyporheic storage, and sorption-desorption dynamics individually contribute to the tailing of compound arrival time. Attributing compound behavior to specific mechanisms and determining mass lost to degradation reactions would require an extensive water balance to account for each converging lampricide block (**Figure 2, a**) and a tandem study on reactive and conservative tracers.

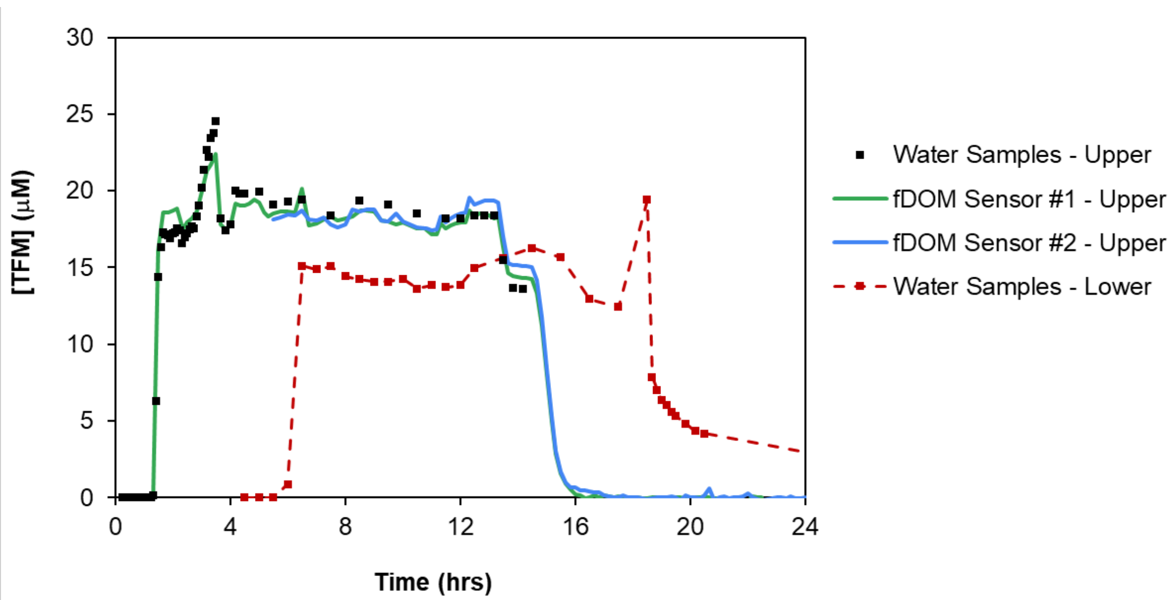

Figure 6. The TFM concentration time series at the upper and lower sites on the Fox River. The continuous series (*fDOM-attributed* TFM concentrations) are shown with solid lines and the discrete sample concentrations are shown with square points (dashed at the lower site for clarity).

Driggs River Tracer Study

At the Driggs River, we conducted a multi-tracer study over the short reach (i.e., 2.6 km; **Figure 2, b**) to characterize the dominant loss mechanisms and assess their role in TFM fate. Concentration time series for bromide, RWT, and uranine were determined at the well-mixed point and short reach (**Figure 7**). Following **Equation 3** and **Equation 4**, discharge was determined at each site (0.68 and 0.77 m^3/s, respectively) to calculate the mass recovered in the water column. Like the fDOM sensors, the submersible uranine and RWT fluorometers were individually calibrated *ex-situ* using analyte concentrations measured in water samples collected during the tracer study.

The pulse injection of the three tracers was visibly consistent at the well-mixed point, but concentration time series and mass recoveries at the short reach varied between tracers. Because the well-mixed point was positioned immediately downstream of the application point, the concentration time series indicates a time of passage on the order of minutes. At the short reach, the bromide time series (**Figure 7, a**) illustrates advection (~3-hour time of passage) and dispersion of the chemical pulse. Following **Equation 2** and **Equation 5**, we calculated a $(112 \pm 8)\%$ bromide mass recovery, suggesting hyporheic exchange was transient and occurred over the study timeframe. Additional uncertainty in recovery could also be introduced by using a single discharge value.

RWT and uranine were subject to the same physical processes over the flow path, but negligible RWT was recovered and only $(10 \pm 34)\%$ of uranine mass was recovered at the short reach (**Figure 7, b-c**). The recovery differences between the conservative and reactive tracers suggest sorption and/or photodegradation can contribute to compound fate over the flow path being treated with TFM. No tracers were detected at the distant site (D3) above our LoDs due to the mass of tracers used.

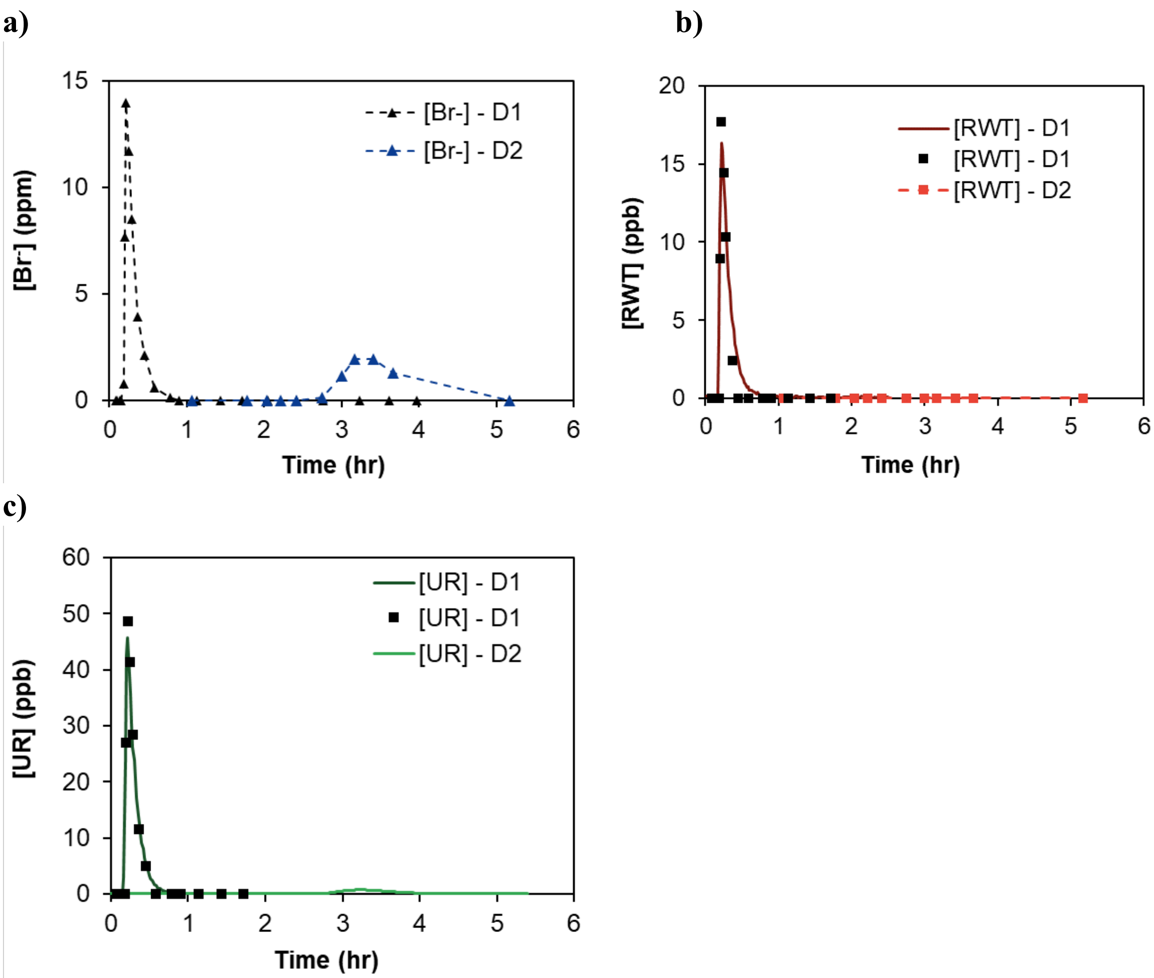

Figure 7. Concentration time series for **a)** bromide, **b)** RWT, and **c)** uranine at the well-mixed point (D1) and short reach (D2) sites at the Driggs River. The continuous series are shown with solid lines and discrete samples are shown with square points.

Driggs River TFM Treatment

Like the tracer study, major mechanisms impacting compound fate were assessed for TFM by developing a concentration time series (**Figure 8**) and calculating the mass recovered at each site. The well-mixed point concentration time series (site D1) resembled a stepwise breakthrough curve with little to no dispersion or broadening. The target TFM concentration was 11.6 μM (SMLC = 5.3 μM) and we observed an average TFM concentration of 12.1 ± 0.7 μM (RSD = 5.7%, n = 301) being maintained for 10.7 hours, excluding the sharp rising and falling limbs. As with the Fox River, the target concentration near the application point was 2-3 times higher than the SMLC to maintain downstream concentrations by accounting for the gradual dilution caused by the net gain of water volume over the flow path. The steady-state concentration and low RSD are resultant of a) the continuous rate of mass injected relative to changes in discharge and b) the lack of opportunity for TFM to undergo physical processes, reactive processes, or phase transitions between the application site and the well-mixed point (i.e., 0.2 km).

At the short reach (site D2), the 4-hour time of passage over a 2.8 km flow path from the application point allowed for environmental loss mechanisms to potentially occur. USFWS did not establish a target TFM concentration for this reach, but we calculated an average of 10.8 ± 1.3 μM (RSD = 12.3%, n = 173) over a ~10-hour window, which is 10% lower than the average concentration at the well-mixed point. Including the rising and falling limbs where concentrations were below the SMLC, the total exposure time was extended to over 15 hours due to curve broadening and tailing. At the short reach, in-stream TFM concentrations slowly increased over time and did not reach steady-state; concentrations at the end of the treatment window (12-16 hours from injection start) were closer to well-mixed point concentrations (~12 μM), indicating hyporheic pore saturation was likely occurring.

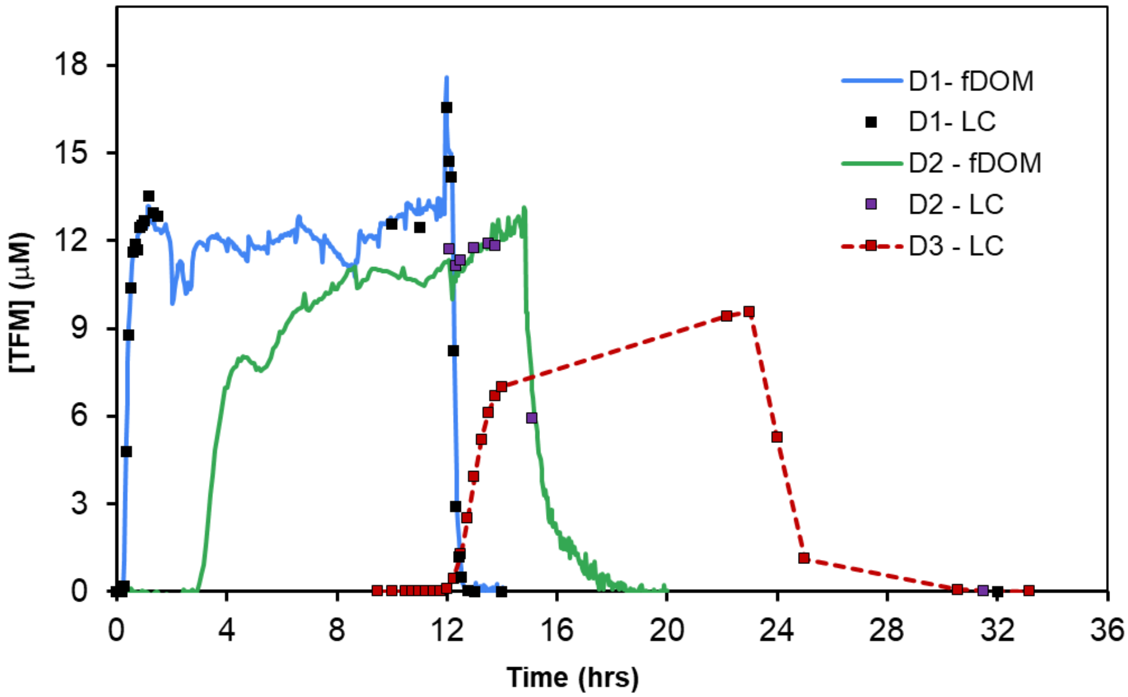

Figure 8. The concentration time series for TFM at the well-mixed point (D1), short reach (D2), and distant site (D3) at the Driggs River. The continuous series (*fDOM-attributed* TFM concentrations) are shown with solid lines and the discrete sample concentrations are shown with square points.

Because of the longer flow path (11.2 km) and time of passage (12 hours) to the distant site (site D3), in-stream transport dynamics and gradual pore saturation were observed to a greater extent. The target TFM concentration was 8.7 μM (SMLC = 7.2 μM) and we calculated an average of 8.7 ± 1.2 μM (RSD = 13.6%, n = 3) over a 9-hour window, excluding the broader rising and falling limbs. This correlates to a 28% drop in average concentration from the well-mixed point. While our observation of non-steady concentrations and declining average concentration at downstream sites suggests physical processes control time series shape, reactive processes that are not destructive (sorption and desorption) may also play a role.

The importance of degradation reactions was determined using a mass balance analysis, which was performed using USFWS river discharge values determined from stage-charge relationships (**Figure 9**). Discharge at our short reach site was interpolated. Relative to the well-mixed point, flow increased by 12% at the short reach and 53% at the distant site, demonstrating that the river is net gaining.

a) **b)**

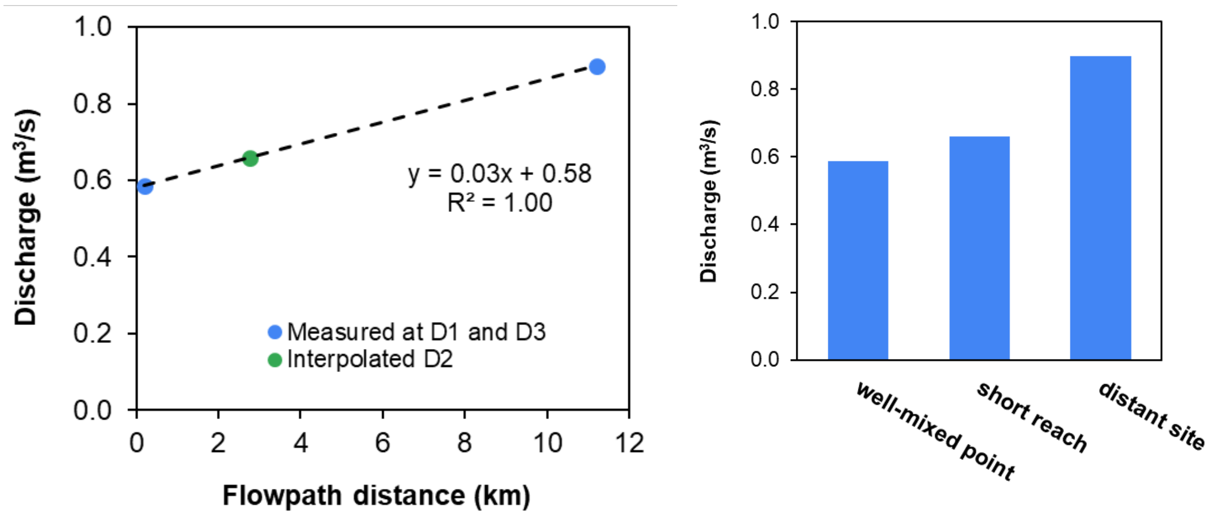

Figure 9. Driggs River discharge for July 26th, 2022, **a)** as a function of flow path distance from application and **b)** by site.

Unlike the assessments of average concentration, the rising and falling limbs of the time series must be included to determine TFM mass with enough accuracy for site-to-site comparisons. This is especially true for downstream sites with greater tailing time of compound arrival. Although the *average steady-state concentration* dropped by 10% and 28% over the two flow paths, there were 18% and 51% losses in the total *time-integrated concentration* at the short reach and distant site, respectively. However, when accounting for comparable increases in river discharge, no TFM mass was lost within the uncertainty of our analysis (**Figure 10**). Masses of (64 ± 1) kg (well-mixed point; D1), (61 ± 2) kg (short reach; D2), and (64 ± 2) kg (distant site; D3) correspond to a (95 ± 4)% and (101 ± 4)% recoveries over the two flow paths, suggesting concentration decreases were driven by dilution and degradation reactions had a negligible impact on TFM fate in the Driggs River over the treatment timescale.

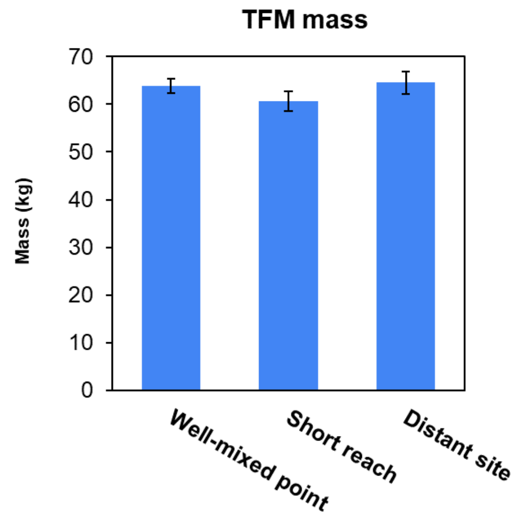

Figure 10. The mass of TFM recovered in-stream at each Driggs River site.

A crude magnitude check was performed to assess mass accuracy. A five-gallon container of 33% active ingredient (ρ = 1.27 g/mL) contains ~8 kg of TFM.[19] The masses we calculated equate to a lampricide volume of ~8 containers applied upstream of the well-mixed point, which aligns with treatment practices for a tributary of this volume.

Laboratory Sorption

To address how interactions between riverbed sediment and TFM may retard its time of arrival in-stream (i.e., cause tailing in the time series), we studied the sorption-desorption kinetics and equilibrium sorption distribution of TFM in laboratory batch experiments using sediment from the Driggs River. In kinetic experiments, sorption equilibrium was achieved within ~4 hours (**Figure 11, a**). Note the initial concentration of 12 μM TFM was chosen to reflect the steady-state concentration at the Driggs River well-mixed point. In a quantitative assessment of the first 30 minutes (**Figure 11, b**), the first-order kinetic constant describing the rate of sorption (k_{sorb}) was calculated to be (0.23 ± 0.07) hr^{-1}, corresponding to a characteristic time (τ) of 4.3 hours (**Equation 6** and **Equation 7**, respectively).

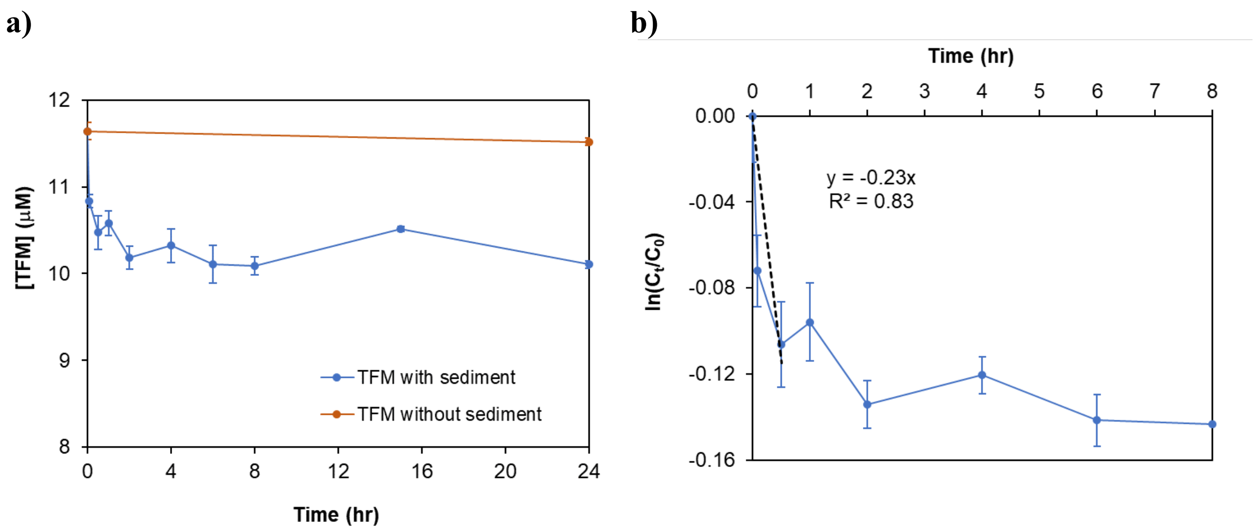

Figure 11. a) The aqueous concentration of TFM in (sacrificial) sorption kinetics reactors over 24 hours and **b)** the first-order kinetics of loss over the first 8 hours (linear, normalized).

There has been little attention given to the sorption kinetics of TFM, but our observation of equilibrium being achieved within a day aligns with previous studies using 4-24 hour equilibration periods in batch laboratory studies.[33,34] The relatively fast TFM sorption kinetics aligns with theory in that sorption kinetic constants are inversely related to equilibrium distribution constants (i.e., weakly sorbed compounds sorb quickly and highly sorbed compounds sorb slowly).[74]

After 8 hours in the kinetic experiment, the equilibrium distribution coefficient (K_d) for TFM was calculated to be (1.1 ± 0.1) L/kg (following the mass balance and linear sorption model respectively described by **Equation 9** and **Equation 10**). Higher organic content and finer texture of riverbed sediment increase the degree of TFM sorption,[33] thus an *organic-carbon normalized* equilibrium distribution coefficient (K_{oc}) is used to make objective comparisons across different sediment types. When factoring the 0.96% fraction of organic content (f_{oc}) in Driggs River sediment, the K_{oc} value was calculated to be (116 ± 13) L/kg (**Equation 11**). We also conducted batch equilibrium experiments to establish a sorption isotherm over a range of initial aqueous concentrations (0-30 μM or ~1-6 mg/L). we calculated K_d to be (0.95 ± 0.07) L/kg, resulting in a K_{oc} of 99 ± 14 L/kg (**Figure 12, a**). When the intercept was calculated normally (slightly deviating from theory), K_d was calculated to be (0.64 ± 0.05) L/kg, resulting in a K_{oc} of 67 ± 9 L/kg (**Figure 12, b**). Both interpretations of the data produce a good fit ($R^2 > 0.95$) and result in comparable K_{oc} values that align with our observation in the sorption kinetics experiment and previously reported laboratory values of 35 – 290 L/kg near pH 7.[33,34]

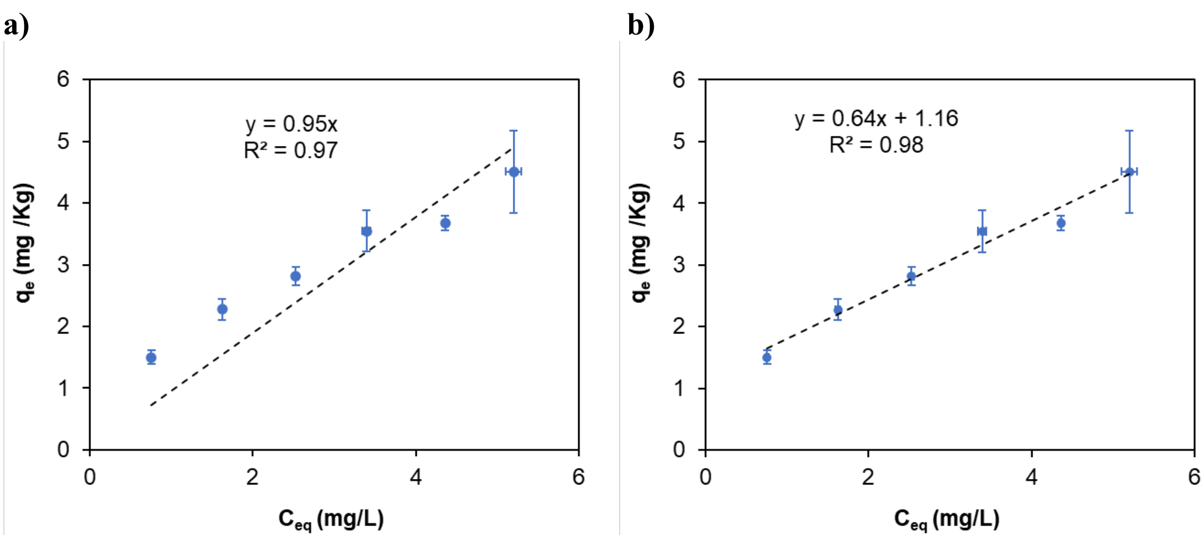

Figure 12. The sorption isotherm for TFM at pH 7.2 with Driggs River sediment (f_{oc} = 0.96 ± 0.11%) after 12 hours of equilibration, shown with a line of best fit **a)** fixed and **b)** not fixed at the origin.

Relating K_{oc} to sorption behavior in natural sediment-water systems (i.e., the hyporheic zone), TFM has *high environmental mobility* according to both McCall's soil mobility classification scheme ($50 < K_{oc} < 150$ L/kg) and the soil mobility classification criteria established by the Food and Agricultural Association (mobile = $10 < K_{oc} < 100$ L/kg, moderately mobile =

100 < K_{oc} < 1,000 L/kg).[75–77] In additional to riverbed organic content, river pH will dictate TFM's protonation state and its partitioning behavior. In most rivers, the majority of TFM is in its anionic, deprotonated state (TFM pK_a = 6.38, Driggs River pH = 7.9).[20,78] In this form, TFM has high solubility (5,000 mg/L at 25 °C) and weakly sorbs to sediment.[79] K_{oc} values broadly classify compound mobility in the environment, but in river systems specifically, K_{oc} influences the retardation factor (R) that describes tailing arrival times. From the fast sorption kinetics and weak sorption to sediment we observed in the laboratory, the majority of TFM is expected to remain in the water column where retardation is governed by a combination of physical processes like in-stream dispersion and transient hyporheic fluxes.

Some organic compounds sorb to sediment irreversibly or only desorb over long periods (i.e., weeks to months).[74] There is some evidence that TFM sorption is irreversible,[13,31,80–82] while other studies report readily reversible sorption.[29,33] We conducted batch experiments using TFM-laden sediment from the Driggs River and buffered, ultrapure water to determine a desorption kinetic constant (k_{desorb}) of (0.19 ± 0.06) hr^{-1}, which corresponds to a characteristic time (τ) of 5.4 hours (**Figure 13**, **Equation 8**). At equilibrium (t = 15.3 hours), K_d and K_{oc} were respectively calculated to be 6.8 and 707 L/kg using a mass balance approach. These values are higher than expected, indicating sorption may not be fully reversible. Although TFM is not very sorptive and can readily desorb, the fraction that remains sorbed may be initially non-labile, contribute to low-level legacy concentrations in-stream, and biotransform in the hyporheic zone.[74,83]

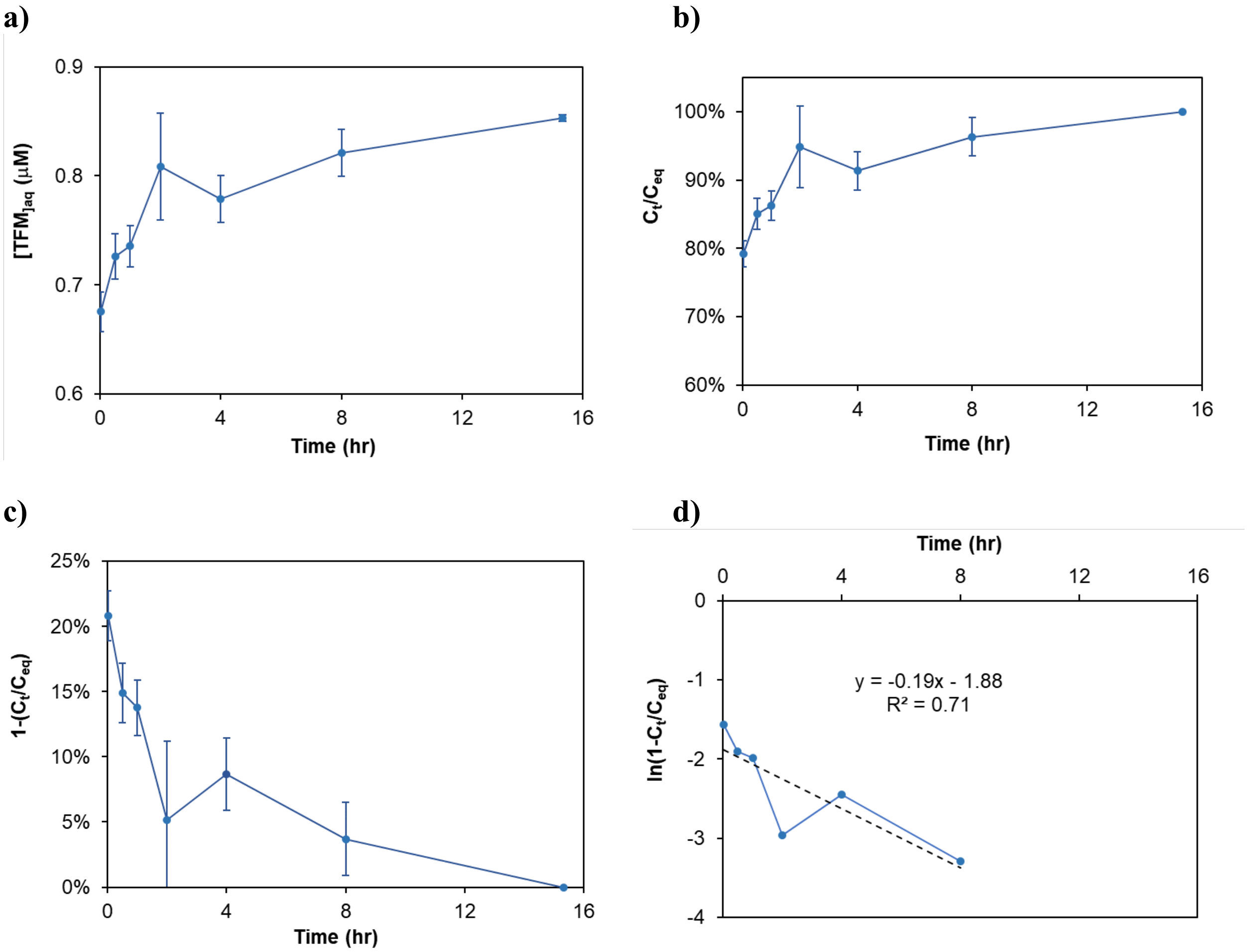

Figure 13. The kinetics of TFM desorption from sediment shown as **a)** increasing aqueous concentration and **b)** increasing aqueous concentration normalized by the maximum, equilibrium concentration at t = 15.3 hours. **c)** Loss from the sediment phase followed first-order kinetics and **d)** the desorption kinetic constant was modeled following **Equation 8**.

Laboratory Microcosms

The fraction of TFM that sorbs to hyporheic sediment or remains in hyporheic porewater is susceptible to biotransformation processes, including reversible reduction to RTFM (non-destructive) or biodegradation to yield lower molecular weight compounds (destructive).[12,13] Using sediment and water from the Fox and Driggs Rivers, we quantified TFM biodegradation kinetics in laboratory batch microcosm experiments (**Figure 14, a-b**).

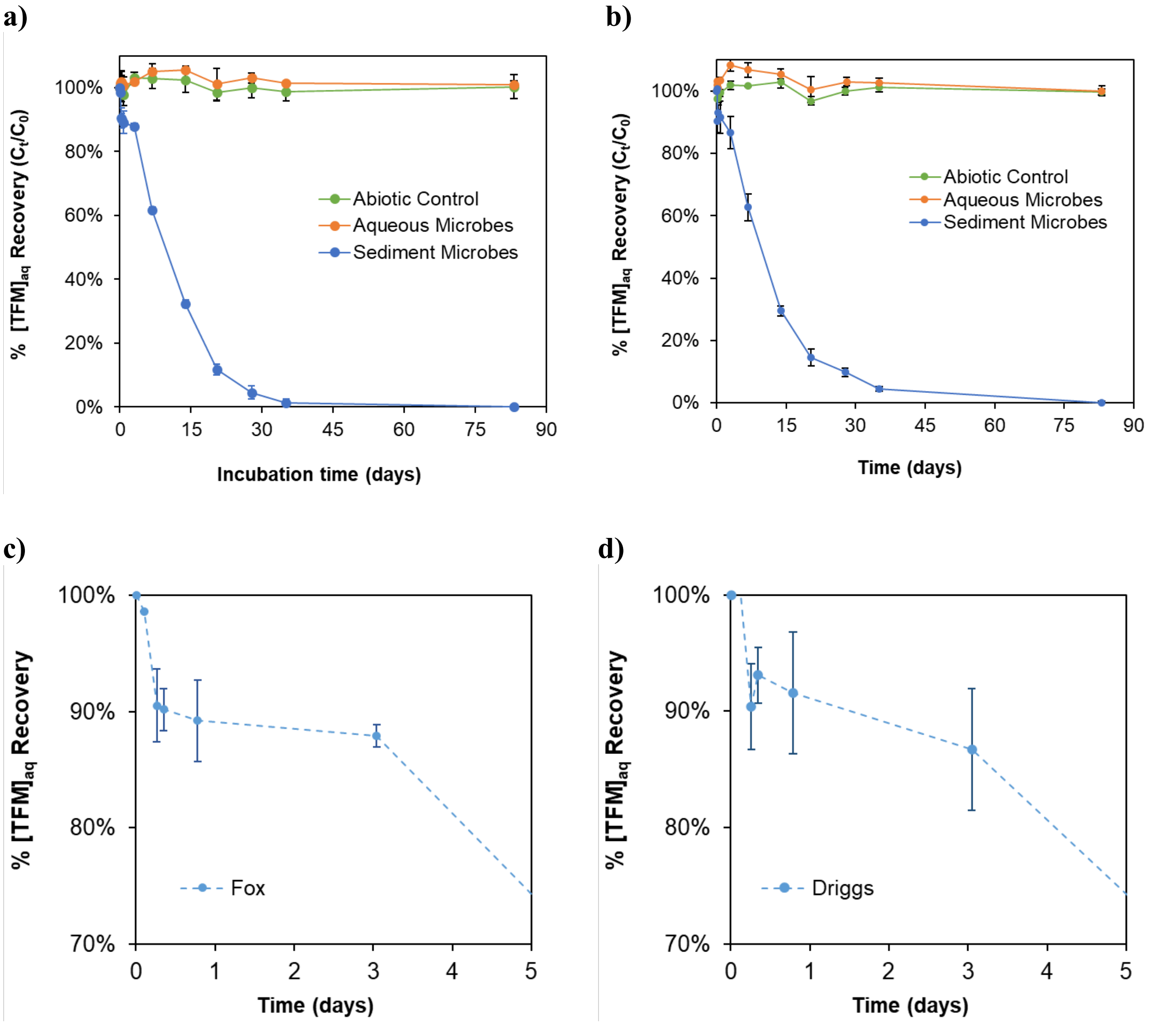

Figure 14. The percent recovery of aqueous TFM in batch microcosm experiments using water and sediment from the **a)** Fox and **b)** Driggs Rivers. The initial sorption kinetics are better visualized for the **c)** Fox and **d)** Driggs Rivers.

In abiotic control and water-only microcosms ("aqueous microbes" in the figure), TFM concentration remained constant. In the sediment-water microcosms, TFM loss followed pseudo-first-order with half-lives (**Equation 13**) of 6.0 ± 0.2 days (Fox) and 7.9 ± 0.1 days (Driggs). TFM was not detected after 35 days. There is no previous evidence of TFM biodegradation in the water column or sediment-free systems,[79,84] but biodegradation in sediment-water systems has been reported with half-lives of 2.1 days (anaerobic)[85] and 5.4 days (aerobic)[86]. After 14 days, DO was

~8 mg/L in the abiotic control and water-only microcosms, but only ~4 mg/L in sediment-water microcosms (**Figure 32**, **SI Section 11**). This indicates oxygen-consuming, aerobic microbial processes were occurring in the sediment-water microcosms.

Sorption equilibrium in sediment-water microcosms was achieved in the first ~10 hours of incubation (**Figure 14, c-d**), which aligns with the equilibrium time observed in our TFM sorption kinetics experiments (**Figure 11**). As expected, TFM was slightly sorptive. For both Fox and Driggs sediment-water microcosms, a ~15% drop in concentration correlates to a K_{oc} of 32 L/kg, which is within a factor of three of the K_{oc} values we determined in isotherm studies (**Figure 12**).

It is evident that sediment microbial communities native to the treatment sites can degrade TFM within days to weeks. Similar organic carbon content between the Fox and Driggs River sediment (respective f_{oc} values = 1.34 ± 0.06% and 1.19 ± 0.09%, remeasured for microcosms), resulted in the same degree of TFM sorption between microcosms. In addition, microbial abundance and composition are linked to organic content, explaining the similarity in TFM biodegradation kinetics.

***In-situ* Sediment Column Studies**

Batch sorption experiments provide valuable information on compound mobility, but do not capture the complexity of the environment. To assess how sorption behavior in laboratory experiments translates to TFM fate in treated rivers, we operated a stream-side sediment column to simulate a vertical, 'homogenous' hyporheic flow path. River water was pumped directly into the column influent during both the Driggs River tracer study and the TFM application.

During the tracer study, we observed the elution of each tracer in column breakthrough curves (**Figure 15**) and used the average column flow rate (0.19 L/hr) to calculate mass recoveries.

The pulse injection visible in the influent time series is the same well-mixed point (site D1) concentration profile from the Driggs River tracer study. Assessing bromide breakthrough, lower effluent concentrations and curve broadening closely resembles the time series at the short reach (**Figure 6, a**), illustrating the importance of physical transport processes. From integration of the breakthrough curve, we observed complete conservation of bromide over the column flow path with a (99 ± 45)% mass recovery. There was complete loss of RWT and a (5 ± 11)% uranine mass recovery. The elution behavior of all three tracers corroborates the concentration time series at the short reach, indicating a complex combination of sorption and physical transport influence compound fate overall.

There is value in translating laboratory constants to field conditions using flow-through, *in-situ* studies, but environmentally relevant column studies are challenging and have their limitations.[87–89] In our study, microbial degradation of the fluorescent tracers could occur, but is assumed negligible over the <4-hour elution time. Another consideration is the low in-stream concentration of fluorescent tracers (i.e., there was complete loss in some scenarios). Lastly, the significant loss of uranine in the column study was unexpected. Rapid photodegradation of uranine in the effluent container cannot be disregarded, but uranine retention to column sediment is unlikely based on negligible sorption observed in batch laboratory experiments (**SI Section 10**).

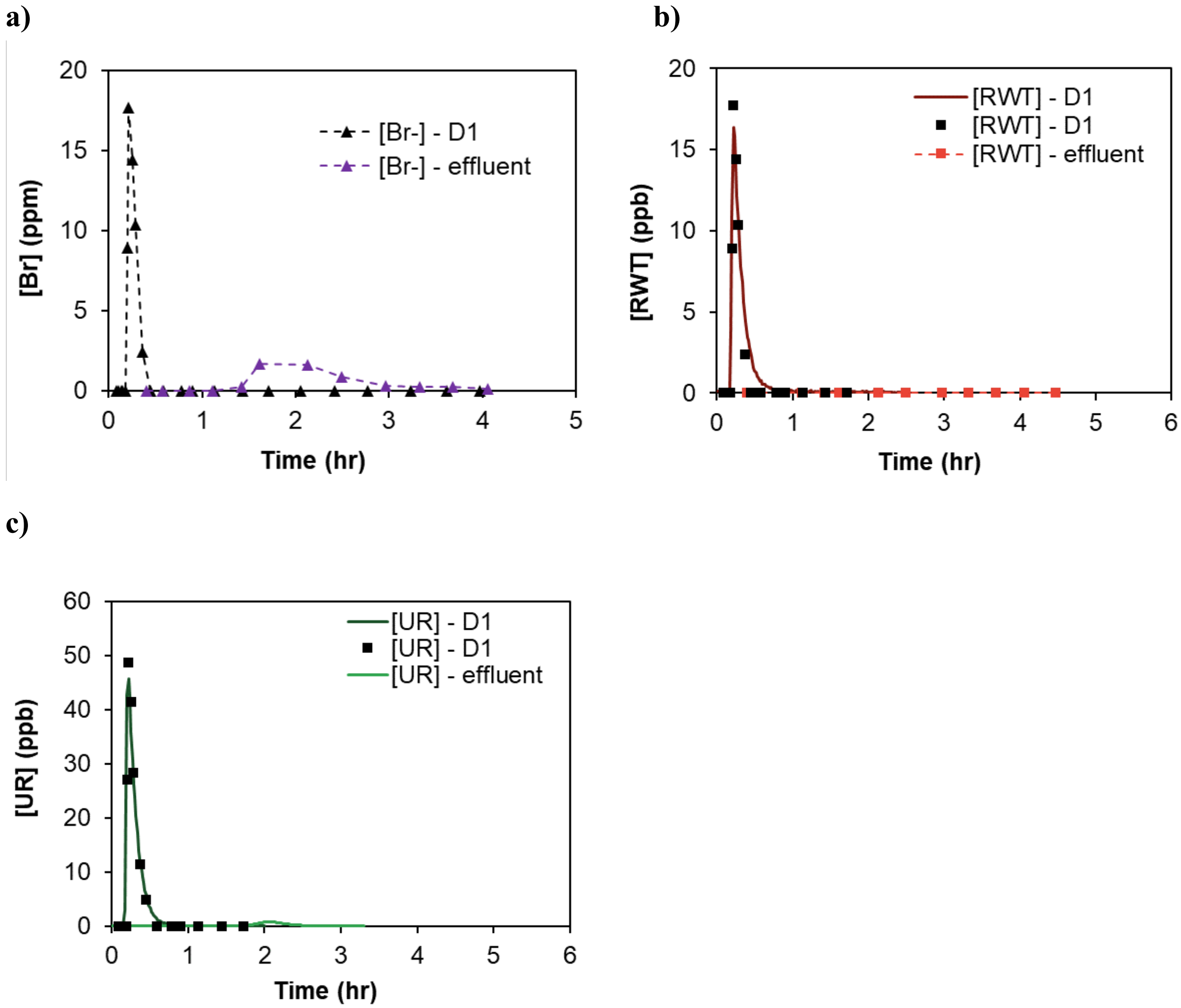

Figure 15. Time series of **a)** bromide, **b)** RWT, and **c)** uranine in the column influent (in-stream, at the well-mixed point) and effluent.

The TFM column study served to evaluate TFM-sediment interactions under steady-state conditions. During treatment, the continuous rate of lampricide injection over a longer period, as well as the constant column flow rate, allowed the influent (i.e., well-mixed point; site D1) and effluent concentrations to respectively reach steady-state (**Figure 16**). The average effluent concentration was 8.3 ± 0.1 μM, which corresponded to a 31% decrease from the well-mixed point concentration (12.1 ± 0.7 μM). The average flow rate into the column was inadvertently higher during TFM treatment (0.32 L/hr), resulting in a shorter residence time (θ = 1.5 hours) for the same water volume (0.5 L). Based on the microcosm results, biodegradation kinetics are negligible relative to the column residence time, deeming the column experiment primarily a flow-through study on compound sorption. We determined a rate of loss over the column flow path to be -2.5 μM/hr, which corresponds to a pseudo-first-order kinetic constant (k_{column}) of 0.2 hr^{-1} and characteristic time (τ) of 5 hours (**Equation 1**). Despite the limitations and challenges associated with column studies, especially when conducted *in-situ*, the kinetics are comparable to those observed in laboratory batch experiments (k_{sorb} = 0.08 hr^{-1}, τ = 12.5 hours).

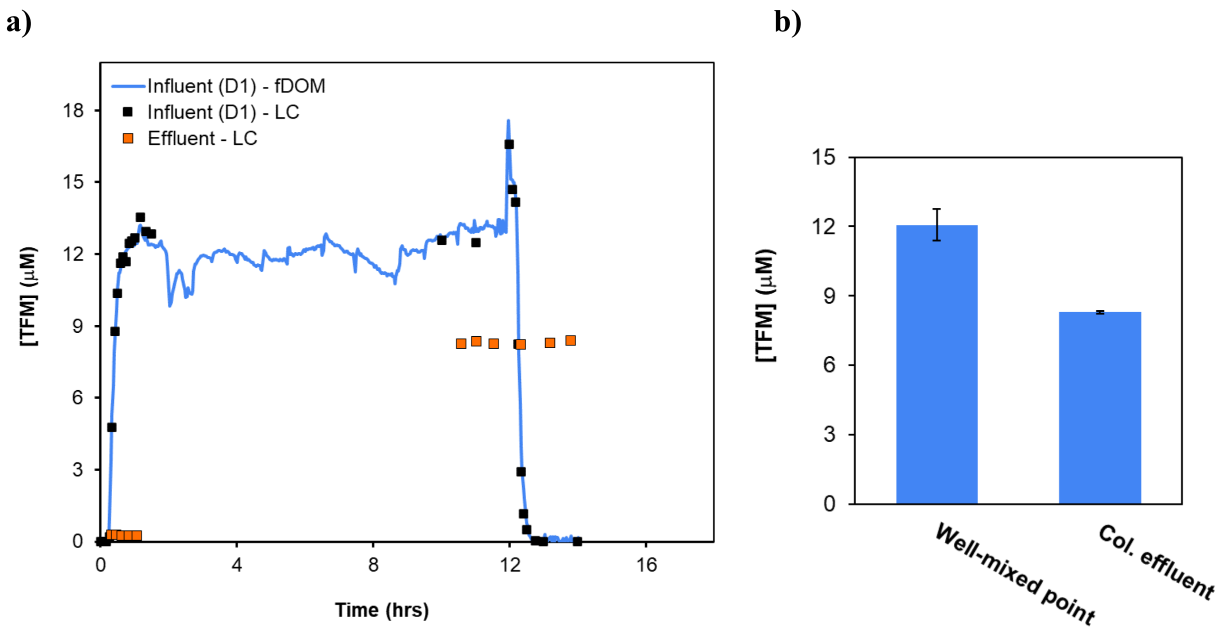

Figure 16. **a)** The TFM time series for the column influent (well-mixed point) and effluent, **b)** the average steady-state concentrations.

Laboratory Photodegradation Study

Photodegradation is a known mechanism of TFM loss based on laboratory experiments,[15,20,28,90] but the conservative behavior of TFM we observed during treatment led us to investigate photodegradation kinetics and reaction efficiencies (quantum yields) under a variety of photochemical conditions. In laboratory photochemistry experiments, TFM and uranine were irradiated using 365 ± 9 nm (UV-A) light. RWT, our photostable tracer, was studied for completeness (**SI Section 12**).

TFM photodegradation (20 μM) followed first-order kinetics in ultrapure water with a direct photodegradation rate constant (k_{screened}) of $(1.16 \pm 0.02) \times 10^{-4}$ s^{-1} ($t_{1/2}$ = 1.9 hr; **Figure 17, a, Equation 14, Equation 15**, and **Equation 16**). This corresponds to a quantum yield (Φ) of $(8.6 \pm 0.2) \times 10^{-5}$ (**Equation 17**) which aligns with previously reported values (8.0×10^{-5} to 1.4×10^{-3}) near pH 7.5-8 using ~365 nm light.[20,28,91] TFM is not susceptible to indirect photodegradation,[90] which was confirmed by irradiating TFM in water from the Fox and Driggs Rivers (i.e., the observed photodegradation rate did not increase in the presence of DOM (**Figure 17, b**). Rather, DOM from this system could have contributed to minor rate inhibition.[92,93]

Uranine (1 μM) also degraded following first-order kinetics with a direct photodegradation rate constant (k_{screened}) of $(4.1 \pm 0.2) \times 10^{-5}$ s^{-1} ($t_{1/2}$ = 4.7 hr; **Figure 18, a**). We calculated a quantum yield of $(9.7 \pm 0.6) \times 10^{-5}$, which is similar to values reported under visible light, $(1.5\text{-}6.5) \times 10^{-5}$.[94,95] Insignificant differences between the control solution and natural waters indicate indirect photodegradation also did not occur for uranine (**Figure 18, b**). For both TFM and uranine, direct photodegradation rate constants were considered in comparisons between measured laboratory kinetics, measured *in-situ* studies, and modeled in-stream kinetics.

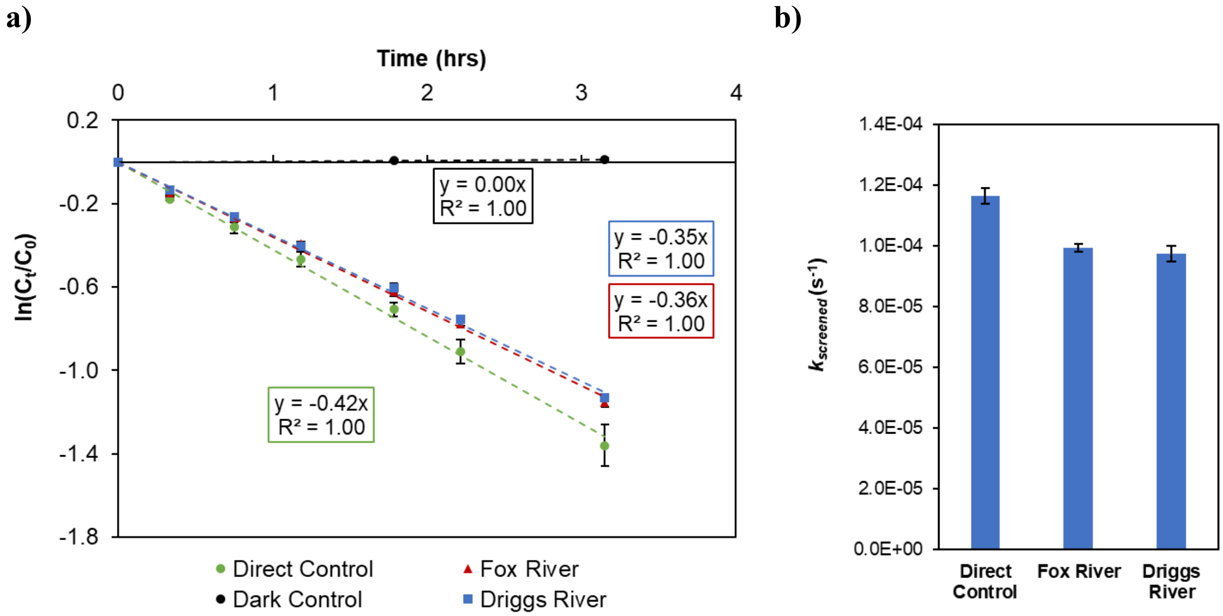

Figure 17. Laboratory photodegradation kinetics of 20 µM TFM under 365 nm light (pH 7.9, light screening corrected) shown as **a)** linear, normalized concentration loss and **b)** the resultant first-order kinetic constants for each matrix.

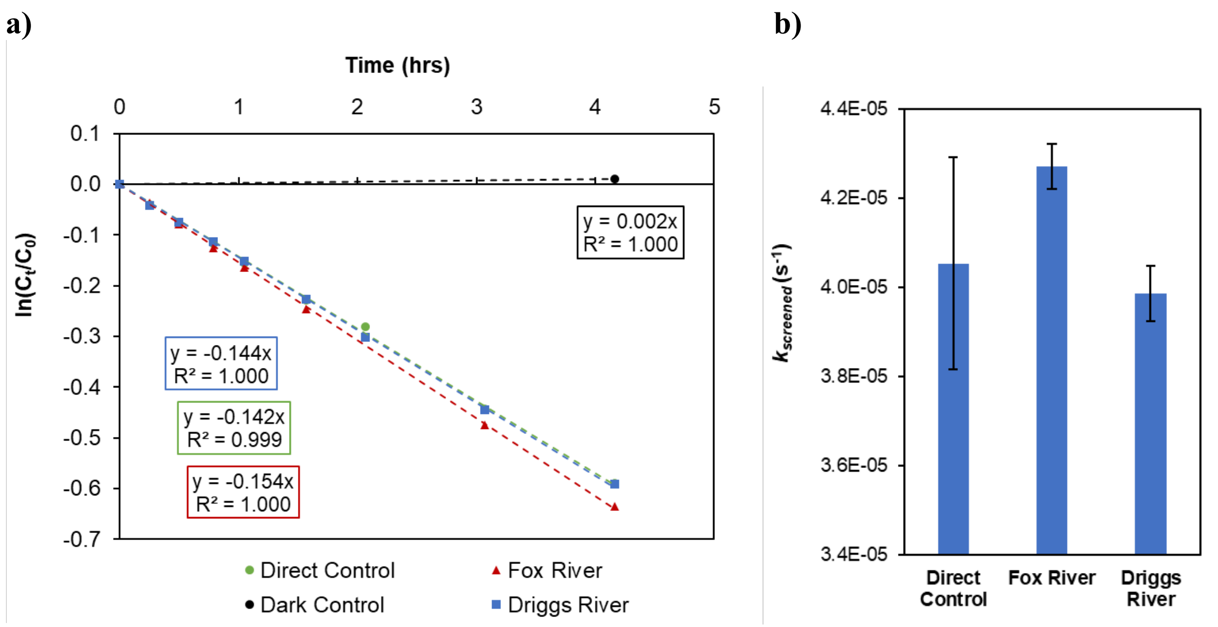

Figure 18. Laboratory photodegradation kinetics of 1 µM UR under 365 nm light (pH 7.8, light screening corrected) shown as **a)** linear, normalized concentration loss and **b)** the resultant first-order kinetic constants for each matrix.

***In-situ* Photodegradation Study**

The laboratory irradiations suggest TFM is more photolabile than uranine, which differs from our observations during treatment (i.e., TFM was conserved and uranine degraded significantly). Therefore, we investigated how the two different light sources (365 nm light vs. sunlight) impact photodegradation kinetics by performing outdoor sunlight irradiations near the treatment site.

While TFM (18.7 μM) and uranine (1.29 μM) both photodegraded in the *in-situ* experiment, kinetics *decreased* for TFM and *increased* for uranine relative to laboratory kinetics (**Figures 19** and **22, a**). For TFM, the photodegradation rate constant ($k_{screened}$) was determined to be 5.1×10^{-6} s^{-1} ($t_{1/2}$ = 38 hr), which is slow compared to uranine *in-situ* kinetics ($k_{screened} = 2.3 \times 10^{-4}$ s^{-1}; $t_{1/2}$ = 0.8 hr). For reference, sunlight experiments previously conducted with 22.5 μM TFM revealed a half-life of $t_{1/2}$ = 72 hours.[28]

The difference between laboratory and *in-situ* half-lives is magnitudes larger for TFM (2 hours vs. 38 hours) than for uranine (5 hours vs. 1 hour). Photodegradation kinetics are concentration-dependent and direct comparison is possible because experiments were conducted at environmentally relevant concentrations reflective of field conditions. Variable light intensity throughout the day caused by dynamic weather conditions and intermittent cloud cover resulted in a deviation of measured photodegradation kinetics from first-order loss, illustrated by lower R^2 values compared to laboratory kinetics.

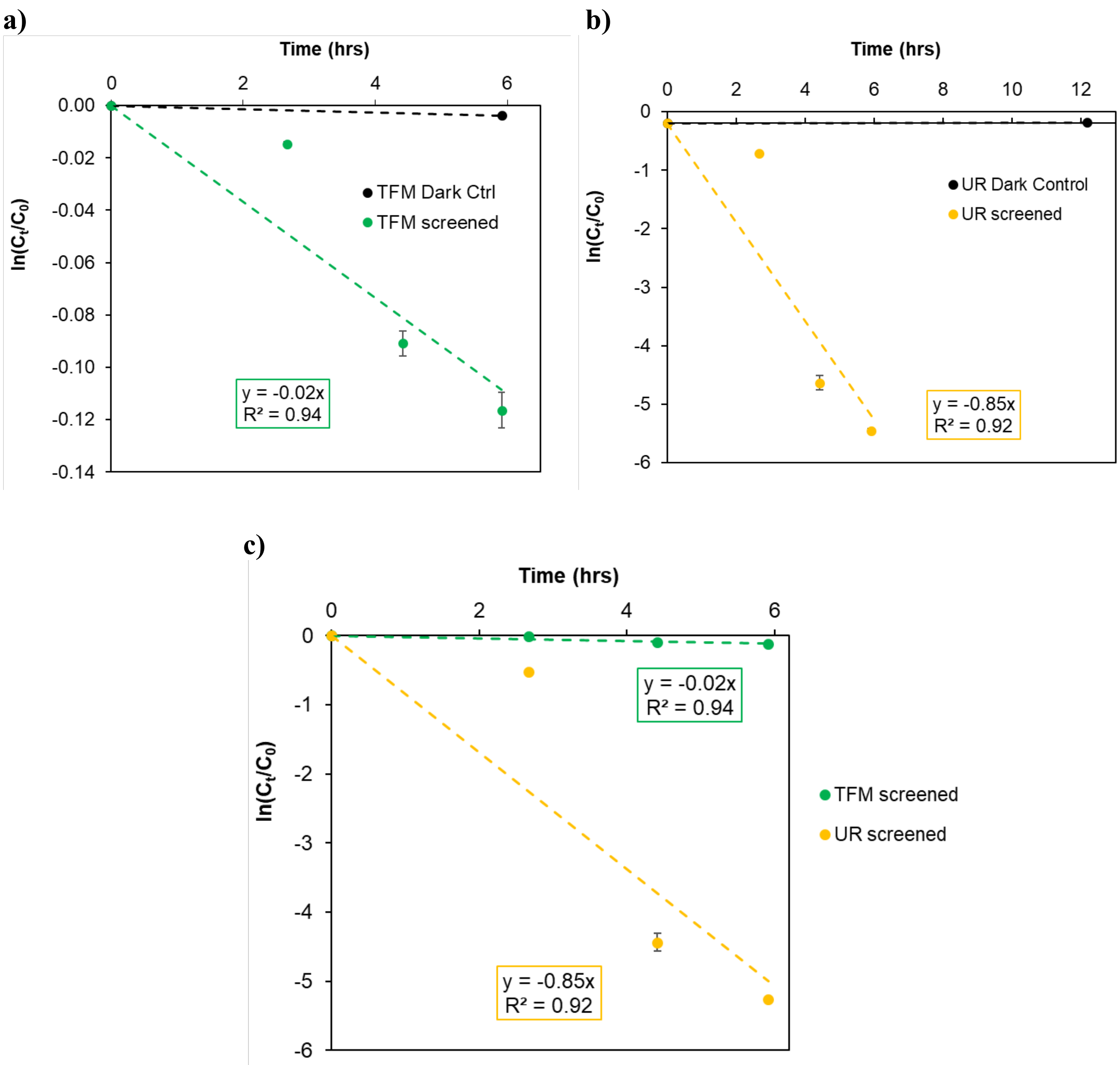

Figure 19. The *in-situ* photodegradation kinetics for triplicate irradiated solutions and a dark control solution of **a)** 18.7 µM TFM in Fox River water and **b)** 1.29 µM uranine in ultrapure water. All kinetics were corrected for light screening. Panel **c)** depicts an overlay of kinetics for both compounds. The experiment began at 9:20 AM EST on August 3, 2022 (concluded at 9:30 PM).

The difference between laboratory and *in-situ* photodegradation kinetics for each compound is driven by their variable rates of light absorption, which are a function of light intensity (**Equation 18**). The degree of overlap between irradiance and the molar absorptivity of a compound governs its rate of light absorption (i.e., it defines its photochemical action spectrum;

Figures 3 and **4**, **c**).[23] The high intensity and narrow wavelength distribution of the 365 nm bulbs greatly differs from natural solar irradiance. In sunlight, TFM exhibited lower rates of light absorption relative to uranine, which has strong absorption in the visible light region (**Figure 20**). Over 200-800 nm, the *integrated* rate of light absorption was determined hourly (**Figure 21**) to calculate a diurnal average for TFM ($k_{abs,TFM}$ = 0.3 s^{-1}) and uranine ($k_{abs,UR}$ = 1.7 s^{-1}). This contrasts laboratory experiments, where TFM absorbed incident light faster than uranine during ($k_{abs,TFM}$ = 1.1 s^{-1} vs. $k_{abs,UR}$ = 0.4 s^{-1}) because its peak absorbance closely overlaps with the 365 nm bulb irradiance (**Figure 22, b**). Following **Equation 19**, the rate of light absorption directly impacts photodegradation kinetics, which is evident based on each batch experiment.

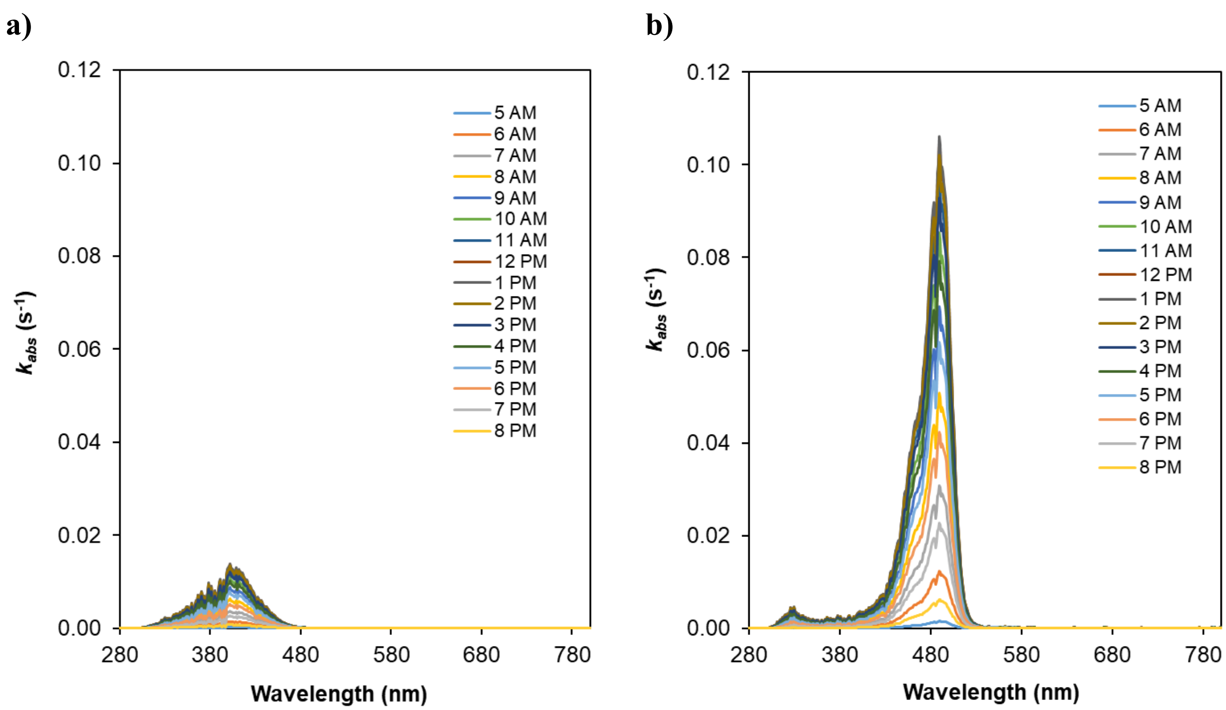

Figure 20. Hourly rates of light absorption for **a)** TFM and **b)** uranine modeled over the relevant solar spectrum (280-800 nm).

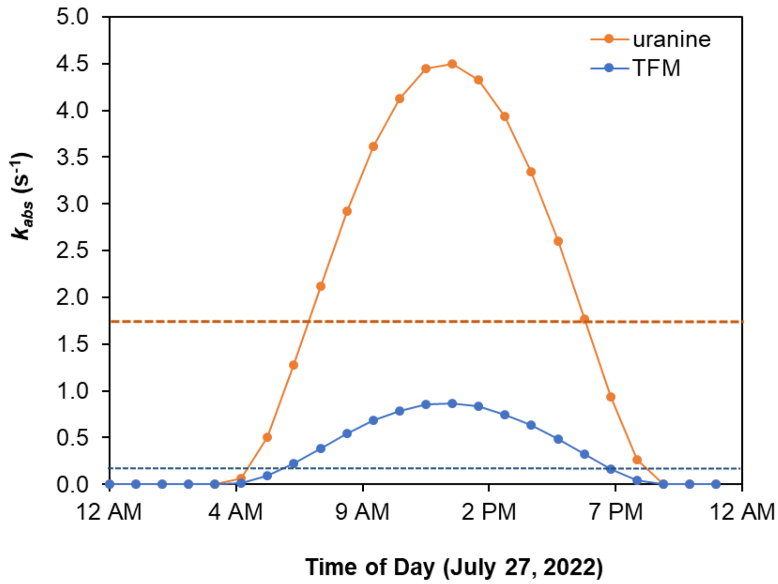

Figure 21. The integrated rates of light absorption for TFM and uranine modeled throughout treatment day. The diurnal averages are shown with dashed lines in blue (TFM, k_{abs} = 0.3 s^{-1}) and orange (uranine, k_{abs} = 1.7 s^{-1}).

Variable photodegradation kinetics under different light sources were also driven by changing quantum yields. Following **Equation 19**, the *in-situ* kinetic constants and *in-situ* integrated rates of light absorption were used to calculate "environmental" quantum yields which account for longer wavelengths in the solar spectrum. For TFM and uranine, the diurnal average environmental quantum yields were calculated to be 3.1×10^{-5} and 3.7×10^{-4}, respectively (**Figure 22, c**). Like the kinetic constants, quantum yield decreased by a factor of ~3 for TFM and increased by a factor of ~4 for uranine relative to laboratory findings. However, the difference is much larger for uranine. This is because the quantum yield of compounds that absorb light over a broad wavelength range (i.e., dyes like uranine) may exhibit more wavelength dependence.[23,67,91,96–99] However, quantum yields can also be wavelength-independent in solution, so laboratory values determined using fixed-wavelength bulbs are commonly used to predict photochemical fate in aquatic systems.[2,3,69,97,100,101] For TFM, a lower environmental quantum yield contributed to slower degradation kinetics, yet the change between laboratory and *in-situ* is relatively smaller because of its peak UV-A absorption. The *magnitude* and *direction* of changes in light absorption and reaction efficiency demonstrate how variable irradiance impacts the photodegradation kinetics of a compound based on its specific optical properties. Overall, the *in-situ* experiment suggests TFM is less photolabile under environmental conditions than under laboratory conditions, but the slower *in-situ* kinetics agrees with our field observations.

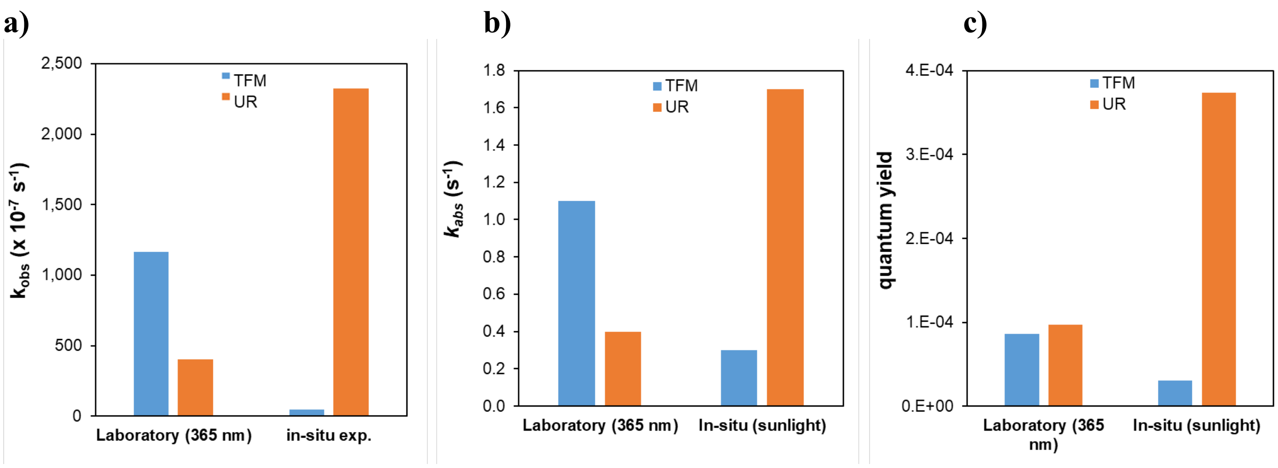

Figure 22. Laboratory and *in-situ* **a)** photodegradation kinetic constants, **b)** integrated rates of light absorption, and **c)** quantum yields for TFM and uranine.

Model-Predicted In-stream Photodegradation Kinetics

Model-predicted values may overpredict loss in the environment. For comparison with the measured values from laboratory and *in-situ* batch experiments, we predicted environmental, or "in-stream", photodegradation kinetic constant using the laboratory quantum yield and modeled solar spectra. The solar spectra First, kinetic constants predicted based on continuous noontime irradiance overestimate loss compared to diurnal average values (**Figure 23**, **Equation 19**). The in-stream kinetic constant for TFM was lowered from 7.3×10^{-5} s^{-1} ($t_{1/2}$ = 2.6 hr) to 2.7×10^{-5} s^{-1} ($t_{1/2}$ = 7.0 hr) and uranine kinetic constants were lowered from 4.3×10^{-4} s^{-1} ($t_{1/2}$ = 0.5 hr) to 1.7×10^{-4} s^{-1} ($t_{1/2}$ = 1.7 hr).

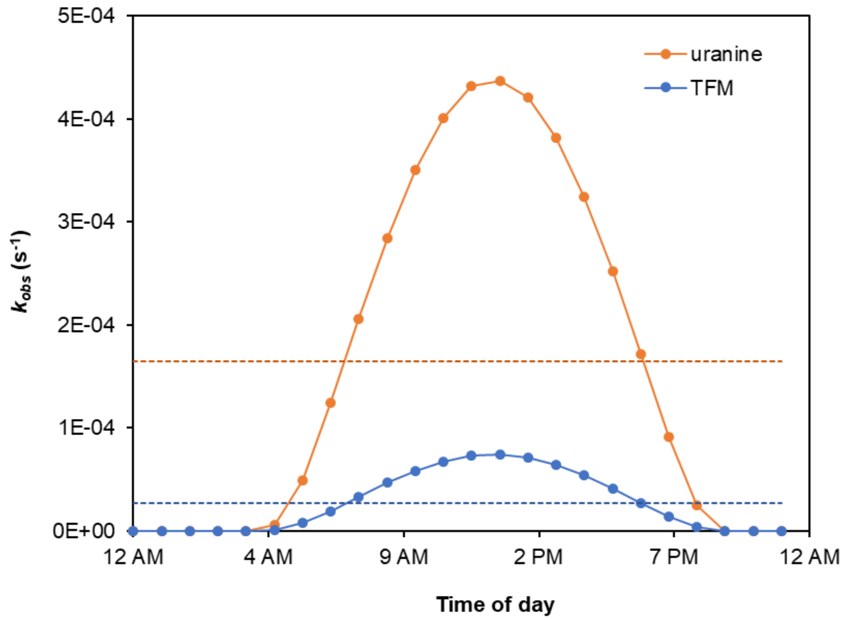

Figure 23. The predicted environmental photodegradation kinetic constants for **a)** TFM and **b)** uranine. The diurnal average is indicated by the dashed line.

Rates of loss are also overestimated by not accounting for environmental complexities such as cloud cover, turbidity and rapid mixing in rivers, in-stream light scattering by analytes or other dissolved organic compounds, and light attenuation down the water column.[102–104] The measured and modeled kinetic constants discussed thus far apply to the near-surface conditions (test tubes or the top 1 cm of the water surface). As light attenuates throughout the water column, decreasing intensity and lower rates of light absorption slow photodegradation. Therefore, we repeated our analysis with variable path lengths up to max depth (60 cm) to obtain depth-integrated kinetic constants (**Figure 24**). For the average depth scenario (30 cm) photodegradation greatly decreased for TFM and uranine, with respective kinetic constants of 1.8×10^{-6} s^{-1} ($t_{1/2}$ = 109 hr) and 7.4×10^{-6} s^{-1} ($t_{1/2}$ = 26 hr) for uranine (**Figure 25**).

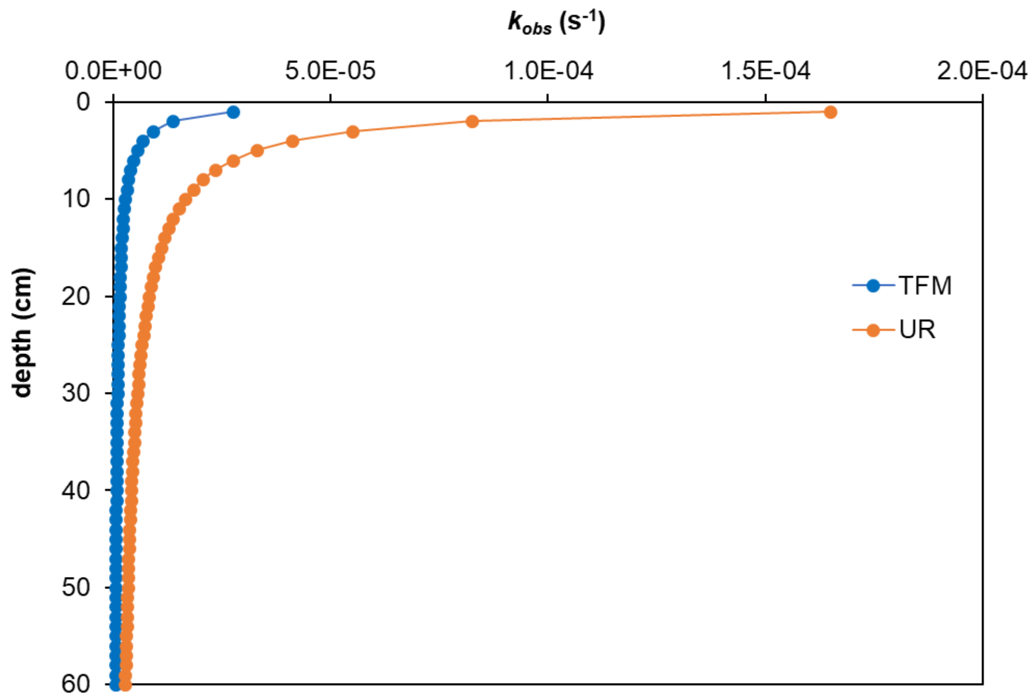

w 24. Model-predicted photodegradation kinetic constants (diurnal averages) for TFM and uranine as a function of water column depth (light path length).

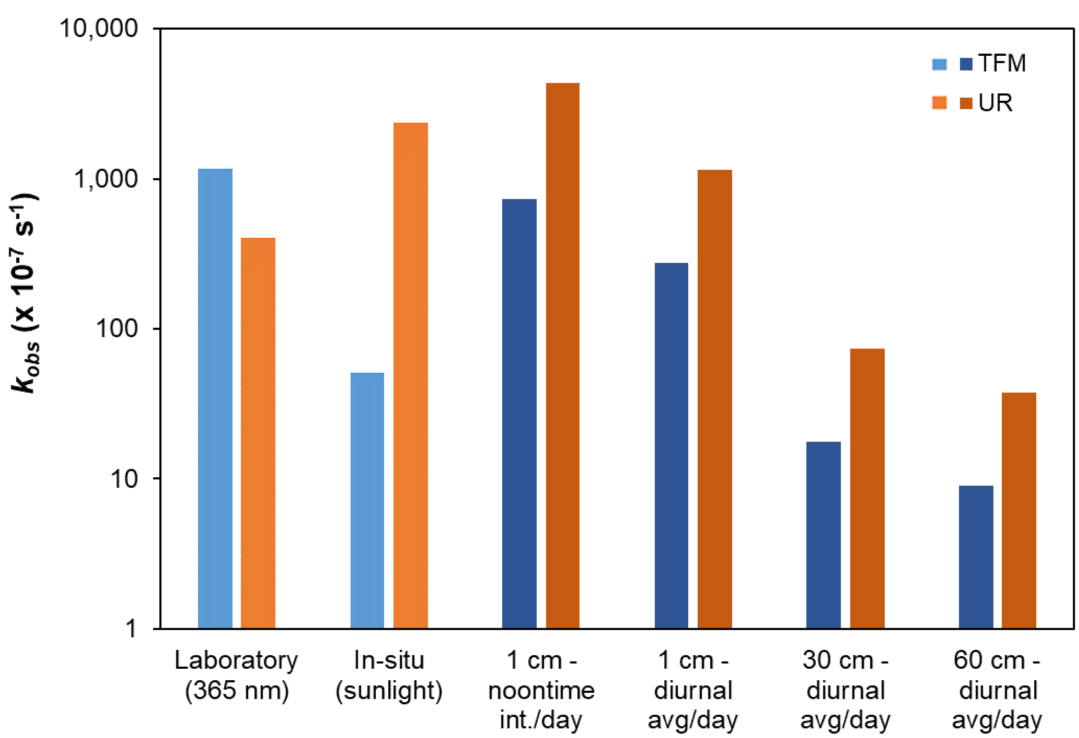

Figure 25. Measured and modeled photodegradation rate constants for TFM and uranine. Note the logarithmic scale. Measured values are lightly colored and modeled values are shaded.

The depth-integrated kinetic predictions are in good agreement with both the *in-situ* kinetics and our field observations in that TFM is less photolabile than laboratory experiments suggest. The laboratory, *in-situ*, and model-predicted values corroborate the laws of photochemistry in multiple ways. First, the model predictions based on laboratory quantum yields underestimated the difference in kinetics between TFM and uranine that was measured *in-situ*, highlighting the need to calculate environmental quantum yields for compounds that absorb light over a broad range of wavelengths. This difference was minimal for TFM compared to uranine. Next, it is evident from the constants averaged over 30 and 60 cm depth that modeled values overpredict photodegradation kinetics when light attenuation is not considered. Lastly, all scenarios that include solar irradiance (*in-situ* measured and all modeled values) predict faster loss of uranine compared to TFM, which aligns with our tracer study and treatment observations. This agreement demonstrates the power of *in-situ* studies to replicate field results and the importance of characterizing photochemical conditions when predicting the aquatic fate of photolabile compounds.

Major Mechanisms Influencing TFM Fate

In the Driggs River, net water gains and physical dispersion respectively lowered the in-stream concentration of TFM (i.e., *diluted* TFM) and increased the exposure time at downstream sites (i.e., *broadened* the time series), but TFM behaved conservatively overall as degradation reactions did not dominate its fate. There is also evidence that transient hyporheic storage controlled the concentrations (i.e., the time series *shape*) based on non-steady-state conditions and tailing at downstream sites. Weak TFM-sediment interactions and rapid sorption-desorption kinetics under river conditions (neutral pH) indicate any retention or retardation of TFM is more so driven by rapid hyporheic fluxes than sorption. Hyporheic dynamics play a role, but storage was transient (~hours) based on full mass recoveries of bromide and TFM within a day.

While biodegradation is negligible in the water column based on microcosm results, biodegradation in sediment-water systems (i.e., the hyporheic zone) is relevant. Reincorporation of TFM back into the water column over treatment timescales indicates subsurface residence times were low,[40,105] thus the opportunity for microbial metabolism and related biogeochemical processes to transform TFM was minimal in the Driggs River. Storage was transient in this study, but previous studies have observed long-term storage and release beyond treatment timescales.[2] Mixed findings agree with our hypothesis that hyporheic processes impact fate, but subsurface residence times are highly dependent on individual river characteristics like streambed morphology and precipitation events.

Because the majority of TFM is expected to remain in the water column, photodegradation is thought to be relevant based on rapid kinetics in laboratory studies. However, laboratory kinetics do not account for the impact of variable irradiance on the rate of light absorption and quantum yield. Like hyporheic processes, variable photochemical conditions can be difficult to model because of environmental complexities like cloud cover, attenuation throughout the water column, or competitive light absorption in high DOC waters. In general, we conclude the majority of TFM will travel long distances untransformed (i.e., to Lake Michigan), which corroborates previous research.[2,13]

CONCLUSIONS

Quantifying dynamic interactions between in-stream and hyporheic processes is challenging. Predicting the *true* fate of a compound in the environment requires synthesis of field observations, laboratory experiments, *in-situ* studies, and theoretical models alongside information on dose, when applicable and available. We propose a novel approach to continuously quantify light-screening compounds *in-situ* using ΔfDOM, thereby increasing the accuracy and temporal resolution of in-stream measurements. We also form broad conclusions on TFM fate by establishing a research framework that includes the dominant physical and chemical loss mechanisms. Kinetic and equilibrium constants describing individual mechanisms were robustly investigated by considering both batch and flow-through style experiments under laboratory and treatment conditions. This synergistic approach is broadly applicable to better understand and predict the fate of polar organic compounds with unknown origins and non-point sources in river systems.

SUPPLEMENTAL INFORMATION

Section 1. Chemicals

All chemicals were used as received. The Fox River and Driggs River were treated with a liquid TFM formulation containing 33% active ingredient (Iofina Chemical, Inc. and Weylchem). Smaller tributaries of the Fox River were treated with TFM bars (23% active ingredient, Iofina Chemical, Inc.) that dissolve between 8-12 hours depending on stream velocity.[19,106,107] 18 MΩ-cm ultrapure water from a Milli-Q purification system was used to prepare analytical standards, aqueous HPLC mobile phases, and buffers used in sediment sorption reactors and photochemistry control samples.

TFM solid standards (99% purity) for laboratory experiments were purchased from Acros Organics and Tokyo Chemical Industry (TCI). Uranine solid standard (96.1% purity) was purchased from TCI. A 20% (v/v) Rhodamine WT solution in water was purchased from Acros Organics. Bromine Booster (99% NaBr solid) was purchased from Spa Choice. 4-Nitroanisole solid (99%, CAS 100-17-4) was purchased from Acros Organics. Pyridine (99%+, CAS 110-86-1) was purchased from Alfa Aesar. Acetonitrile (HPLC grade, CAS 75-05-8) was purchased from Fisher. Monobasic potassium phosphate (CAS 7778-77-0) and dibasic potassium phosphate (CAS 7778-11-4) were purchased from Sigma Aldrich. Dibasic sodium phosphate (CAS 7558-79-4) was purchased from EMD Millipore. pH 4 and 10 probe calibrants were purchased from Aqua Solutions. Sodium hydroxide pellets (98% purity, CAS 1310-72-3) were purchased from Macron/Avantor. Ammonium acetate (99.2% purity, CAS 631-61-8) was purchased from Honeywell (Fluka). Bromide standard was purchased from inorganic ventures. Formic acid (CAS 64-18-6) was purchased from Fisher Chemical.

Table 1. Chemical information for the organic analytes studied.

Compound information		Structure
Name	3-trifluoromethyl-4-nitrophenol (TFM)	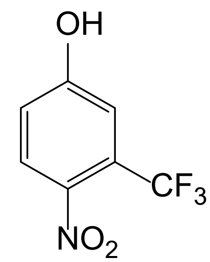
Molecular formula	$C_7H_4F_3NO_3$	
Molecular weight	207.1 g/mol	
CAS	88-30-2	
Acid dissociation constant[20]	$pK_a = 6.38$	
Peak absorbance (in water)	295 nm (pH < pK_a, phenol) 395 nm (pH > pK_a, phenolate anion)	
Name	Uranine (UR) (fluorescein disodium salt)	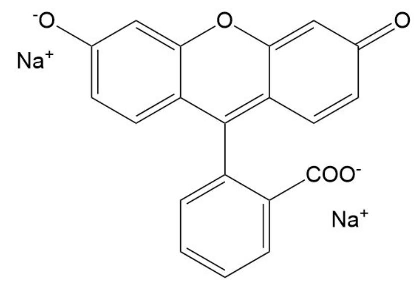
Molecular formula	$C_{20}H_{10}Na_2O_5$	
Molecular weight	376.27 g/mol	
CAS	518-47-8	
Acid dissociation constant(s)[108,109]	$pK_{a1} = 2.08$ $pK_{a2} = 4.31$ $pK_{a3} = 6.43$	
Peak absorbance (in water)	491 nm (pH > pK_{a3}, xanthene dianion)	
Name	Rhodamine-WT (RWT) (meta-para isomer mixture)	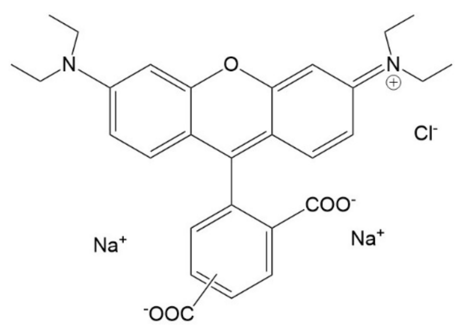
Molecular formula	$C_{29}H_{29}ClN_2Na_2O_5$	
Molecular weight	566.99 g/mol	
CAS	37299-86-8	
Acid dissociation constant(s)[48]	$pK_{a1,meta} = 2.8$, $pK_{a1,para} = 2.8$ $pK_{a2,meta} = 3.5$, $pK_{a2,para} = 3.6$ $pK_{a3,meta} = 4.4$, $pK_{a3,para} = 4.4$	
Peak absorbance (in water)	556 nm (pH > pKa_3, iminium cation and two anionic carboxylates)	

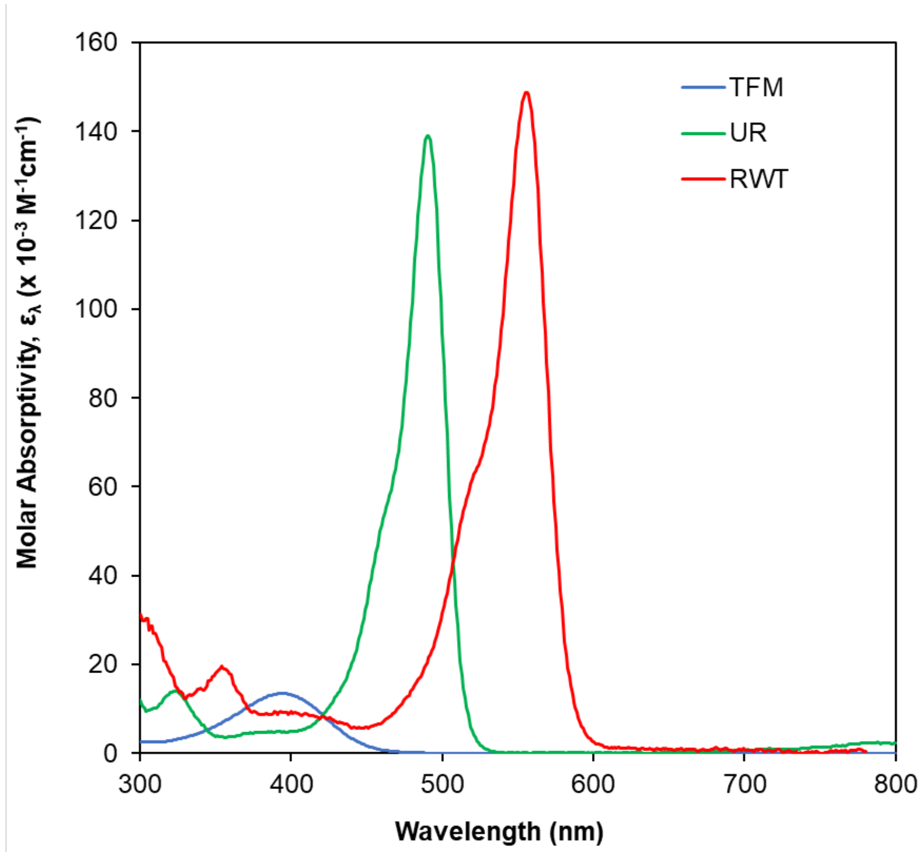

Figure 26. The molar absorptivity of TFM, UR, and RWT in water at pH 7.5 (5 mM phosphate) as a function of wavelength, with respective peak absorbances at 375, 491, and 554 nm.

Section 2. Field Sites

Table 2. Site coordinates and stream flow paths from the most upstream 1° application points (AP) and the closest 2° application point.

1° AP or study site	Coordinates	Distance from 1° AP (km)	Distance from nearest 2° AP (m)
Fox 1° AP (Casey Lake outlet)	46.51641, -86.05042	--	--
Fox Upper	46.50692, -86.04978	2.0	240
Fox Lower	46.47206, -86.06507	7.6	80
Driggs 1° AP (Driggs Truck Trail)	46.44822, -86.18794	--	--
Driggs well-mixed point	46.44747, -86.18713	0.2	--
Driggs Short Reach	46.43391, -86.17629	2.8	--
Driggs Distant Site	46.40525, -86.13937	11.2	--

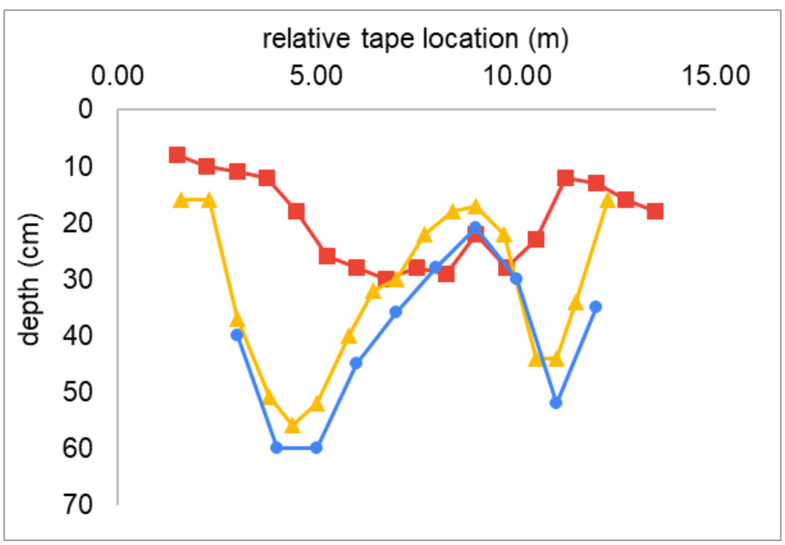

Figure 27. Three depth profiles collected at the Driggs River well-mixed point. In-stream photodegradation kinetics were modeled for the max depth (60 cm) and average depth (30 cm) scenarios.

a) b)

Figure 28. Stream-side sediment packed column during **a)** TFM treatment (fDOM sensors) and **b)** the tracer study (fluorometers).

Section 3. Pre-treatment Sampling

Background water chemistry parameters are summarized in **Table 10** (**SI Section 8**). A month before the two treatments, bulk sediment and river water samples were collected from the Fox and Driggs Rivers and transported back to UW-Madison for characterization and use in laboratory experiments. Using a shovel, sediment was collected from the top few centimeters of the riverbed and sealed in 10-gallon buckets. Bulk surface water samples were collected in 4-liter amber jars and immediately stored on ice in the dark. All glassware was amber and baked at 450 °C for 8 hours before sampling. The pretreatment samples were transported within 48 hours and then stored in the dark at 4 °C. Upon arrival, the water was vacuum filter sterilized (0.45 μm, nylon).

Section 4. Fox River TFM Sampling Scheme

On July 22, 2022, the 1° application near Casey Lake outlet began at 7:30 a.m. EST and the 2° application immediately above our upper site began at 9 a.m. At the upper site, duplicate fDOM sensors were deployed with acquisition frequencies of 2-5 minutes and water samples were collected at 5-minute intervals from 7:45–11 a.m. Thereafter, samples were collected every 10 minutes from 11–12 p.m., then every 30 minutes from 12–2 p.m. Samples were collected on the hour from 2–7 p.m., every 30 minutes from 7–8 p.m., and every 20 minutes from 8–9:40 p.m. 1 sample was collected every day for 4 days following treatment.

As for the lower site, TFM from the upstream applications began appearing around 1:30 p.m. The 2° application immediately upstream of the lower site began at 1:43 p.m. Samples were collected every 30 minutes from 12–8 p.m., then collected on the hour from 8 p.m.–2 a.m. (July 23rd). The nearby 2° application halted at ~2 a.m. and samples were collected every 10 minutes for the following hour (2–3 a.m.). From 3–4 a.m., samples were collected every 20 minutes. For the four days following treatment, 1-3 daily samples were collected from both sites.

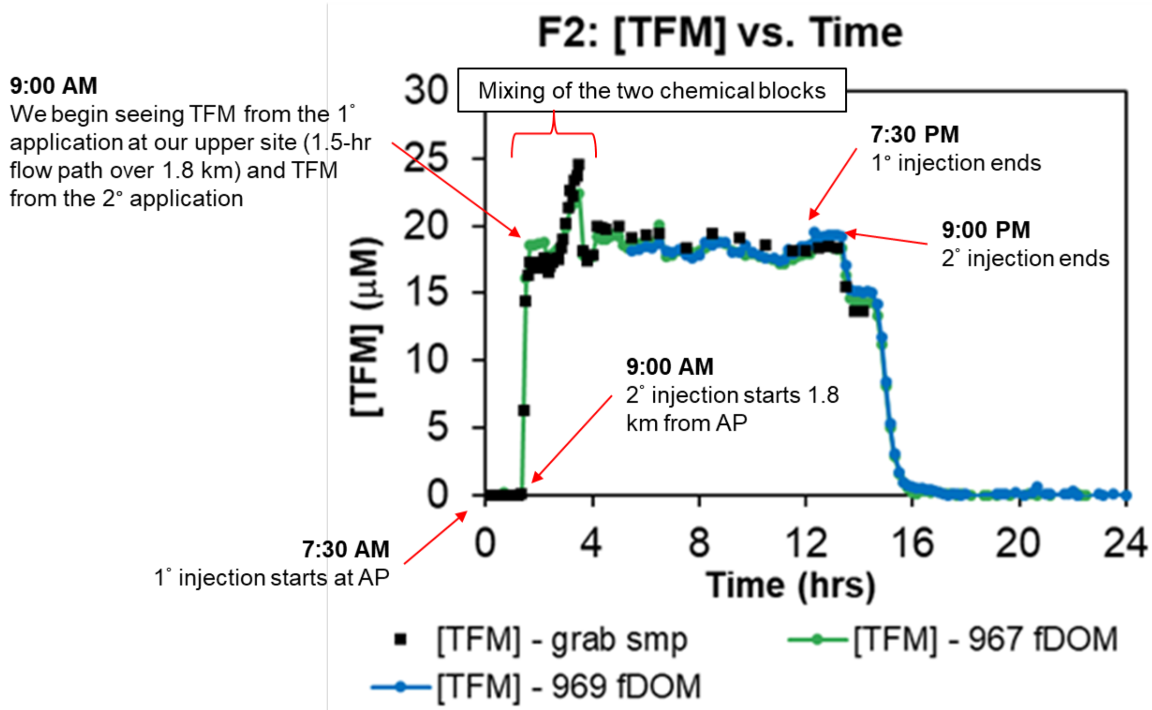

Figure 29. Further annotation of the Fox River time series at the upper site (details mixing of two upstream applications).

Section 5. Driggs River TFM Sampling Scheme

On July 27, 2022, application began at Driggs Truck Trail at 5 a.m. during a period of heavy precipitation. There were clear skies in the afternoon and evening. An fDOM sensor was deployed at the well-mixed point and the short reach. At the well-mixed point, samples were collected every five minutes from 4:55—6 a.m. to capture the steep rising limb during treatment start. Samples were collected every 10 minutes until 6:30 a.m. Samples were collected at 3 p.m., 4 p.m., and 5 p.m. before rapid sampling began again. Application halted at 5 p.m. and samples were collected every five minutes to capture the rapid falling limb from 5—5:30 p.m. Samples were collected every 15 minutes until 6 p.m. and another sample was collected at 7 p.m. A single sample was collected the following day and three days later. For the sediment column effluent, 50-60 mL was accumulated in a large syringe every ~10 minutes from 5:15—6:10 a.m. Tailing of the time series was expected, thus effluent samples were collected later in the day from 3:20—7 p.m. Another volume was collected the following day.

Section 6. Driggs River Tracer Sampling Scheme

At 9:30 AM on July 31, 2022, a pulse injection of uranine, RWT, and bromide was conducted at the 1° application point on the Driggs. 56 g of uranine stock solution, 115 g of RWT stock solution, and 7.3 kg NaBr solid were added to a 55-gallon bin containing river water. The tracer solution was mixed before injection. At the well-mixed point downstream, several samples were collected before injection to assess background signals. Samples were rapidly collected (every 1-2 minutes) from 9:35 – 9:47 a.m., then every 5–15 minutes until 10:30 a.m. Thereafter, samples were collected every 20-30 minutes until 1:30 p.m. Like TFM treatment, time-integrated samples were slowly collected from the column effluent container at ~10-30-minute intervals. At the short reach, samples were collected every 10-20 minutes from 11:30 a.m.–2:40 p.m. Background samples were periodically collected immediately before and after the pulse was expected. In the two days following the tracer study, a sample was collected from the well-mixed point, column effluent container, and the short reach to potentially observe legacy concentrations.

Section 7. Analytical Methods

Table 3. TFM single analyte assay: DAD/MWD detection (standard C18 column)

TFM HPLC Method: 120 EC-C18	
Method Name	
Column	Agilent InfinityLab Poroshell 120 EC-C18 (3.0 x 50 mm) 2.7 um
Guard column	Agilent InfinityLab Poroshell 120 EC-C18 (3.0 x 5 mm) 2.7 um
Flow Rate	0.5 mL/min
Mobile Phase A	0.1% Formic Acid
Mobile Phase B	100% ACN
Elution	Isocratic: 65% A, 35% B
Method Duration	3.0 min
Injection volume	50 µL
Column Temperature	30º C (Combined Compartment)
DAD Parameters	
Detector	Diode-Array Detection (DAD)/Photodiode-Array Detection (PDA)
Absorbance Wavelength	300 nm
Bandwidth	4.0 nm
Reference Wavelength	450 nm
Reference Bandwidth	100 nm
Peak width	>0.10 min (2.0 s response time) (2.5 Hz)
Zero Offset	5%
Attenuation	1000 mAU
Margin for Negative Absorbance	100 mAU

Table 4. TFM single analyte assay: DAD/MWD detection (C18 column with embedded polar groups)

Agilent HPLC 1260 Infinity Method: TFM, on C18 with Amide Embedded Polar Group (EPG)		
Method/ Column Info	Method Name	LDA_TFM_BONUS RP.M **- or -** LDA_TFM_BONUS RP_50 uL.M
	Column	Agilent InfinityLab Poroshell Bonus-RP (3.0 x 100 mm) 2.7 um
	Guard column	Agilent InfinityLab Poroshell Bonus-RP (3.0 x 5 mm) 2.7 um
Binary Pump	Flow Rate	0.55 mL/min
	Mobile Phase A	10 mM $NH_4CH_3CO_2$ adjusted to pH 7.5 (w/ NaOH), 0.2 um filtered
	Mobile Phase B	100% ACN
	Elution Method	Isocratic: 45% A, 55% B
	Method Duration	4.5 min (5.75 min with transition time)
Sampler	Injection volume	20 uL (was 30 uL) **– or –** 50 uL
	Draw Speed	200 uL/min
	Eject Speed	200 uL/min
Column Compart.	Temperature	30º C (Combined)
Multi-Wavelength Detector (MWD) (HPLC 2) or **Diode-Array Detection (DAD)/ Photodiode-Array Detection (PDA) (HPLC 1)**	Absorbance Wavelength	375 nm
	Bandwidth	4 nm
	Reference Wavelength	450 nm
	Reference Bandwidth	100 nm
	Peak width	>0.10 min (2.0 s response time) (2.5 Hz)
	Zero Offset	5%
	Attenuation	1000 mAU
	Margin for Neg. Absorbance	100 mAU
	Auto-balance	Prerun
Additional MWD Parameters	Slit	4 nm
	Visible Lamp	Off

Table 5. TFM single analyte assay: MS/MS detection.

<table>
<tr><th colspan="3">LCMS Method: TFM on 120 Bonus-RP (Amide Column)</th></tr>
<tr><td rowspan="3">Method/ Column Info</td><td>Method Name</td><td>LDA_TFMQuickAssay.m</td></tr>
<tr><td>Column</td><td>Agilent InfinityLab Poroshell Bonus-RP (3.0 x 100 mm) 2.7 um</td></tr>
<tr><td>Guard column</td><td>Agilent InfinityLab Poroshell Bonus-RP (3.0 x 5 mm) 2.7 um</td></tr>
<tr><td rowspan="5"></td><td>Flow Rate</td><td>0.55 mL/min</td></tr>
<tr><td>Mobile Phase A</td><td>(100%) 0.2% Formic Acid, 0.2 um filtered</td></tr>
<tr><td>Mobile Phase B</td><td>(100%) Methanol</td></tr>
<tr><td>Elution Method</td><td>Gradient:
<table>
<tr><th>Time (min)</th><th>A (%)</th><th>B (%)</th><th>Flow (mL/min)</th><th>Max Pressure Limit (bar)</th></tr>
<tr><td>0.00</td><td>60</td><td>40</td><td>0.55</td><td>400</td></tr>
<tr><td>0.50</td><td>5</td><td>95</td><td>0.55</td><td>400</td></tr>
<tr><td>2.00</td><td>5</td><td>95</td><td>0.55</td><td>400</td></tr>
<tr><td>2.10</td><td>60</td><td>40</td><td>0.55</td><td>400</td></tr>
<tr><td>5.00</td><td>60</td><td>40</td><td>0.55</td><td>400</td></tr>
</table></td></tr>
<tr><td>Method Duration</td><td>5 min</td></tr>
<tr><td>Sampler</td><td>Injection volume</td><td>25 uL</td></tr>
<tr><td>Column Compartment</td><td>Column Temperature</td><td>50º C (Combined Compartment)</td></tr>
<tr><td>detection</td><td>Scan type</td><td>MRM</td></tr>
<tr><td></td><td>Drying gas temp</td><td>300 C</td></tr>
<tr><td></td><td>Drying gas flow</td><td>7 L/min</td></tr>
<tr><td></td><td>Nebulizer pressure</td><td>45 psi</td></tr>
<tr><td></td><td>Sheath gas temp</td><td>350 C</td></tr>
<tr><td></td><td>Sheath gas flow rate</td><td>10 L/min</td></tr>
<tr><td></td><td>Capillary</td><td>3500 V</td></tr>
<tr><td></td><td>Nozzle voltage</td><td>500 V</td></tr>
<tr><td></td><td>Ionization mode</td><td>AJS Electrospray ionization</td></tr>
</table>

<table>
<tr><th rowspan="2">Target Analyte</th><th>Precursor Ion</th><th>Retention Time</th><th>Fragmentor Voltage</th><th>Product Ion</th><th>Collision Energy Voltage</th><th>Dwell time</th><th>Cell accelerator</th></tr>
<tr><th>m/z</th><th>min</th><th>V</th><th>m/z</th><th>V</th><th>s</th><th>V</th></tr>
<tr><td rowspan="2">-TFM</td><td rowspan="2">206</td><td rowspan="2">2.4</td><td rowspan="2">125</td><td>160</td><td>16</td><td>100</td><td>4</td></tr>
<tr><td>176</td><td>12</td><td>100</td><td>4</td></tr>
</table>

Table 6. PNA single analyte assay: DAD/MWD detection

Agilent HPLC 1260 Infinity Method: *para*-nitroanisole (PNA) by C18 reverse phase chromatography		
Method/ Column	Method Name	LDA_PNA.M
	Column	Agilent InfinityLab Poroshell 120 EC-C18 (3.0 x 100 mm) 2.7 um
	Guard column	Agilent InfinityLab Poroshell 120 EC-C18 (3.0 x 5 mm) 2.7 um
Binary Pump	Flow Rate	0.6 mL/min
	Mobile Phase A	0.1 % Formic Acid in MQ
	Mobile Phase B	100% ACN
	Method Duration	2.5 min (3.5 min with transition time)
	Elution Method	Isocratic (55% A, 45% B)
Sampler	Injection volume	5 μL
	Draw Speed	200 μL/min
	Eject Speed	200 μL/min
Column Compartment	Column Temperature	30º C (Combined Compartment)
Multi-Wavelength Detector (MWD)	Wavelength	314 nm
	Bandwidth	4 nm
	Ref. Wavelength	400 nm
	Ref. Bandwidth	16 nm
	Peak width	>0.1 min (2 s response time) (2.5 Hz)
	Zero Offset	5%
	Attenuation	1000 mAU
	Margin for Neg. Absorbance	100 mAU
	Slit	4 nm

Table 7. Uranine single analyte assay: DAD/MWD detection.

Agilent HPLC 1260 Infinity Method: Uranine (UR) by C18 reverse phase chromatography		
Method/ Column	Method Name	LDA_URANINE.M
	Column	Agilent InfinityLab Poroshell 120 EC-C18 (3.0 x 100 mm) 2.7 um
	Guard column	Agilent InfinityLab Poroshell 120 EC-C18 (3.0 x 5 mm) 2.7 um
Binary Pump	Flow Rate	0.6 mL/min
	Mobile Phase A	10 mM $NH_4CH_3CO_2$, pH 7.5 (adjusted w/ NaOH for HPLC, NH_3OH on MS), 0.2 um vacuum-filtered
	Mobile Phase B	100% ACN
	Method Duration	1.5 min (2.75 min with transition)
	Elution Method	Isocratic (80% A, 20% B)
Sampler	Injection volume	5 μL
	Draw Speed	200 μL/min
	Eject Speed	200 μL/min
Column Compartment	Column Temperature	30º C (Combined Compartment)
Diode-Array Detection (DAD)/ Photodiode-Array Detection (PDA)	Wavelength	491 nm
	Bandwidth	4 nm
	Ref. Wavelength	575 nm
	Ref. Bandwidth	16 nm
	Peak width	>0.1 min (2 s response time) (2.5 Hz)
	Zero Offset	5%
	Attenuation	1000 mAU
	Margin for Neg. Absorbance	100 mAU
Fluorescence Detector (FLD)	Excitation Wavelength	491 nm
	Emission Wavelength	513 nm
	Peak width	>0.2 min (4 s response time) (2.31 Hz)
	Zero Offset	5%
	Attenuation	1000 LU
	PMT Gain	8

Table 8. RWT single analyte assays: DAD/MWD detection.

RWT Method	
Column	Agilent Poroshell 120 EC-C18 (3.0 x 100 mm)
Guard column	Agilent Poroshell 120 EC-C18 (3.0 x 5 mm)
Injection volume	5 µL
Mobile Phase A	10 mM NH_4Acetate, pH 7.5 (adjusted with 0.1 M NaOH), 0.45 um filtered
Mobile Phase B	ACN
Flow Rate	0.5 mL/min 30ºC
Column Temperature	30º C (combined)
Detector	FLD
Threshold	1.0 mAU
Elution Method	Gradient, 75% A, 25% B
Method Duration	7.00 min
Excitation Wavelength	554
Emission Wavelength	583
Retention Time	1.25, 4

RWT Method	
Column	Agilent Poroshell Bonus-RP (3.0 x 100 mm)
Guard column	Agilent Poroshell Bonus-RP (3.0 x 5 mm)
Injection volume	30 µL
Mobile Phase A	10 mM NH_4Acetate, pH 7.5 (adjusted with 0.1 M NaOH), 0.45 or 0.2 um filtered
Mobile Phase B	100% ACN
Flow Rate	0.55 mL/min 30ºC
Column Temperature	30º C (combined)
Detector	FLD
Threshold	1.0 mAU
Elution Method	Gradient: %A/%B 0 min 75/10 1.5 min 90/10 3.5 min 50/50 4.5 min 50/50 4.6 min 90/10 7.5 min 90/10
Method Duration	7.00 min
Excitation Wavelength	554
Emission Wavelength	583
Retention Time	1.25, 4

Table 9. TFM, UR, and RWT mixture: DAD and FLD detection.

<table>
<tr><th colspan="3">Agilent HPLC 1260 Infinity Method: TFM + RWT + UR, C18 with Amide EPG</th></tr>
<tr><td rowspan="3">Method/ Column</td><td>Method Name</td><td>LDA_SARAHS TRIPLE COMBO SURPRISE.M</td></tr>
<tr><td>Column</td><td>Agilent InfinityLab Poroshell 120 Bonus-RP (3.0 x 100 mm) 2.7 um</td></tr>
<tr><td>Guard column</td><td>Agilent InfinityLab Poroshell 120 Bonus-RP (3.0 x 5 mm) 2.7 um</td></tr>
<tr><td rowspan="5">Binary Pump</td><td>Flow Rate</td><td>0.55 mL/min</td></tr>
<tr><td>Mobile Phase A</td><td>10 mM $NH_4CH_3CO_2$, pH 7.5
(with NaOH for HPLC, NH_3OH on MS), 0.2 um vacuum-filtered</td></tr>
<tr><td>Mobile Phase B</td><td>100% ACN</td></tr>
<tr><td>Method Duration</td><td>8 min stop time (9.3 min with transition)</td></tr>
<tr><td>Elution Method</td><td>Gradient:
<table>
<tr><th>Time (min)</th><th>A (%)</th><th>B (%)</th><th>Flow (mL/min)</th><th>Max Pressure Limit (bar)</th></tr>
<tr><td>0.00</td><td>98</td><td>2</td><td>0.100</td><td>400</td></tr>
<tr><td>0.50</td><td>80</td><td>20</td><td>0.550</td><td>400</td></tr>
<tr><td>4.00</td><td>50</td><td>50</td><td>0.550</td><td>400</td></tr>
<tr><td>4.10</td><td>80</td><td>20</td><td>0.550</td><td>400</td></tr>
<tr><td>8.00</td><td>80</td><td>20</td><td>0.550</td><td>400</td></tr>
</table></td></tr>
<tr><td rowspan="3">Sampler</td><td>Injection volume</td><td>25 uL</td></tr>
<tr><td>Draw Speed</td><td>200 uL/min</td></tr>
<tr><td>Eject Speed</td><td>200 uL/min</td></tr>
<tr><td>Column Compartment</td><td>Column Temperature</td><td>30º C (Combined Compartment)</td></tr>
<tr><td rowspan="9">Diode-Array Detection (DAD)/ Photodiode-Array Detection (PDA)</td><td>Wavelength</td><td>375 nm</td></tr>
<tr><td>Bandwidth</td><td>4 nm</td></tr>
<tr><td>Ref. Wavelength</td><td>450 nm</td></tr>
<tr><td>Ref. Bandwidth</td><td>100 nm</td></tr>
<tr><td>Peak width</td><td>>0.10 min (2 s response time) (2.5 Hz)</td></tr>
<tr><td>Zero Offset</td><td>5%</td></tr>
<tr><td>Attenuation</td><td>1000 mAU</td></tr>
<tr><td>Margin for Neg. Absorbance</td><td>100 mAU</td></tr>
<tr><td>Autobalance</td><td>Prerun</td></tr>
<tr><td rowspan="3">FLD</td><td>Peak width</td><td>>0.20 min (4 s response time) (2.31 Hz)</td></tr>
<tr><td>Zero Offset</td><td>5%</td></tr>
<tr><td>Attenuation</td><td>1000 LU</td></tr>
</table>

		Time (min)	Function	Parameter
	Gain + Wavelength Timetable	0.0	Change PMT gain	PMT gain: 7
		0.0	Change baseline	Mode: zero
		0.0	Change signal A excitation	Wavelength: 491 nm
		0.0	Change signal A emission	Wavelength: 513 nm
		3.4	Change PMT gain	PMT gain: 10
		3.4	Change baseline	Mode: zero
		3.4	Change signal A excitation	Wavelength: 554 nm
		3.4	Change signal A emission	Wavelength: 583 nm

Section 8. Background Water Chemistry

Table 10. Background water chemistry for pretreatment water collected from each river.

Parameter		Fox River	Driggs River
pH	--	7.66	7.90
Alkalinity	mg/L as $CaCO_3$	78.5	71.5
Total Organic Carbon	ppm	3.77	4.03
Inorganic Carbon	ppm	16.85	15.50
Al	ppm	--	--
Ca	ppm	20.08	21.04
Cu	ppm	--	--
Fe	ppm	0.21	0.19
K	ppm	0.71	0.54
Mg	ppm	6.65	5.23
Mn	ppm	0.01	0.01
Na	ppm	1.53	1.11
P	ppm	0.02	0.01
Pb	ppm	0.04	--
S	ppm	1.50	1.02
Sr	ppm	0.03	0.03

Section 9. Additional fDOM Calibrations

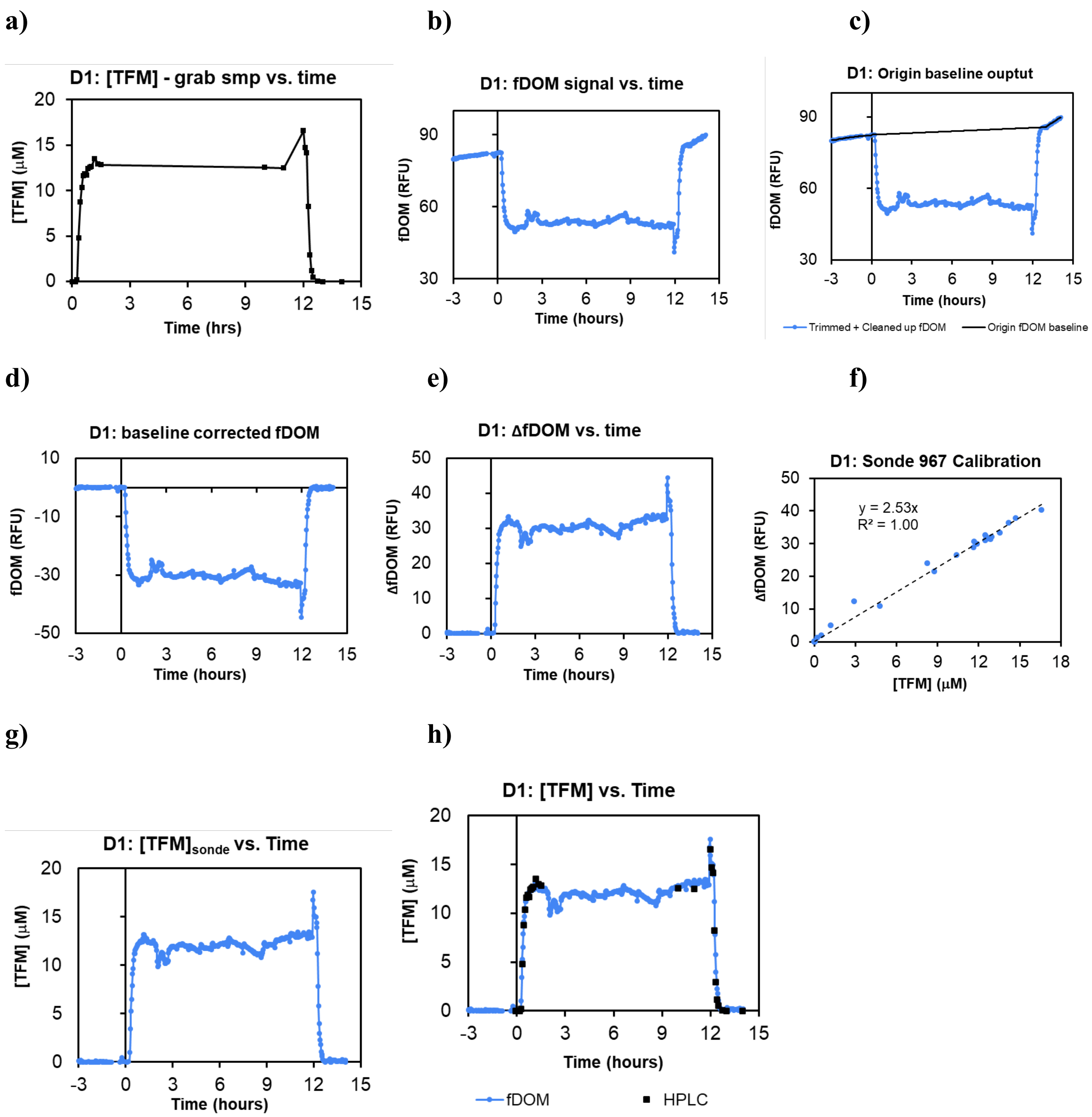

Figure 30. Driggs River fDOM calibration example.

Section 10. Uranine Sorption

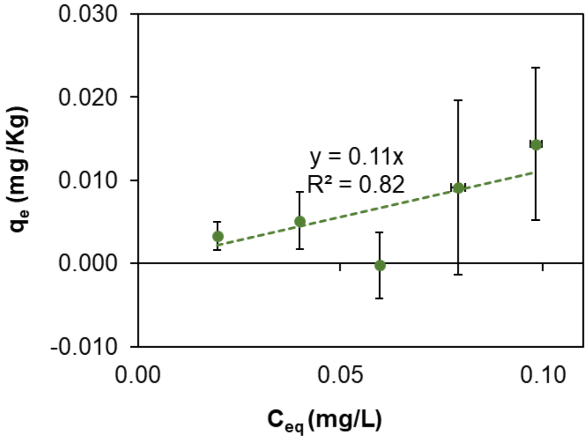

Figure 31. Sorption isotherm for uranine (pH 7.3) with Driggs River sediment (f_{oc} = 0.96 ± 0.11%).

Equilibrium sorption with uranine resulted in a K_d of 0.11 ± 0.03 L/kg, corresponding to a K_{oc} of 12 ± 3 L/kg (**Figure 31**). Uranine is primarily in a dianionic state (pK_a = 6.43) under river conditions, is highly soluble, and is very environmentally mobile. Our laboratory results suggest sorption should be negligible for uranine, and losses in-stream are primarily driven by photolysis and dilution.[20,110] In contrast, RWT is highly sorptive, with literature K_{oc} values ranging from 3,000 – 35,000 L/kg.[111–113] RWT is immobile in the sediment-water systems, with chemical loss largely driven by irreversible sorption.

Section 11. Microcosm pH and DO

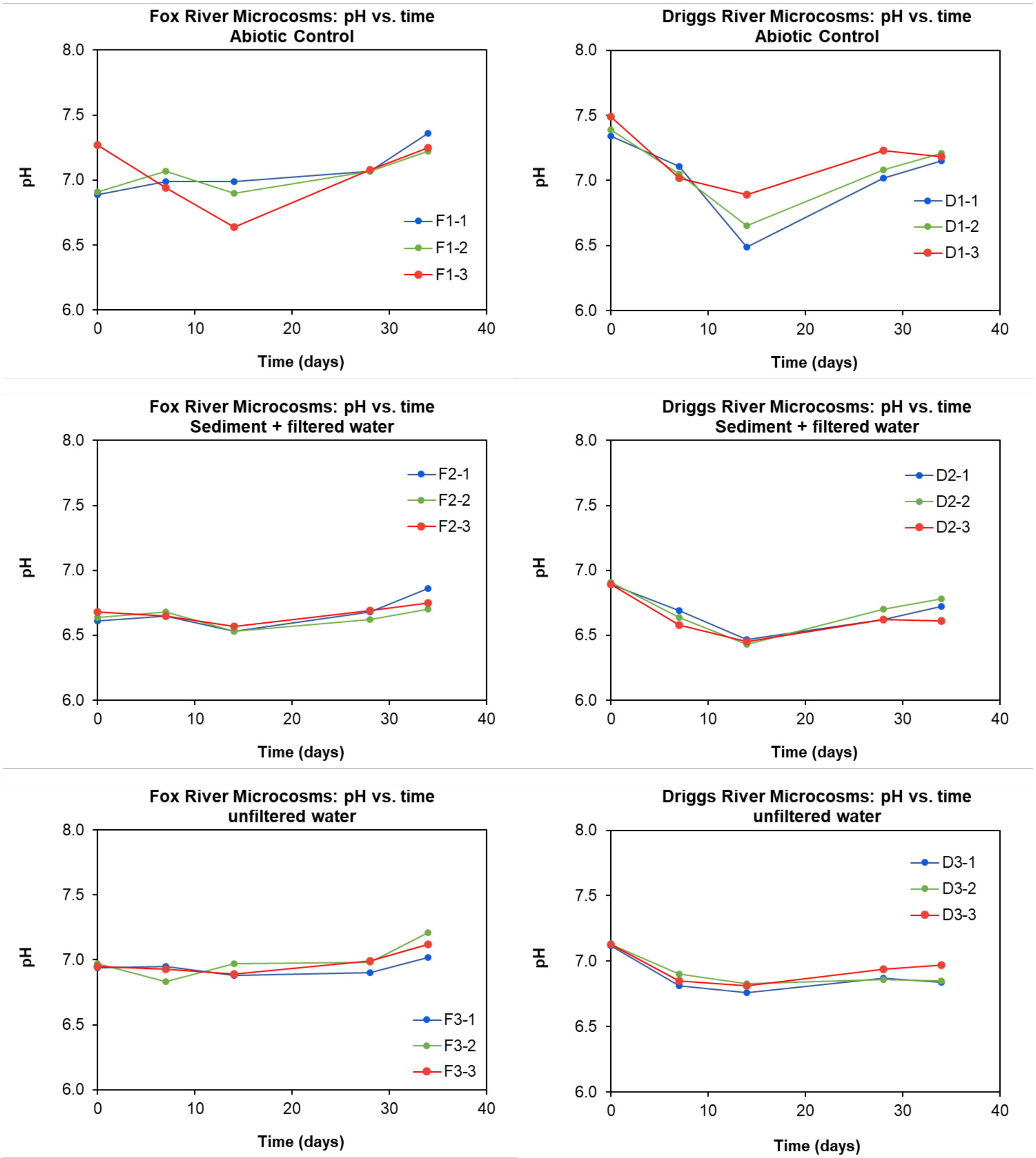

Figure 32. Microcosm pH measurements.

Table 111. Microcosm DO and temperature recordings.

Site	reactor	DO (mg/L)	±	temp (°C)	±
FOX	abiotic	8.18	0.05	21.80	0.00
	sed	3.76	0.18	21.80	0.00
	aq	7.97	0.14	21.97	0.05
DRIGGS	abiotic	8.08	0.01	22.63	0.21
	sed	4.40	0.25	22.57	0.25
	aq	8.01	0.04	22.63	0.21

Section 12. Actinometer and RWT Photodegradation Kinetics

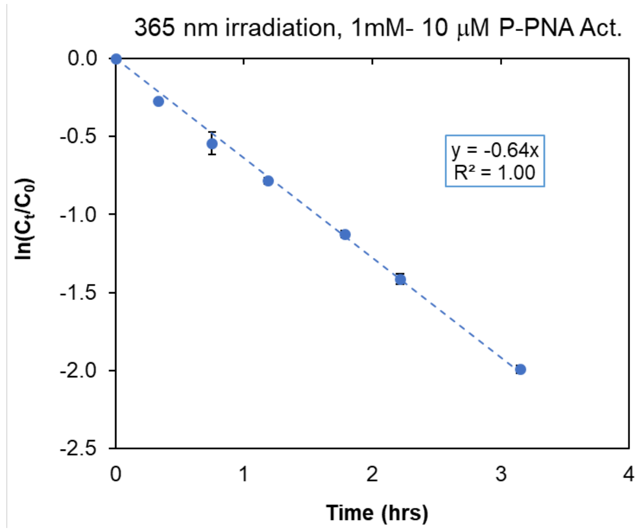

Figure 33. Actinometer kinetics during TFM experiment.

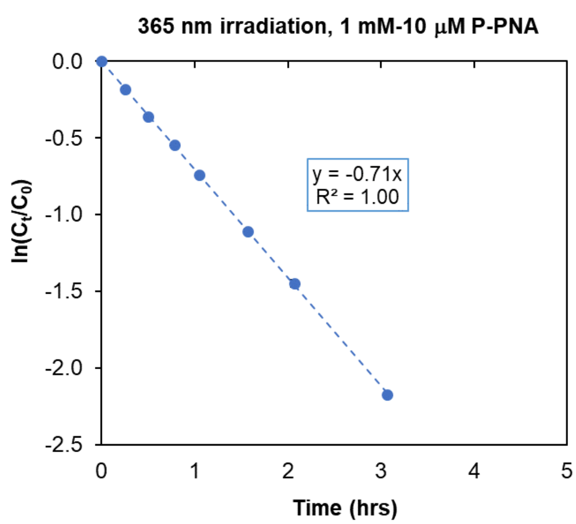

Figure 34. Actinometer kinetics during uranine experiment.

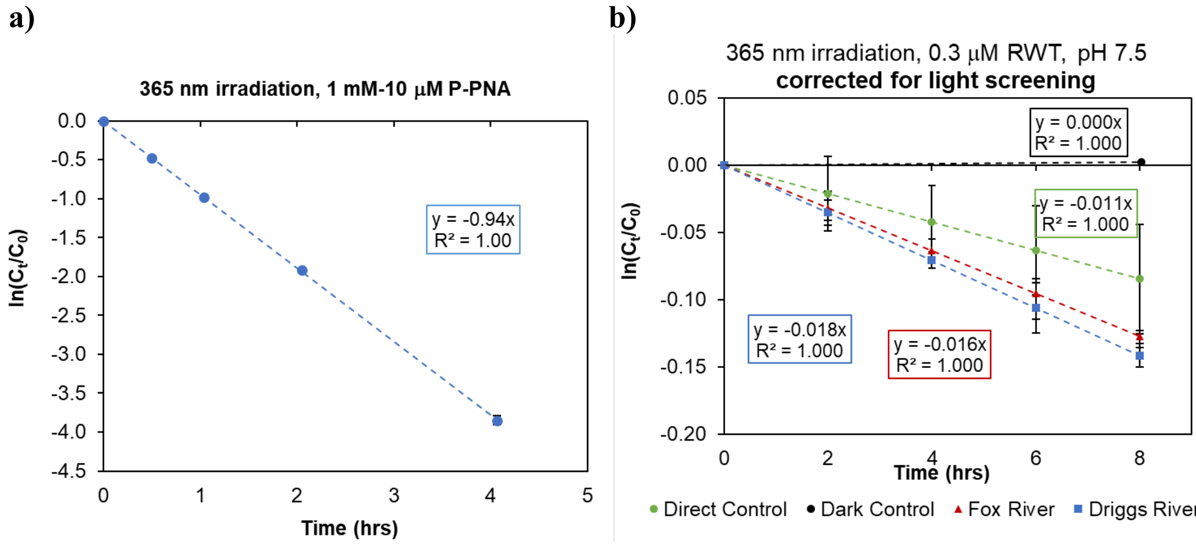

Figure 35. **a)** P-PNA actinometer and **b)** RWT photodegradation kinetics.

Photodegradation of 0.3 µM RWT was slow in ultrapure and river water **(Figure 35).** Despite relatively high light absorption in the visible light region, RWT has a low photochemical quantum yield, on the order of 10^{-7}, which was determined in a 200-hr irradiation at 488 nm (near peak absorbance) by Tai & Rathbun (1988).[100] Minimal photoreactivity of RWT has been documented under a variety of light sources; thus, RWT is considered photostable over timescales used in aquatic tracer studies.[95,99,114–116]

RWT did not photodegrade in sunlight, either: *In-situ* RWT photodegradation was also negligible, therefore *In-situ* quantum yield was not determined. In-stream photodegradation kinetics were not modeled for RWT, either. Negligible photodegradation of RWT under a variety of light sources supports our use of it as a primarily sorptive hydrological tracer for in-stream tracer studies and *in-situ*, stream-side column studies.

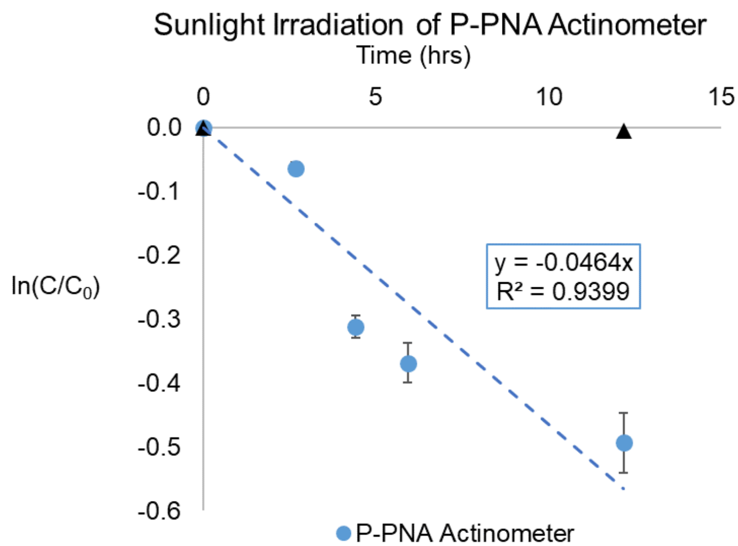

Figure 36. In-situ P-PNA actinometer kinetics.

Section 13. SMARTS Cards

Table 12. The SMARTS input parameter cards used to model solar spectra.

Card Number/ Description	**Input parameters**
1. Comment	'Driggs River - Well Mixed Point'
1. Manually input pressure	1
2a. Pressure (mb), surface altitude (km), and height (km)	1013.25 0.363 0
3. Option to use default atmosphere	1
3a. Midlatitude Summer	'MLS'
4. Use default Water vapor	1
5. Use default ozone abundance	1
6. Use default gas abundance except CO_2	1
7. Carbon dioxide from June 2021 and 2022	419
7a. Use default synthetic spectrum	0
8.Use continental aerosol model	'SRA_CONTL'
9. Use aerosol optical depth of 55 nm	5
9a.	0.084
10. Select "water" for albedo	2
10b. ITILT	1
ITILT is an option for tilted surface calculations. Leave box unchecked	51 37. 180.
11. Minimal spectral range, max spectral range, variability in irradiance, and default solar constant.	280 4000 1.0 1366.1
12. Option to generate results with spreadsheet	2
12a: Interval for printing results	280 4000 1
12b. Total number of outputs	5
12c. Outputs: (1) extraterrestrial spectrum, (2) direct normal irradiance, (3) diffuse horizontal irradiance, (4) global horizontal irradiance and (5) direct horizontal irradiance	1 2 3 4 5
13. Bypass circumsolar radiation	0
14. Bypass smoothing calculation	0
15. Illuminance using CIE photopic curve	1

16. No special UV calculations	0
17. Set inputs for card 17	3
17a. Year, month, day, hour*, latitude, longitude, time zone.	2022 07 27 12.1 46.44747 -86.18713 -5

*this field was updated to generate hourly solar spectra for July 27, 2022.

Section 14. Filtrate Recoveries

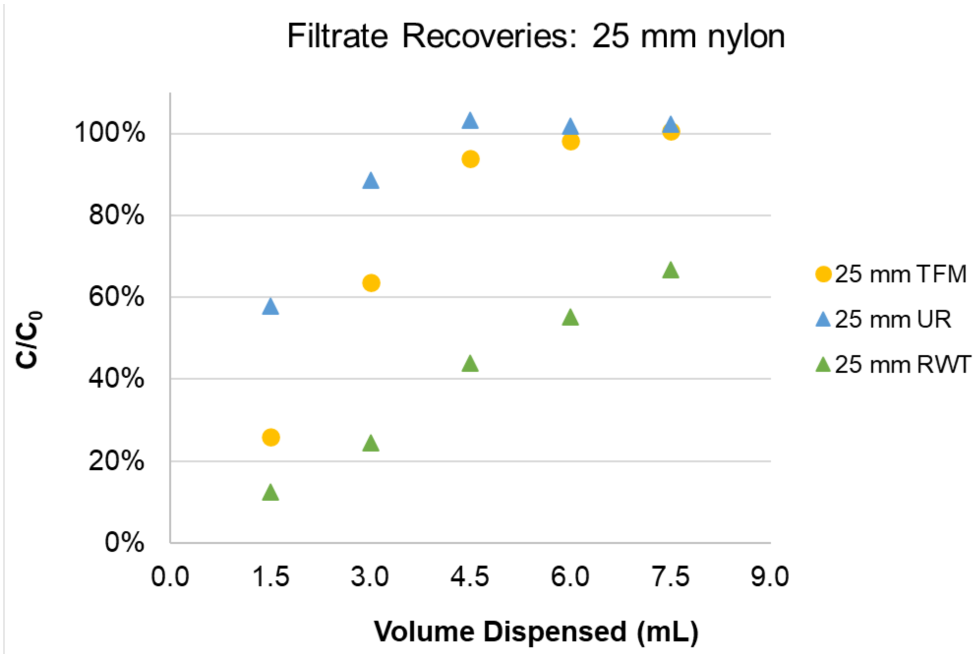

Figure 37. The filtration conditioning volume was determined for each organic analyte (for 25 mm nylon syringe filters). Standard solutions in water were filtered and 1.5 mL fractions were collected to construct an elution curve.

REFERENCES

(1) Zhi, H.; Mianecki, A. L.; Kolpin, D. W.; Klaper, R. D.; Iwanowicz, L. R.; LeFevre, G. H. Tandem Field and Laboratory Approaches to Quantify Attenuation Mechanisms of Pharmaceutical and Pharmaceutical Transformation Products in a Wastewater Effluent-Dominated Stream. *Water Res.* **2021**, *203* (June), 117537. https://doi.org/10.1016/j.watres.2021.117537.

(2) McConville, M. B.; Cohen, N. M.; Nowicki, S. M.; Lantz, S. R.; Hixson, J. L.; Ward, A. S.; Remucal, C. K. A Field Analysis of Lampricide Photodegradation in Great Lakes Tributaries. *Environ. Sci. Process. Impacts* **2017**, *19* (7), 891–900. https://doi.org/10.1039/c7em00173h.

(3) White, A. M.; Frost, S. R. Van; Jauquet, J. M.; Magness, A. M.; Mcmahon, K. D.; Remucal, C. K. (Article)_Quantifying the Role of Simultaneous Transformation Pathways in the Fate of the Novel Aquatic Herbicide Florpyrauxifen-Benzyl. **2023**. https://doi.org/10.1021/acs.est.3c03343.

(4) Christensen, E. R.; Wang, Y.; Huo, J.; Li, A. Properties and Fate and Transport of Persistent and Mobile Polar Organic Water Pollutants: A Review. *J. Environ. Chem. Eng.* **2022**, *10* (2). https://doi.org/10.1016/j.jece.2022.107201.

(5) Zaramella, M.; Packman, A. I.; Marion, A. Application of the Transient Storage Model to Analyze Advective Hyporheic Exchange with Deep and Shallow Sediment Beds. *Water Resour. Res.* **2003**, *39* (7). https://doi.org/10.1029/2002WR001344.

(6) Hubert, T. D. Environmental Fate and Effects of the Lampricide TFM: A Review. *J. Great Lakes Res.* **2003**, *29* (SUPPL. 1), 456–474. https://doi.org/10.1016/S0380-1330(03)70508-5.

(7) Wilkie, M. P.; Hubert, T. D.; Boogaard, M. A.; Birceanu, O. Control of Invasive Sea Lampreys Using the Piscicides TFM and Niclosamide: Toxicology, Successes & Future Prospects. *Aquat. Toxicol.* **2019**, *211* (July 2018), 235–252. https://doi.org/10.1016/j.aquatox.2018.12.012.

(8) The Great Lakes Fishery Commission (GLFC). Strategic Vision of the Great Lakes Fishery Commission 2011-2020. *Ann Arbor, Michigan*. 2011, pp 1–29.

(9) McDonald, D. G.; Kolar, C. S. Research to Guide the Use of Lampricides for Controlling Sea Lamprey. *J. Great Lakes Res.* **2007**, *33* (2), 20–34. https://doi.org/10.3394/0380-1330(2007)33[20:RTGTUO]2.0.CO;2.

(10) Meyer, F. P.; Schnick, R. A. Sea Lamprey Control Techniques: Past, Present, and Future. *J. Great Lakes Res.* **1983**, *9* (3), 354–358. https://doi.org/10.1016/S0380-1330(83)71906-4.

(11) Applegate, V. C. Natural History of the Sea Lamprey (Petromyzon Marinus) in Michigan. *Spec. Sci. Rep. Fish.* **1950**, *55* (55), 1–237.

(12) United States Environmental Protection Agency (US EPA). *Reregistration Eligibility Decision (RED) FACTS: 3-Trifluoromethyl-4-Nitrophenol*; 1999.

(13) United States Environmental Protection Agency (US EPA). *Reregistration Eligibility*

Decision (RED): 3-Trifluoro-Methyl-4-Nitro-Phenol and Niclosamide; 1999.

(14) Siefkes, M. J.; Steeves, T. B.; Sullivan, W. P.; Twohey, M. B.; Weiming, L. Sea Lamprey Control: Past , Present, and Future. *Gt. Lakes Fish. policy Manag. A Binatl. Perspect.* **2013**, No. Daniels 2001, 651–704.

(15) Ellis, D. A.; Mabury, S. A. The Aqueous Photolysis of TFM and Related Trifluoromethylphenols. An Alternate Source of Trifluoroacetic Acid in the Environment. *Environ. Sci. Technol.* **2000**, *34* (4), 632–637. https://doi.org/10.1021/es990422c.

(16) Barber, J.; Steeves, M. Sea Lamprey Control in the Great Lakes: 2020. Annual Report to the Great Lakes Fishery Commission. **2020**.

(17) Dawson, V. K.; Gumming, K. B.; Gilderhus, P. A. Laboratory Efficacy of 3-Trifluoromethyl-4-Nitrophenol (TFM) as a Lampricide. *Investig. Fish Control* **1975**, *63*, 1–13.

(18) Marking, L. L.; Olson, L. E. Toxicity of the Lampricide 3-Trifluoromethyl-4-Nitrophenol (TFM) to Nontarget Fish in Static Tests. **1975**, *19* (3), 1–27.

(19) Barber, J.; Steeves, M. Standard Operating Procedures for Application of Lampricides in the Great Lakes Fishery Commission Integrated Management of Sea Lamprey (Petromyzon Marinus) Control Program. Sea Lamprey Control Special Report 92-001.4. **2021**.

(20) McConville, M. B.; Hubert, T. D.; Remucal, C. K. Direct Photolysis Rates and Transformation Pathways of the Lampricides TFM and Niclosamide in Simulated Sunlight. *Environ. Sci. Technol.* **2016**, *50* (18), 9998–10006. https://doi.org/10.1021/acs.est.6b02607.

(21) Bhat, A. P.; Pomerantz, W. C. K.; Arnold, W. A. Finding Fluorine: Photoproduct Formation during the Photolysis of Fluorinated Pesticides. **2022**. https://doi.org/10.1021/acs.est.2c04242.

(22) Freeling, F.; Scheurer, M.; Koschorreck, J.; Ho, G.; Ternes, T. A.; Karsten, N. Levels and Temporal Trends of Trifluoroacetate (TFA) in Archived Plants: Evidence for Increasing Emissions of Gaseous TFA Precursors over the Last Decades. **2022**. https://doi.org/10.1021/acs.estlett.2c00164.

(23) Schwarzenbach, R. P.; Gschwend, P. M.; Imboden, D. M. *Environmental Organic Chemistry: 2nd Edition*; Hoboken, New Jersey, 2003.

(24) Boutonnet, J. C.; Bingham, P.; Calamari, D.; Rooij, C. de; Franklin, J.; Kawano, T.; Libre, J.-M.; McCul-loch, A.; Malinverno, G.; Odom, J. M.; Rusch, G. M.; Smythe, K.; Sobolev, I.; Thompson, R.; Tiedje, J. M. Environmental Risk Assessment of Trifluoroacetic Acid. *Hum. Ecol. Risk Assess. An Int. J.* **1999**, *5* (1), 59–124. https://doi.org/10.1080/10807039991289644.

(25) The National Oceanic and Atmospheric Administration (NOAA). Great Lakes ecoregion: This lake system contains the largest supply of freshwater in the world. https://www.noaa.gov/education/resource-collections/freshwater/great-lakes-ecoregion#:~:text=The large lakes are Superior,system for clean drinking water. (accessed Mar 5, 2024).

(26) The Great Lakes Fishery Commission (GLFC. About the Lakes https://www.glc.org/lakes/ (accessed Mar 5, 2024).

(27) The Great Lakes Fishery Commission (GLFC). Lampricides: theme overview https://www.glfc.org/lampricides-theme.php (accessed Mar 5, 2024).

(28) Carey, J. H.; Fox, M. E. Photodegradation of the Lampricide 3-Trifluoromethyl-4-Nitrophenol (TFM) 1. Pathway of the Direct Photolysis in Solution. *J. Great Lakes Res.* **1981**, *7* (3), 234–241. https://doi.org/10.1016/S0380-1330(81)72050-1.

(29) Carey, J. H.; Fox, M. E.; Schleen, L. P. Photodegradation of the Lampricide 3-Trifluoromethyl-4-Nitrophenol (TFM). 2. Field Confirmation of Direct Photolysis and Persistence of Formulation Impurities in a Stream During Treatment. *J. Great Lakes Res.* **1988**, *14* (3), 338–346. https://doi.org/10.1016/S0380-1330(88)71563-4.

(30) McConville, M. B.; Hubert, T. D.; Remucal, C. K. SI_Direct Photolysis Rates and Transformation Pathways of the Lampricides TFM and Niclosamide in Simulated Sunlight. *Environ. Sci. Technol.* **2016**, *50* (18), 9998–10006. https://doi.org/10.1021/acs.est.6b02607.

(31) Kempe, L. L. *Microbial Degradation of the Lamprey Larvicide 3-Trifluoromethyl-4-Nitrophenol in Sediment-Water Systems*; 1973.

(32) Reynolds, J. *Hydrolysis of [14C] TFM. Performed by XenoBiotic Laboratories, Inc. Submitted by Great Lakes Fishery Commission, Ann Arbor, Michigan. MRID 44429501*; 1997.

(33) Dawson, V. K.; Johnson, D. A.; Allen, J. L. Loss of Lampricides by Adsorption on Bottom Sediments. *Can. J. Fish. Aquat. Sci.* **1986**, *43* (8), 1515–1520. https://doi.org/10.1139/f86-189.

(34) Hussain, M. Fate of the Lampricide 3-Trifluoromethyl-4-Nitrophenol (TFM) in the Environment. MS Thesis., Michigan State University, 1998.

(35) Schaper, J. L.; Posselt, M.; McCallum, J. L.; Banks, E. W.; Hoehne, A.; Meinikmann, K.; Shanafield, M. A.; Batelaan, O.; Lewandowski, J. Hyporheic Exchange Controls Fate of Trace Organic Compounds in an Urban Stream. *Environ. Sci. Technol.* **2018**, *52* (21), 12285–12294. https://doi.org/10.1021/acs.est.8b03117.

(36) Ward, A. S. The Evolution and State of Interdisciplinary Hyporheic Research. *Wiley Interdiscip. Rev. Water* **2016**, *3* (1), 83–103. https://doi.org/10.1002/wat2.1120.

(37) Lewandowski, J.; Arnon, S.; Banks, E.; Batelaan, O.; Betterle, A.; Broecker, T.; Coll, C.; Drummond, J. D.; Grabowski, R. C.; Herzog, S. P.; Hinkelmann, R.; Höhne, A.; Raza, M.; Riml, J.; Robertson, A.; Rutere, C.; Singh, T.; Ward, A. S.; Wolke, P.; Wörman, A.; Wu, L. Is the Hyporheic Zone Relevant beyond the Scientific Community ? **2019**.

(38) Briggs, M. A.; Day-lewis, F. D.; Zarnetske, J. P.; Harvey, J. W. A Physical Explanation for the Development of Redox Microzones in Hyporheic Flow. **2015**, 4402–4410. https://doi.org/10.1002/2015GL064200.Received.

(39) Buffington, J. M.; Tonina, D. Hyporheic Exchange in Mountain Rivers II: Effects of Channel Morphology on Mechanics, Scales, and Rates of Exchange. *Geogr. Compass*

2009, *3* (3), 1038–1062. https://doi.org/10.1111/j.1749-8198.2009.00225.x.

(40) Fox, A.; Boano, F.; Arnon, S. Impact of Losing and Gaining Streamflow Conditions on Hyporheic Exchange Fluxes Induced by Dune-Shaped Bed Forms. **2014**, 5375–5377. https://doi.org/10.1002/2013WR014979.

(41) Gutowski, L.; Olsson, O.; Lange, J.; Kümmerer, K. Science of the Total Environment Photolytic Transformation Products and Biological Stability of the Hydrological Tracer Uranine. *Sci. Total Environ.* **2015**, *533*, 446–453. https://doi.org/10.1016/j.scitotenv.2015.07.002.

(42) Smart, P. L.; Laidlaw, I. M. S. An Evaluation of Some Fluorescent Dyes for Water Tracing. *Water Resour. Res.* **1977**, *13* (1), 15–33. https://doi.org/10.1029/WR013i001p00015.

(43) Lange, J.; Schuetz, T.; Gregoire, C.; Elsässer, D.; Schulz, R.; Passeport, E.; Tournebize, J. Multi-Tracer Experiments to Characterise Contaminant Mitigation Capacities for Different Types of Artificial Wetlands. *Int. J. Environ. Anal. Chem.* **2011**, *91* (7–8), 768–785. https://doi.org/10.1080/03067319.2010.525635.

(44) Shiau, B. -J; Sabatini, D. A.; Harwell, J. H. Influence of Rhodamine WT Properties on Sorption and Transport in Subsurface Media. *Groundwater* **1993**, *31* (6), 913–920. https://doi.org/10.1111/j.1745-6584.1993.tb00864.x.

(45) Dierberg, F. E.; DeBusk, T. A. An Evaluation of Two Tracers in Surface-Flow Wetlands: Rhodamine-WT and Lithium. *Wetlands* **2005**, *25* (1), 8–25. https://doi.org/10.1672/0277-5212(2005)025[0008:AEOTTI]2.0.CO;2.

(46) Ptak, T.; Schmid, G. Dual-Tracer Transport Experiments in a Physically and Chemically Heterogeneous Porous Aquifer: Effective Transport Parameters and Spatial Variability. *J. Hydrol.* **1996**, *183* (1–2), 117–138. https://doi.org/10.1016/S0022-1694(96)80037-0.

(47) Sutton, D. J.; Kabala, Z. J.; Vasudevan, D. Rhodamine WT as a Reactive Tracer: Laboratory Study and Field Consequences. *IAHS-AISH Publ.* **2000**, No. 262, 201–205.

(48) Vasudevan, D.; Fimmen, R. L.; Francisco, A. B. Tracer-Grade Rhodamine WT: Structure of Constituent Isomers and Their Sorption Behavior. *Environ. Sci. Technol.* **2001**, *35* (20), 4089–4096. https://doi.org/10.1021/es010880x.

(49) Soerens, T. S.; Sabatini, D. A. Interpretation of Sorption Studies for Compound Isomers or Mixtures. *Ground Water* **1996**, *34* (4), 605–609. https://doi.org/10.1111/j.1745-6584.1996.tb02047.x.

(50) Leibundgut, C.; Seibert, J. Tracer Hydrology. *Treatise Water Sci.* **2011**, *2* (December 2011), 215–236. https://doi.org/10.1016/B978-0-444-53199-5.00036-1.

(51) The US Geological Survey. The National Map. https://apps.nationalmap.gov/viewer/ (accessed Feb 16, 2024).

(52) TOP 018.7: Procedures for Conducting Spectrophotometric Analysis for TFM in Stream Water. **2012**, No. 0, 1–9.

(53) YSI (Xylem). CDOM-fDOM: YSI Webinar - A Closer Look at fDOM Measurement https://www.ysi.com/parameters/cdom-fdom#:~:text=Chromophoric Dissolved Organic

Matter or,fraction of CDOM that fluoresces (accessed Dec 4, 2023).

(54) YSI (Xylem). *YSI EXO User Manual: Section 1.9 FDOM Sensor Overview*; 2020.

(55) Lee, E. J.; Yoo, G. Y.; Jeong, Y.; Kim, K. U.; Park, J. H.; Oh, N. H. Comparison of UV-VIS and FDOM Sensors for in Situ Monitoring of Stream DOC Concentrations. *Biogeosciences* **2015**, *12* (10), 3109–3118. https://doi.org/10.5194/bg-12-3109-2015.

(56) Watras, C. J.; Hanson, P. C.; Stacy, T. L.; Morrison, K. M.; Mather, J.; Hu, Y. H.; Milewski, P. A Temperature Compensation Method for CDOM Fluorescence Sensors in Freshwater. *Limnol. Oceanogr. Methods* **2011**, *9* (JULY), 296–301. https://doi.org/10.4319/lom.2011.9.296.

(57) YSI (Xylem). EXO User Manual: Advanced Water Quality Monitoring Platform. Item# 603789REF, Revision K.

(58) Algae, B. G.; Oil, C.; Brighteners, O.; Fuels, R. Cyclops-7 Interchangeable Logger Cyclops-7 Sensor Specifications.

(59) Pallud, C.; Meile, C.; Laverman, A. M.; Abell, J.; Cappellen, P. Van. The Use of Flow-through Sediment Reactors in Biogeochemical Kinetics : Methodology and Examples of Applications. **2007**, *106*, 256–271. https://doi.org/10.1016/j.marchem.2006.12.011.

(60) Gupta, R. S. *Hydrology and Hydraulic Systems: Third Edition*; Waveland Press, 2008.

(61) Organisation for Economic Co-operation and Development (OECD). OECD 106 Adsorption - Desorption Using a Batch Equilibrium Method. *OECD Guidel. Test. Chem.* **2000**, No. January, 1–44.

(62) Roy, W. R.; Krapac, I. G.; Chou, S.-F. J.; Griffin, R. A. Technical Resource Document: Batch-Type Procedures for Estimating Soil Adsorption of Chemicals. *EPA Tech. Doc.* **1992**, *EP A/530-S*.

(63) Dean, W. Determination Of Carbonate and Organic Matter in Calcareous Sediments and Sedimentary Rocks by Loss on Ignition: Comparison with Other Methods. *J. Sediment. Petrol.* **1974**, *44* (1), 242–248.

(64) Laszakovits, J. R.; Berg, S. M.; Anderson, B. G.; O'Brien, J. E.; Wammer, K. H.; Sharpless, C. M. P-Nitroanisole/Pyridine and p-Nitroacetophenone/Pyridine Actinometers Revisited: Quantum Yield in Comparison to Ferrioxalate. *Environ. Sci. Technol. Lett.* **2017**, *4* (1), 11–14. https://doi.org/10.1021/acs.estlett.6b00422.

(65) Zepp, R. G.; Cline, D. M. Rates of Direct Photolysis in Aquatic Environment. *Environ. Sci. Technol.* **1977**, *11* (4), 359–366. https://doi.org/10.1021/es60127a013.

(66) Leifer, A. *The Kinetics of Environmental Aquatic Photochemistry: Theory and Practice*; American Chemical Society, 1988.

(67) Dullin, D.; Mill, T. Development and Evaluation of Sunlight Actinometers. *Environ. Sci. Technol.* **1982**, *16* (11), 815–820. https://doi.org/10.1021/es00105a017.

(68) McConville, M. B.; Cohen, N. M.; Nowicki, S. M.; Lantz, S. R.; Hixson, J. L.; Ward, A. S.; Remucal, C. K. SI_A Field Analysis of Lampricide Photodegradation in Great Lakes Tributaries. *Environ. Sci. Process. Impacts* **2017**, *19* (7), 891–900. https://doi.org/10.1039/c7em00173h.

(69) Van Frost, S. R.; White, A. M.; Jauquet, J. M.; Magness, A. M.; McMahon, K. D.; Remucal, C. K. Laboratory Measurements Underestimate Persistence of the Aquatic Herbicide Fluridone in Lakes. *R. Soc. Chem.* **2024**. https://doi.org/10.1039/d3em00537b.

(70) Downing, B. D.; Pellerin, B. A.; Bergamaschi, B. A.; Saraceno, J. F.; Kraus, T. E. C. Seeing the Light: The Effects of Particles, Dissolved Materials, and Temperature on in Situ Measurements of DOM Fluorescence in Rivers and Streams. *Limnol. Oceanogr. Methods* **2012**, *10* (OCTOBER), 767–775. https://doi.org/10.4319/lom.2012.10.767.

(71) Bertone, E.; de Oliveira, G. F.; Stewart, R.; O' Halloran, K. Using Compensated Fluorescence Probes Data for Proactive Water Treatment Management. **2018**, *3* (July), 227–217. https://doi.org/10.29007/tq71.

(72) Zhao, H. A.; Garnier, C.; Redon, R.; Mounier, S. 3D Fluorescence Quenching of Dissolved Organic Matter Applying PARAFAC Treatment. No. 2, 3–4.

(73) Wang, Z.; Cao, J.; Meng, F. Interactions between Protein-like and Humic-like Components in Dissolved Organic Matter Revealed by Fluorescence Quenching. *Water Res.* **2015**, *68*, 404–413. https://doi.org/10.1016/j.watres.2014.10.024.

(74) Karickhoff, S. W.; Morris, K. R. Sorption Dynamics of Hydrophobic Pollutants in Sediment Suspensions. *Environ. Toxicol. Chem.* **1985**, *4* (4), 469–479. https://doi.org/10.1002/etc.5620040407.

(75) Swann, R. L.; Laskowski, D. A.; McCall, P. J. A Rapid Method of the Estimation of the Environmental Parameters Octanol/Water Partition Coeffient, Soil Sorption Constant, Water to Air Ratio, and Water Solubility. *Residue Rev.* **1983**, *Vol. 85*, 17–28. https://doi.org/10.1007/978-1-4612-5462-1_3.

(76) United States Environmental Protection Agency (US EPA). Fate, Transport and Transformation Test Guidelines - OPPTS 835.1230 Adsorption/Desorption (Batch Equilibrium). **2008**, No. October, 1–55.

(77) The Food and Agricultural Association (FAO). Parameters of pesticides that influence processes in the soil https://www.fao.org/3/X2570E/X2570E06.htm (accessed Sep 4, 2024).

(78) Applegate, V. C.; Howell, J. H.; Moffett, J. W.; Johnson, B. G. H.; Smith, M. A. *Use of 3-Trifluormethyl-4-Nitrophenol as a Selective Sea Lamprey Larvicide*; 1961.

(79) Thingvold, D. A.; Lee, G. F. Persistence of 3-(Trifluoromethyl)-4-Nitrophenol in Aquatic Environments. *Environ. Sci. Technol.* **1981**, *15* (11), 1335–1340. https://doi.org/10.1021/es00093a004.

(80) Thingvold, D. A. Adsorption, Degradation and Persistence of 3-Trifluoromethyl-4-Nitrophenol (TFM) in Aquatic Environments. Ph.D. Thesis., University of Wisconsin--Madison, 1975.

(81) Bothwell, M. L.; Beeton, A. M.; Lech, J. J. Degradation of the Lampricide 3-Trifluoromethyl-4-Nitrophenol by Bottom Sediments. *Fish. Res. Board Canada* **1973**, 1–6.

(82) Magadanz, H. E.; Kempe, L. L. The Removal of 3-Trifluoromethyl-4-Nitrophenol from

Natural Water by Bottom Sediments; Indianapolis, Indiana, 1986; p 11.

(83) Saalfield, S. L.; Wnuk, J. D.; Murray, M. M.; Dunnivant, F. M. A Comparison of Two Techniques for Studying Sediment Desorption Kinetics of Hydrophobic Pollutants. *Chemosphere* **2007**, *66* (2), 384–389. https://doi.org/10.1016/j.chemosphere.2006.04.043.

(84) Liu, D.; Fox, M. E. *Biodegradation of TFM in a Cyclone Fermentor System: Technical Report Number PESTAB/81/2137*; 1978.

(85) Fathulla, R. N. Anaerobic Aquatic Metabolism of 14C-Labeled 3-Trifluoromethyl-4-Nitrophenol (14C-TFM) Great Lakes Fishery Commission; 1996.

(86) Fathulla, R. N. Aerobic Aquatic Metabolism of 14C-Labeled 3-Trifluoromethyl-4-Nitrophenol (14C-TFM) Great Lakes Fishery Commission; 1995; pp 1–64.

(87) Rao, A. M. F.; Mccarthy, M. J.; Gardner, W. S.; Jahnke, R. A. Respiration and Denitrification in Permeable Continental Shelf Deposits on the South Atlantic Bight : Rates of Carbon and Nitrogen Cycling from Sediment Column Experiments. **2007**, *27*, 1801–1819. https://doi.org/10.1016/j.csr.2007.03.001.

(88) Lewis, J.; Sjöstrom, J. Optimizing the Experimental Design of Soil Columns in Saturated and Unsaturated Transport Experiments. *J. Contam. Hydrol.* **2010**, *115* (1–4), 1–13. https://doi.org/10.1016/j.jconhyd.2010.04.001.

(89) Ali, S.; Nakhli, A.; Tian, J.; Thomas, P. MethodsX Preparing and Characterizing Repacked Columns for Experiments in Biochar-Amended Soils. **2021**, *8*. https://doi.org/10.1016/j.mex.2020.101205.

(90) McConville, M. B.; Mezyk, S. P.; Remucal, C. K. Indirect Photodegradation of the Lampricides TFM and Niclosamide (Article). *Environ. Sci. Process. Impacts* **2017**, *19* (8), 1028–1039. https://doi.org/10.1039/c7em00208d.

(91) Bhat, A. P.; Pomerantz, W. C. K.; Arnold, W. A. Wavelength-Dependent UV-LED Photolysis of Fluorinated Pesticides and Pharmaceuticals. *Environ. Sci. Technol.* **2023**. https://doi.org/10.1021/acs.est.3c00627.

(92) Canonica, S.; Gunten, U. Von; Wenk, J. Effect of Dissolved Organic Matter on the Transformation of Contaminants Induced by Excited Triplet States and the Hydroxyl Radical. *Environ. Sci. Technol.* **2011**, *45* (18), 7947–7948. https://doi.org/10.1021/es202439z.

(93) Wenk, J.; Canonica, S. Phenolic Antioxidants Inhibit the Triplet-Induced Transformation of Anilines and Sulfonamide Antibiotics in Aqueous Solution. *Environ. Sci. Technol.* **2012**, *46* (10), 5455–5462. https://doi.org/10.1021/es300485u.

(94) El-Din, M. Z.; Elsayed, K.; Al-Sherbini, S. M.; Harith, M. A. Photostability of Uranine via Crossed-Beam Thermal Lens Technique. *Laser Chem.* **2007**, *2007*. https://doi.org/10.1155/2007/36024.

(95) Minor, E. C.; James, E.; Austin, J. A.; Nelson, V.; Lusk, R.; Mopper, K. A Preliminary Examination of an in Situ Dual Dye Approach to Measuring Light Fluxes in Lotic Systems. **2013**, 631–642. https://doi.org/10.4319/lom.2013.11.631.

(96) Walden, S. L.; Carroll, J. A.; Unterreiner, A. N.; Barner-Kowollik, C. Photochemical

Action Plots Reveal the Fundamental Mismatch Between Absorptivity and Photochemical Reactivity. *Adv. Sci.* **2024**, *11* (3), 1–8. https://doi.org/10.1002/advs.202306014.

(97) Miller, G. C.; Zepp, R. G. Extrapolating Photolysis Rates from the Laboratory to the Environment. *Residue Rev.* **1983**, *Vol. 85*, 89–110. https://doi.org/10.1007/978-1-4612-5462-1_8.

(98) Haag, W. R.; Mill, T. Direct and Indirect Photolysis of Water-soluble Azodyes: Kinetic Measurements and Structure-activity Relationships. *Environ. Toxicol. Chem.* **1987**, *6* (5), 359–369. https://doi.org/10.1002/etc.5620060505.

(99) Minor, E. C.; Austin, J. A.; Sun, L.; Gauer, L.; Zimmerman, R. C.; Mopper, K. Mixing Effects on Light Exposure in a Large-Lake Epilimnion: A Preliminary Dual-Dye Study. *Limnol. Oceanogr. Methods* **2016**, *14* (8), 542–554. https://doi.org/10.1002/lom3.10111.

(100) Tai, D. Y.; Rathbun, R. E. Photolysis of Rhodamine-WT Dye. *Chemosphere* **1988**, *17* (3), 559–573.

(101) Zepp, R. G. *Photochemical Transformations Induced by Solar Ultraviolet Radiation In Marine Ecosystems*; U. S. Environmental Protection Agency Environmental Research Laboratory College Station Road Athens, Georgia 30613, 1982.

(102) Wilson, J. F.; Cobb, E. D.; Kilpatrick, F. A. Fluorometric Procedures for Dye Tracing. *U.S. Geol. Surv. Tech. Water-Resources Investig. B. 3* **1986**.

(103) Partanen, S. B.; Apell, J. N.; Lin, J.; McNeill, K. Factors Affecting the Mixed-Layer Concentrations of Singlet Oxygen in Sunlit Lakes. *Environ. Sci. Process. Impacts* **2021**, *23* (8), 1130–1145. https://doi.org/10.1039/d1em00062d.

(104) Apell, J. N.; McNeill, K. Updated and Validated Solar Irradiance Reference Spectra for Estimating Environmental Photodegradation Rates. *Environ. Sci. Process. Impacts* **2019**, *21* (3), 427–437. https://doi.org/10.1039/c8em00478a.

(105) Findlay, S. Importance of Surface-subsurface Exchange in Stream Ecosystems: The Hyporheic Zone. *Limnol. Oceanogr.* **1995**, *40* (1), 159–164. https://doi.org/10.4319/lo.1995.40.1.0159.

(106) Inc., I. C. TFM SDS. *Mater. Saf. Data Sheet* **2012**, *4* (2), 8–10.

(107) *TFM Bar: Registration Number 22610 Pest Control Products Act. For the United States Department of the Interior: U.S. Fish and Wildlife Service and the Canadian Agent: Department of Fisheries and Oceans (Canada)*; 2005.

(108) Niazi, A.; Yazdanipour, A.; Ghasemi, J.; Bozorgzad, S.; Kubista, M.; Republic, C. Spectrophotometric Investigation of the Acidity Constants of Fluorescein in Various Water-Organic Solvent Media. **2008**, No. October 2014, 37–41. https://doi.org/10.1080/00986440801943677.

(109) Król, M.; Wrona, M.; Page, C. S.; Bates, P. A. Macroscopic PKa Calculations for Fluorescein and Its Derivatives. *J. Chem. Theory Comput.* **2006**, *2* (6), 1520–1529. https://doi.org/10.1021/ct600235y.

(110) Kubista, M.; Sjiiback, R.; Nygren, J. Quantitative Spectral Analysis of Multicomponent Equilibria. **1995**, *302*, 121–125.

(111) Trudgill, S. T.; Pickles, A. M.; Smettem, K. R. J.; Crabtree, R. W. Soil Water Residence Time and Solute Uptake, 1. Dye Tracing and Rainfall Events. *J. Hydrol.* **1983**, *60:257 279*.

(112) Everts, C. J.; Kanwar, R. S. Evaluation of Rhodamine WT as an Adsorbed Tracer in an Agricultural Soil. *J. Hydrol.* **1994**, *153* (1–4), 53–70. https://doi.org/10.1016/0022-1694(94)90186-4.

(113) Sabatini, F.; Degano, I.; Colombini, M. P. Development of a Method Based on High-performance Liquid Chromatography Coupled with Diode Array, Fluorescence, and Mass Spectrometric Detectors for the Analysis of Eosin at Trace Levels. *Sep. Sci. Plus* **2020**, *3* (6), 207–215. https://doi.org/10.1002/sscp.202000002.

(114) Abood, K. A.; Lawler, J. P.; Disco, M. D. Utility of Radioisotope Methodology in Estuary Pollution Control Studies: Evaluation of the Use of Radioisotopes and Fluorescent Dyes for Determining Longitudinal Dispersion Coefficient in Estuaries. **1969**.

(115) Upstill-Goddard, R. C.; Suijlen, J. M.; Malin, G.; Nightingale, P. D. The Use of Photolytic Rhodamines WT and Sulpho G as Conservative Tracers of Dispersion in Surface Waters. *Limnol. Oceanogr.* **2001**, *46* (4), 927–934. https://doi.org/10.4319/lo.2001.46.4.0927.

(116) Keefe, S. H.; Barber, L. B.; Runkel, R. L.; Ryan, J. N.; Mcknight, D. M.; Wass, R. D. Conservative and Reactive Solute Transport in Constructed Wetlands. *Water Resour. Res* **2004**, *40*, 1201. https://doi.org/10.1029/2003WR002130.